Production and characterization of metal oxide nanoparticles and study of their incorporation into polymeric membranes

Gabriel Ribeiro

Thesis report submitted to

Escola Superior de Tecnologia e Gestão

Instituto Politécnico de Bragança

Master Degree in

Chemical Engineering

within the scope of the double diploma with

Universidade Tecnológica Federal do Paraná Campus Apucarana

Supervisors

Profª. Dra. Maria Filomena Filipe Barreiro

Prof. Dr. Helder Teixeira Gomes

Profª. Dra. Juliana Guerra Sgorlon

Profª. Dra. Maria Carolina Sérgi Gomes

Bragança

2021

ACKNOWLEDGEMENTS

First, I would like to thank my parents, my mother Gina and my father Valdir, who always have done everything that was possible for them to help me along my journey in Apucarana and in Bragança. They always have given me love and support.

Thanks to my supervisors from Portugal, Professor Dra. Filomena Barreiro and Professor Dr. Helder Teixeira Gomes of Instituto Politécnico de Bragança (IPB). Also, to my supervisors from Brazil, Professor Dra. Juliana Guerra Sgorlon and Professor Dra. Maria Carolina Sérgi Gomes of Universidade Tecnológica Federal do Paraná (UTFPR) for helping me with my work and give me all the support that I needed to complete it.

Thanks to Dr. Jose Luis and Dra. Isabel Fernandes for their help on the laboratory work, for helping and doing everything that they could for the success of this work. I thank the researchers that were always with me during the lab days, Adriano dos Santos Silva and Fernanda Fontana Roman, for the availability and energy to support and teach me everything I needed. Also thank to the researcher Ana Carolina Spaciari for the help in the final experiments.

I would like to express my sincere gratitude to IPB and UTFPR for enabling me to experience this Double Degree agreement opportunity and for the structure to perform the project. And also to CIMO to provide all the structure to do the laboratory research.

All my gratitude to my teachers from UTFPR – Apucarana and from IPB, that contributed to my personal and professional growth during all the time.

I also extend my thanks to those involved in my undergraduate years in Apucarana who have contributed to my growth, being important to my journey, and to my friends in Portugal who made part of my journey in IPB.

ABSTRACT

Membrane technology is applied as a separation process in different process, such as gas separation, wastewater treatment, biodiesel purification, food and fermentation industry. This technology contributes to reduce water used and save energy in these processes. They can be defined as a physical barrier between two phases, which regulates the mass transport between them. The performance of this type of technology in purification processes depends on parameters such as permeability and selectivity with the material to be filtered. Membranes can be produced from different materials. This study aimed to produce polymeric membranes composed of polyvinylpyrrolidone (PVP) and polyethersulfone (PES) with and without the addition of metal oxide nanoparticles, such as zinc oxide and iron oxides. The membranes were synthesized using the phase inversion method, with different amounts of solvent, PVP and nanoparticles. Nanoparticles were synthesized by the co-precipitation method. The nanoparticles were characterized by techniques such as infrared spectrum (FTIR), thermogravimetric analysis (TGA) and laser diffraction (LS). Membranes were characterized by techniques such as water absorption, porosity, hydraulic permeability, thermogravimetric analysis and optical microscopy. With the incorporation of nanoparticles, it is intended to study whether they change important properties such as hydrophilicity, pore size and permeability, to prevent membrane pore blocking, a phenomenon known as fouling, which is responsible for the drop in membrane performance in processes of filtration. Through the analyses, the relationship between membrane permeability and water absorption, pore size and permeate flux of each of the different compositions studied was verified. The analyses carried out, allowed to verify that the properties of the membranes were modified when the nanoparticles were incorporated. Permeability analysis allowed to verify the behaviour of membranes when applied to a fluid pressure. In this study, distilled water was used and even so it was verified a reduction in the permeate flux, which is due to membrane compaction. However, the incorporation of nanoparticles and the variation in the amount of PVP were able to reduce the reduction in permeate flux.

Keywords: Polymeric membranes; nanoparticles; coprecipitation; phase inversion; permeability.

RESUMO

Dentre os processos de separação de materiais existentes, a tecnologia de membrana é aplicada como um processo de separação em diferentes campos, como separação de gases, no tratamento de águas residuais, na purificação de biodiesel, na indústria de alimentos e fermentação. Esta tecnologia contribui para a redução de água utilizada e economia de energia desses processos. Elas podem ser definidas como uma barreira física entre duas fases, que regula o transporte de massa entre elas. A performance desse tipo de tecnologia em processos de purificação depende de parâmetros como a permeabilidade e a seletividade com o material a ser filtrado. As membranas podem ser produzidas de diferentes materiais. Este estudo teve como objetivo produzir membranas poliméricas compostas por polivinilpirrolidona (PVP) e polietersulfona (PES) com e sem a adição de nanopartículas de óxidos metálicos, como o óxido de zinco e óxidos de ferro. As membranas foram sintetizadas utilizando o método de inversão de fases, com diferentes quantidades de solvente, PVP e nanopartículas. As nanopartículas foram sintetizadas pelo método de coprecipitação. As nanopartículas foram caracterizadas por técnicas como espectro infravermelho (FTIR), análise termogravimétrica (TGA) e difração de laser (LS). A caracterização das membranas se deu por técnicas como absorção de água, porosidade, permeabilidade hidráulica, análise termogravimétrica e microscopia óptica. Com a incorporação das nanopartículas pretende-se estudar se elas alteram propriedades importantes tais como hidrofilicidade, tamanho de poros e permeabilidade, para a prevenção do entupimento de poros da membrana, fenômeno conhecido como *fouling*, que é responsável pela queda da performance da membrana em processos de filtração. Através das análises citadas foi verificado a relação entre permeabilidade da membrana e absorção de água, tamanho de poros e fluxo permeado de cada uma das diferentes composições estudadas. Com as análises realizadas foi possível verificar que as propriedades das membranas foram alteradas quando as nanopartículas foram incorporadas. A análise de permeabilidade permitiu verificar o comportamento das membranas quando aplicadas a pressão de um fluido. No estudo se utilizou água destilada e mesmo assim foi verificação de redução do fluxo permeado, o que se deve a compactação da membrana. Porém a incorporação de nanopartículas e a variação da quantidade de PVP, foram capazes de diminuir a redução do fluxo permeado.

Palavras-chave: Membranas poliméricas; nanopartículas; coprecipitação; inversão de fases; permeabilidade.

INDEX OF FIGURES

INDEX OF TABLES

INDEX OF ACRONYMS

CA – cellulose acetate;

DLS – diffractive light scattering;

DMF – N,N-Dimethylformamide;

FFAs – free fatty acids;

FTIR – transform infrared spectroscopy;

LD – Laser diffraction;

NP – nanoparticle;

OM – Optical Microscope;

PAN – polyacrylonitrile;

PES – polyethersulfone;

PP – polypropylene;

PSF – polysulfone;

PVC – polyninylchloride;

PVDF – polyvinyldiene fluorine;

PVP – polyvinylpyrrolidone;

SEM – scanning electron microscopy;

TAGs – tracylglycerol;

TEM – transmission electron microscopy;

TGA – thermogravimetric analysis;

THF – tetrahydrofuran;

XRD – X-ray diffraction;

TABLE OF CONTENTS

MOTIVATIONS AND OBJECTIVES

1 MOTIVATION AND OBJECTIVES

The emission of toxic gases and the generated air pollution is presently a subject of high concern for society. Several strategies are being developed to reduce atmospheric pollution and to improve air quality, including the study and development of biofuels. However, the economic and environmental viability of the biofuels implies the optimization of the productive processes and procedures, including, among others, the purification stage, in order to guarantee a higher quality of the final product.

The conventional purification process in biodiesel production is washing with water. However, this process increases the operation cost and is not ecofriendly. Membrane technology can be applied to avoid the water washing step. Purification using membranes is widely implemented, having, however, a main drawback: which is membrane fouling. This problem has been addressed and reported by different studies in literature [1–4]. One of the strategies mentioned as alternative to solve this problem consists in the incorporation of nanomaterials into the membranes. In fact, the application of nanotechnology finds diverse uses, due to the variety of materials with unique characteristics, which makes their choice important for certain applications to achieve the expected result. Several studies show that the incorporation nanoparticles (NP) into polymeric membranes produced from specific polymers allows to reduce the fouling phenomenon.

This project aims to develop new membranes with potential to be used in biodiesel production process, having in view both the increment of process efficiency and reduction of environmental impact by minimizing the amount of water used in the biofuel purification stage. For this purpose, a systematic study concerning production of membranes was performed, using different polymers and NPs of metallic oxides, to overcome the fouling phenomena.

The membranes were prepared using the phase inversion process, evaluating the influence of polymer concentration, type of solvent and NPs in the casting solution. The polymers used were polyvinylpyrrolidone (PVP) and polyethersulfone (PES) and the solvent N,N-Dimethylformamide (DMF). The selected NPs to be incorporated were zinc oxide (ZnO) and iron oxide, which were synthetized by the co-precipitation method.

The produced NPs were characterized by techniques such as Fourier-transform infrared spectroscopy (FTIR), Thermogravimetric Analysis (TGA) and Laser diffraction (LD). The produced membranes were characterized by optical microscopy (OP), thermogravimetry (TGA), water absorption, porosity the hydraulic permeability evaluated.

STATE OF THE ART

2 STATE OF THE ART

2.1 Biodiesel production and purification process

The worldwide concern about the negative impact that the different activities carried out by man cause to the environment and to human health has been growing, leading to the search of alternative solutions with lower environmental impact. Among the different concerns, the emission of gases generated from use of the fossil fuels, together with the limited availability of those sources are critical. In this context, biodiesel appears as a friendly and viable alternative, once it has a lower environmental impact, mostly in the quality of air [5,6].

Biodiesel is a renewable source of energy, sulphur free, oxygenated, sustainable, biodegradable and with a calorific value similar to fossil fuel [6]. It can be produced from different feedstocks, such as vegetal oils, animal fats or residual oils, once these contain long chains of free fatty acids (FFAs) or triacylglycerols (TAGs) [5]. Biodiesel can be produced by different methods, being transesterification the most applied, also known as alcoholysis due to reaction of the free fatty acids with alcohol. After the reaction is over, biodiesel and glycerol are formed [7]. The produced biodiesel contains impurities such as soap, catalysts, residual alcohols, diglycerides and monoglycerides (raw material residues) besides the secondary generated product - glycerol [5–7].

According to the standard specifications imposed to biofuels, such as the American ASTM D6751 and the European EN14214, those contaminants must be removed from the final product before use [8], thus implying the application of purification processes. Traditionally, the most common method used to separate the ester and glycerol phases from the crude biodiesel is decanting, while the removal of the residual alcohol from both phases, is usually performed by distillation or flash unit [9]. However, these processes are not 100% efficient, since impurities are still remaining on the ester phase, requiring an additional purification step. The alternatives for this final purification are wet washing, dry washing, membrane extraction, precipitation and complexation [10].

Among these methods, the wet and dry washing are those generally applied at industrial scale. Wet washing is the most frequently used method due to its simplicity and high efficiency in removing glycerol and methanol. The dry washing has no risk of contamination of the fuel with water, allows to work in continuous mode, improves the fuel quality and reduces the time of the process and the required amount of water [10,11].

Nevertheless, these conventional methods have some associated disadvantages, which make them uneconomically and non-environmentally friendly. Wet washing requires large

amounts of water (from 0.2 to 10 liters per liter of produced biodiesel) to remove the impurities, and has high energetic costs, being time consuming to complete the process. Dry washing uses ion exchange resins that do not remove the residual alcohol, thus requiring an extra equipment for this elimination, increasing the process costs [9–12].

Given the importance of the biodiesel purification to obtain a final product with the intended specifications, thus enabling its use, research works are carried on trying to find the best alternative to make the overall productive process economically efficient, and applicable on a large scale to reduce the negative impact on the environment. In this context, one of the most studied alternatives is the separation of the biodiesel contaminants using membranes. It has been verified some positive points about membrane technology, in addition to the reduction of water consumption, such as the use of moderate temperature and pressure conditions, low usage of energy, low elimination of wastewater and required treatment, higher mechanical, thermal and chemical stability, which have led to the use of membrane in the biodiesel purification [11].

In the field of membrane processes, Torres et al. [13] compared different types of membranes in biodiesel refining. Their results pointed out for differences in performance related with the composition of membranes. A polyvinyldiene fluorine (PVDF) membrane reached 67.3% of glycerol rejection. Nevertheless, it was noticed a decrease in the initial flow of biodiesel filtration, which was attributed to the membrane fouling. Saiful et al. [14] conducted a study on the separation of contaminants from crude biodiesel products by using a membrane produced with chitosan, dimethyl formamide and purolite particles. The developed membranes reached 63.93% removal efficiency of glycerol from crude biodiesel.

Alves et al. [9] also studied biodiesel purification using ultrafiltration and microfiltration processes. Different membranes were compared, namely polyethersulfone membranes (PES) of 10 and 30 kDa and mixed cellulose ester microfiltration membranes of 0.22 and 0.3 μm of pore size. Among all the performed tests, only the 10 kDa PES membrane was able to reduce glycerol content below 0.02% (w/w). Gomes et al. [15] studied the influence of the oil quality used for the production of biodiesel by transesterification, in the purification step by ultrafiltration. It was observed that there was an increase in the flow at the beginning of the filtration, but after the transient period, a reduction in the flow was noticed. This fact was probably originated due to the size of the agglomerated glycerol and the pressure used, which led to the fouling of the membrane. Nevertheless, ultrafiltration was efficient on glycerol removal since the highest glycerol content in the permeate was 0.013 wt%.

These studies put in evidence the importance of using membranes-based processes for biodiesel purification.

2.2 Membranes

A membrane can be defined as a physical barrier between two phases, which regulates the transport of substances between the phases [16]. In other words, a membrane is a third phase that controls mass transfer between the other phases. Membrane technology has been studied and applied as a separation process in a variety of fields, such as gas separation, wastewater treatment, leather industry, biodiesel purification, food industry and fermentation industry. This technology is considered cleaner than those conventionally used, contributing for environmental protection, and energy savings [17].

Membranes used in such processes must fulfil specific technical requirements, such as guarantying higher filtration flux and lower filtration pressure, being compact to contribute for space saving and having high efficiency in order to eliminate pre-treatment processes [16].

The performance of membranes in the filtration process usually depends on selectivity and permeability. Selectivity (α) is related to the properties of the materials under certain operating conditions. If there is a defect in its morphological structure, the material selectivity may change. Permeability (Lp) usually indicates the membrane ability to process the permeate, also representing the rate of mass flow through the membrane ($Q_{filtrate}$) per unit of area (A) and time, at a given pressure gradient (ΔP). High permeability is related to a high process yield. Membrane productivity depends on material characteristics and film thickness. The smaller the thickness, the greater the productivity [18,19]. The described membrane relations are demonstrated in Equations 1 and 2 [18].

$$Permeability, Lp = \frac{Q_{filtrate}}{A\Delta P} \quad (1)$$

$$Selectivity, \alpha = \frac{Flux\ of\ impurity}{Flux\ of\ product} \quad (2)$$

In membrane separation processes, the driving force is usually the pressure or the concentration gradient. Another significant parameter affecting the process is the transmembrane pressure, which is the hydrostatic pressure that allows ultrafiltration across the membrane [11]. Figure 1 represents a simplified scheme of the process.

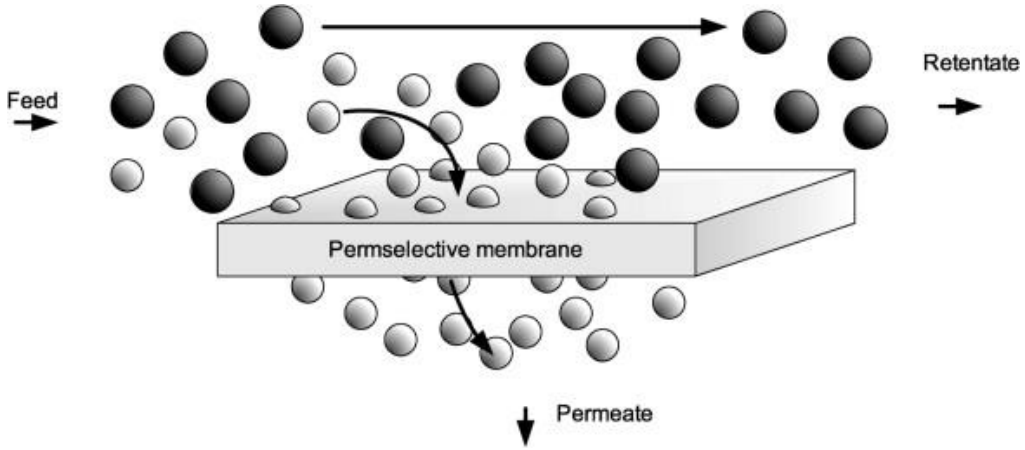

Figure 1. Simplified schematic concept of membrane separation.
Source: Adapted from [19]

This technology offers some significant advantages on separation processes as it is a simple operation, and easily scaled-up. Moreover, it has performance reliability, energy-efficiency, and compatibility with integrated systems [17].

Membranes can be produced from different materials, being these usually selected based on the specific application. Membranes can be composed by organic polymers, inorganic materials (oxides, ceramics and metals) or composite materials.

When compared with polymeric based membranes, the use of inorganic membranes has as main advantages the greater thermal, chemical, and mechanical stability, making this type of membranes advantageous for purification and separation processes. However, they are based in materials of higher economical cost, limiting their application. In this context, the membranes based on organic polymers are an immediate alternative due to their lower price [16].

2.2.1 Polymeric membranes: materials and synthesis processes

Polymeric membranes have as main advantages the low operation costs, and relatively small footprints, complying with environmental regulations, when compared with other conventional technologies [16]. In comparison with ceramic membranes, the polymeric membranes have operational limitations related with pH, pressure, organic solvents or high concentrations of chlorine. In addition, the regeneration of membranes after use is more difficult [20]. Due to such disadvantages, polymers must be carefully selected, since they will delimit the structural conditions, affinity to compounds and the subsequent application. In Table 1 it is possible to see an overview of some advantages and disadvantages of inorganic and polymeric membranes.

Table 1. Comparison of polymeric and inorganic membranes

Membrane	Advantages	Disadvantages
Inorganic	▪Long term durability; ▪High thermal stability; ▪Chemical stability in wide pH; ▪High structural integrity;	▪Expensive; ▪Some have low hydrothermal stability.
Polymeric	▪Cheap; ▪Mass production; ▪Good quality control.	▪Structurally weak; ▪Temperature limited; ▪Short life.

Source. Adapted from [19]

Polymeric membranes are produced from one unique polymer or by using a mixture of polymers. During the preparation of the membrane, the polymer can be added with inorganic materials that will be embedded into the membrane physical structure. Different preparation techniques can be applied to produce membranes. Their selection is made based on the specificity of the final separation application. Among the available options, techniques such as sintering, stretching, track-etching and phase inversion can be applied [20].

The sintering method involves compressing a powder composed of polymer particles of a certain size followed by sintering at high temperature. The required temperature depends on the used material. During sintering, the "interface" between the particles in contact disappears. In the stretching method, an extruded film or sheet made of a partially crystalline polymeric material, the only type of polymeric materials suitable for this technique, is stretched perpendicularly to the direction of extrusion so that the crystalline regions are positioned parallel to the extrusion direction. When mechanical stress is applied small fractures occur, and a porous structure is obtained. In track-etching, the film or sheet is subjected to high energy radiation applied perpendicularly to the film. The particles can damage a polymeric matrix and create marks. The film is then immersed in an acid or alkaline bath and the polymeric material evaluated along these tracks to form uniform cylindrical pores with a narrow pore size distribution. [20].

Beyond those methods, the most common process is phase inversion [21–27], where a polymer is transformed from a liquid to a solid state under controlled conditions. The method consists of spreading the polymeric solution onto a support, then immersing it in a non-solvent bath for a certain period under controlled volume and temperature conditions. The phase inversion can be performed by different techniques, being the most common applied the immersion precipitation. Others available techniques are solvent evaporation, precipitation by controlled evaporation, thermal precipitation and precipitation from the vapor phase [20].

Considering the immersion precipitation, a solution of polymer and solvent is prepared and casted onto a suitable support and immersed in a coagulation bath containing a nonsolvent. Here, the combination of mass transfer and phase separation makes the precipitation to occur, resulting in the formation of the membrane [20].

In general, the preparation of a composite membrane can be carried out by two methods, by dispersing the NPs in the casting solution, to prepare the membrane via phase inversion, or by dipping the membrane in a suspension with NPs [28].

Polymeric materials such as polyvinylidene fluoride (PVDF), polysulfone (PSF), polyethersulfone (PES), polyvinyl chloride (PVC), polypropylene (PP), polyacrylonitrile (PAN) and cellulose acetate (CA) can be applied in the production of films [11,29]. The most used polymers to produce membranes are PES, PSF and PVDF, due to the excellent chemical and physical stabilities of these polymers, and superior thermal and mechanical properties. However, these three polymers are hydrophobic, which leads the membrane to be easily fouled [4]. Besides these, others like polyvinylpyrrolidone (PVP), have been also studied [30]. In Table 2 is possible to observe some characteristics of the most used polymers.

Table 2. Polymeric materials comparison

Polymer	Advantages	Disadvantages	Ref
PES	• Excellent thermal, chemical, and physical resistance (range of pH of 1 to 13); • Mechanical strength; • Easy processing;	• Susceptible to fouling and a low membrane flux.	[22,31]
PSF	• Physiochemical and thermal stability; • Resistance to oxidation and chlorine;	• Susceptible to fouling by molecules much smaller than the membrane pore.	[21,32]
PVDF	• Thermal stability; • Resistance to radiation, acids and bases; • Highly organic selectivity;	• Liable to be contaminated by foulant materials, resulting in a dramatic decrease of membrane flux	[33,34]

Among the referred polymers, PES has been used for industrial and biological applications. It is the most common polymer used for fabrication of ultrafiltration or nanofiltration membranes. PES provides high chemical, oxidative and thermal stability to the membrane, having a wide pH tolerance. It can be easily processed and is cost-effective, which

makes it a great candidate for membrane preparation [35–37]. In the Figure 2 it is possible to observe the morphological differences of PES membrane at different PES concentrations.

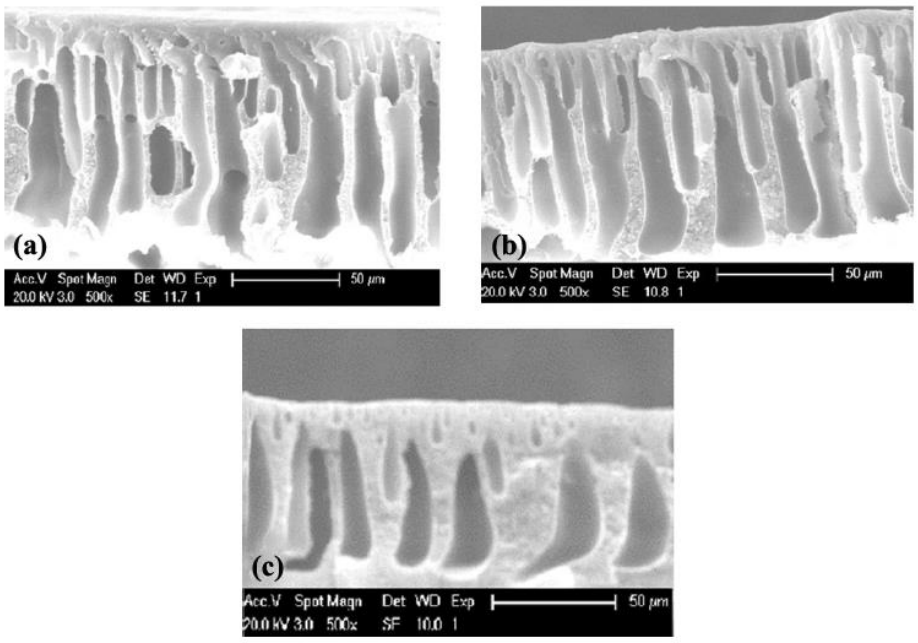

Figure 2. Cross-sectional SEM images of PES membranes at different PES concentrations: (a) 27% PES, (b) 30% PES and (c) 32% PES.
Source: Adapted from [28]

PVP has been widely used as an additive during the preparation of ultrafiltration membrane and is the most common additive used in the synthesis of PES membranes, in order to increase membrane hydrophobicity. Its use plays an important role during the synthesis of membranes by phase inversion once it promotes the pore generation in this process, providing the formation of more and larger porous in the membranes [38,39]. This occurs due to additives, such as PVP, that direct the phase inversion mechanism towards instantaneous demixing. Its presence on the synthesis mixture increases the viscosity of the solution, improving the casting [30]. In Figure 3 it is possible to observe the morphological differences of PVDF membranes when different PVP concentrations were used to produce a polymer mixed membrane.

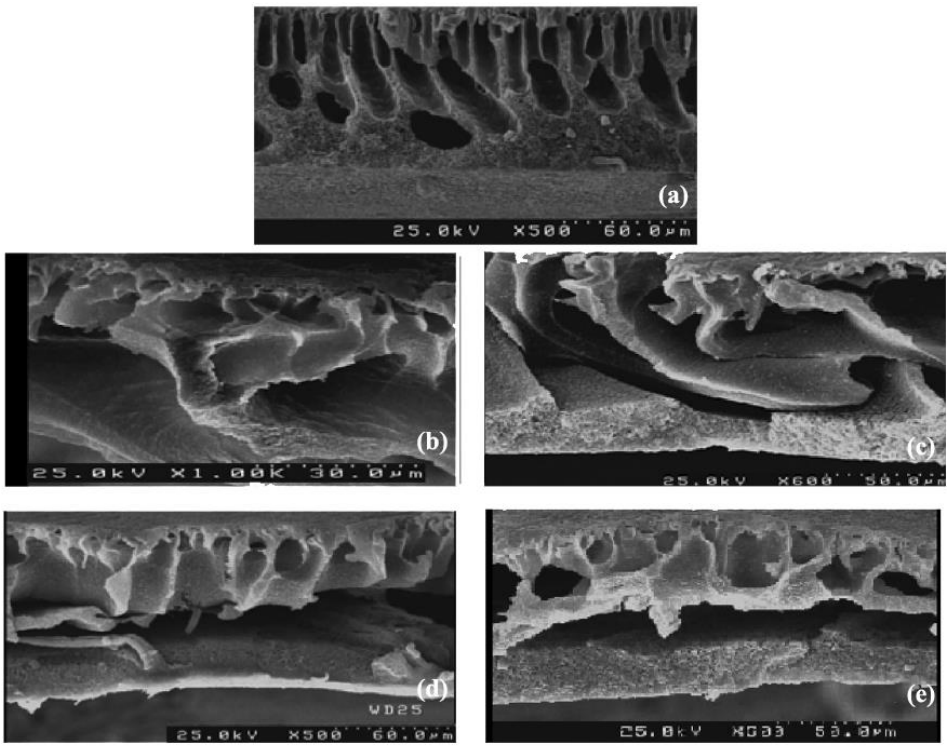

Figure 3. FESEM images of PVDF membranes at different PVP concentrations: (a) no additive, (b) 1%PVP, (c) 3% PVP, (d) 5% PVP and (e) 7% PVP
Source: Adapted from [40]

PES has a hydrophobic nature that is maintained even with the addition of additives, impacting on the most common membrane problem, which is membrane fouling. This type of problem occurs due to the presence of suspended particles, dissolved macromolecules, and emulsions present in the solution to be filtered, which can be deposited or adsorbed on the filtration membrane pores. The deposited material creates an additional layer on the membrane that acts like an additional barrier to the permeation. Thus, the pores of the membranes are blocked causing an irreversible reduction of permeate flux. In addition, the materials that originate the fouling, can shorten the membrane's service life and even destroy it [11,16,41].

Due to fouling, the flux decline is unavoidable during the filtration process. To minimize the fouling's impact, different approaches have been studied [1–4], such as the design of membrane modules, the optimization of operational parameters and the modification of the membrane material or structure. Among these alternatives, membrane modifications by the incorporation of nanomaterials have been studied as promising paths to increase the antifouling properties, as the permeation flux and hydrophilicity. The inorganic fillers are known as an effective way to enhance permeability without sacrificing the separation properties of the membrane [2].

Since permeability depends on porosity and hydrophilicity, and that nanomaterials enhance the selective features of the membrane including porosity, hydrophilicity, mechanical strength, and pore size, different types of nanomaterials are incorporated based on the application of the membrane. For this reason, even though different materials have been used for the preparation of membranes, polymeric membranes are gaining extreme popularity [42].

2.3 Characterization of the polymeric membranes

The characterization of membranes can be performed by scanning electron microscopy (SEM), Thermogravimetric Analysis (TGA), contact angle measurements, water uptake and porosity.

To analyze the morphological characteristics of the produced membranes, SEM is usually used. The surface and cross-section of the produced membranes are analyzed using the images obtained by SEM. It is also an important technique to check and compare polymeric membranes that have been modified by the incorporation of some additives [3,28,43,44]. Before the observations the samples need to be frozen, and liquid nitrogen is normally used for this purpose. The membrane samples need to be broken into small sizes in order to produce a clean and regular cross section [43].

To evaluate the surface hydrophilicity of the membranes, the contact angle between a water droplet and the membrane surface is measured. The tendency of water droplets to spread on the membrane surface is attributed to the hydrophilicity of the membrane surface. A lower contact angle indicates that the surface of the membrane is more hydrophilic [3,13,43–45].

As mentioned before, the permeability of the membrane depends on porosity. Porosity (ε) can be determined by the ratio of the pore volume to the geometrical volume of the membranes. To evaluate this parameter, Equation 3 can be used [40].

$$\varepsilon = \frac{W_w - W_d}{\rho_w . A . L} \tag{3}$$

Briefly, the membrane sample, with a certain area (A), is immersed in distilled water and weighed in the wet state (W_w). Then, the sample is dried until a constant mass is reached (W_d). The ρ_w is the density of pure water and (L) is the thickness of the membrane.

Water uptake can be determined from the measure of the dry and wet masses of the membrane samples, as show in Equation 4. Usually, the membranes are soaked in water for 24h and weighed after the excess of water is removed with blotting paper. After that, the membrane is dried to determine the dry weight [46,47].

$$\%\, Water\ uptake = \frac{W_w - W_d}{W_d}\ X\ 100 \qquad (4)$$

In Equation 4, W_w stands for the membrane weight in the wet state, and W_d stand for the membrane weight after the drying process.

To analyze the thermal properties of the membrane, a TGA analysis is carried out. Through this analysis it is possible to verify the thermal stability of the membrane. This method can be used to investigate the loss of mass of the material due to oxidation, reduction or loss of volatiles, such as the moisture contained in a fixed rang of temperature, which generally results in a temperature (or time) versus mass (or weight percentage) plot [4,48].

2.4 Nanomaterials

Nanotechnology has recently revolutionized science and engineering. This area of science deals with the development, manufacture and application of materials at the nanoscale, i.e., materials with sizes lower than 100 nm, called nanomaterials. Nanomaterials have several applications, but they have been mostly applied on the environmental science field, health, engineering and industrial. Compared to materials in another scale, these nanomaterials show a higher surface/volume ratio, allowing good performances for its diverse applications [2,49].

Inside the nanotechnology world, there are material's nanoparticles (NPs) that can be incorporated into other materials to improve or change some characteristics. This is achieved due to the extended surface effect, quantum effect and their size. Those nanomaterials can also act on different properties on the embedded material such as physical, chemical, morphological, mechanical, thermal, optical, magnetic and conductive [49].

NPs are smaller than 10-20 nm and are responsible for the drastically changes of the physical properties when compared with the solid material themselves. Their small size brings the most important information to its applicability [9]. Due to the unique characteristics of each material, the selection of the material and the synthesis method should be based on the final application and on its requirements [49].

2.4.1 Synthesis of the nanoparticles

One of the areas of fundamental importance to the understanding and development of nanomaterials is the development of synthetic methods, which allows control over the main variables, such as reaction kinetics, concentrations of reagents, reaction temperature, pH and

the order of reagents addition, which determine the particle size, size distribution, crystallinity and crystalline structure.

The preparation of metal oxide NPs is characterized in two main groups, physical and chemical methods. In the chemical route, a precursor is prepared in a solution or suspension (aqueous or non-aqueous), later converted into solid nanoparticles by a chemical reaction. Its disadvantages are some process complexity and particle agglomerations. The latter can change the properties of the developed material [50]. Metal oxide NPs are made up of different metals, and can be classified in insulating oxides (MgO, CaO, Al_2O_3 and SiO_2), semiconducting oxides (ZnO, TiO_2, NiO, Fe_2O_3 and Cr_2O_3) and transition metal oxides (Ru, Mo, W, Pt and V).

The crystallization process occurs in two phases, the nucleation (spontaneous or heterogeneous) and the growth of the particle. The latter requires that the clusters exceed a certain critical radius. Above this critical radius the clusters will not dissociate and increase their size [51]. Among these methods, the common synthesis methods involve co-precipitation, sol-gel processing, microemulsion techniques and solvothermal methods [52]. By varying the synthesis method and the stoichiometric parameters, the size and the morphology of the NPs can be altered [53].

In the sol-gel technique, the metal oxide nanoparticle (ZnO, TiO_2, SiO_2 and CuO_2) is prepared through the hydrolysis of precursors containing metals, mainly alkoxides in alcohol solutions, such as the precursor metal acetate, for example $Zn(CH_3COO)_2$, in ethanol or propanol [54]. The formation of the metal hydroxide network occurs by the condensation of molecules by the release of water. The polymerization and condensation of hydroxyl groups provides a thick and porous gel. After the appropriate drying and calcination steps, the ultrafine porous metal oxide powder is obtained [53,55,56]. The sol-gel method presents several advantages over other methods, such as relatively low annealing temperatures, excellent control of stoichiometry of the precursor solution and high purity of the synthesized material. However, the precursors presents a high cost [53].

In the microemulsion techniques, a ternary reaction system is created containing water, surfactant and oil. Then the metal oxide precursor is dropped into the emulsion and the NPs with narrow size are formed [57]. The particles obtained by this method are generally very uniform, but it requires a large amount of solvent to synthesize NPs and adverse effects on the NPs proprieties, due to residual surfactants [58].

The solvothermal method is based on the thermal decomposition of metal complexes under pressure in inert conditions. The size and aggregation of NPs can be controlled using appropriate surfactants under the reaction conditions [59]. Several surfactants such as oleic

acid, polyacrylic acid and sodium dodecyl benzene sulfonic have been used. The advantages of this method are that there is no requirement for any reducing agent or surfactant, kinetically control experimental conditions and easy scaling-up. However, this technique is very sensitive to the concentration of water and alkalinity [58].

In co-precipitation methods, the control of size and chemical uniformity, are the main challenge of the method, due to the uncontrolled aggregation of particles. However, particle size and shape can be tuned by adjusting parameters that are responsible for the synthesis, such as type of salts (chlorides, sulfates or nitrates), ionic strength and pH. Co-precipitation is the simplest technique to obtain large quantities of NPs but the large amount of water in the washing step of the material, due to a strong base solution, such as NaOH or NH_4OH in order to increase the amount of OH^- ions in the solution, makes the method not eco-friendly [52,58,60].

This method can be performed to synthesize metal oxide NPs, such as ZnO, FeO, Fe_2O_3, Fe_3O_4, CuO, TiO_2 and from other metals (Co, Ni, Mn) [45,61–63]. The solution of salt precursors, such as chlorides, sulfates and nitrates, have an important role on the morphology of the NPs, since the crystal growth depends on the nature of the precursor used and the growth rate difference pertaining to different planes [64].

2.4.2 Characterization techniques of the NPs

To analyze and characterize the produced NPs, techniques such as Fourier-transform infrared spectroscopy (FTIR), Thermogravimetric Analysis (TGA), Dynamic light scattering (DLS), Transmission electron microscopy (TEM) and X-ray diffraction (XRD), can be performed. These techniques allow the determination of particle size, atoms interaction, physical and chemical properties.

FTIR is a common technique to evaluate the binding characteristics of the dried powder of the synthetized NPs, by analyzing the emitted spectra [65,66]. The analysis of the diameter, morphology and shape of the synthesized NPs can be performed through TEM images. TEM is a microscopy technique in which an electron beam is transmitted through the sample to form image [66,67].

DLS is the most common technique used to analyze the hydrodynamic size of the nanoparticles, due its fastness and simplicity of use. It provides the information about the presence of NPs and allows obtaining information about the number-base size distribution [68].

TGA is most widely used for qualitative measurements. The variations of temperature in weight obtained by TGA can be used to classify the composition of NPs, to determine the effect of additives and to evaluate oxidation and thermal stability [48].

XRD is a rapid and powerful technique to identify and characterize materials. It is based on the constructive interference of monochromatic X-rays in a crystalline sample. For the NPs, this technique is used to identify crystal lattice indices and particle sizes of the samples [65–67].

2.4.3 NPs as additives in membranes

Among the vast application fields of nanomaterials, their incorporation into polymeric membranes has an important role, since they allow to increase the permeability, selectivity, strength, hydrophilicity, and antifouling properties, through the increment of the membrane pore size and wettability while reducing surface roughness [36,49].

The application of nanomaterials by incorporation in membrane to minimize the fouling effect has been reported. For example, Li et al. [1] tested PES/Pluronic-F127/TiO_2 mixed matrix membrane. They found that the improved hydrophilicity (due to the presence of TiO_2) was able to decrease the humic acid adsorption at the surface of the membrane. Aguilar et al.[37] presented a process to change the surface characteristics and to mitigate fouling of commercially available PES microfiltration membranes using nanoporous and nano-textured layers composed of cellulose nanocrystals or TEMPO-oxidized cellulose nanofibrils. The coated membranes showed significant reduction in organic fouling due to a decrease in the surface roughness, as well as increased wettability.

Abdulkarem et al. [69] prepared poly(vinylidene fluoride) (PVDF)-alpha-zirconium phosphate (PVDF-α-ZrP) mixed matrix membranes by the phase inversion method, with different loadings of α-ZrP NPs. The membranes demonstrated anti-fouling properties with lower fouling rates than the pristine PVDF membrane, due to its highest hydrophilic character, pore size and porosity. The produced membranes can be used to treat industrial wastewater containing traces of heavy metals.

Despite all the above mentioned, the amount of NPs needed to enhance the performance of the membrane may change depending on the types of the nanoparticle, the material used for its synthesis and its application. Low nanoparticle loading may not be sufficient to enhance the properties of the membrane, whereas high loading may cause aggregation of the NPs during immersion precipitation. High loading can also plug the pores

of the membrane, which can greatly affect the membrane morphology and filtration ability, suppressing all positive effects rather than improving them [70].

Several inorganic nanomaterials can be used for membranes to be applied in filtration processes, such as metal oxides (ZnO, TiO_2, SiO_2, Al_2O_3, FeO, Fe_2O_3, Fe_3O_4, ZrO_2 and zeolites), metals (Ag and Cu), nanostructured carbon materials (carbon nanofibers and nanotubes, among others) and nanofiber polymers (polyurethane, polylactic acid and polyethylene oxide) [2].

Due to this diversity of inorganic nanomaterials, it is important to choose the right material to achieve the desired final characteristics of the membrane with incorporated NPs. Oxide metal NPs, such as ZnO and iron oxides, are typically used to minimize the fouling phenomenon.

2.4.3.1 ZnO NPs incorporated in membranes

ZnO is one of the most important multifunctional semiconductor materials and exceptionally important for applications in photo-catalysis, due to its excellent optical, electrical, mechanical and chemical proprieties [71]. Characteristics such dipole-dipole structure, high active surface area, excellent photocatalysis properties with its wide bandgap (3.37eV), low toxicity and the possibility to be shaped in different nanoshapes, has brought much attention to ZnO materials [72].

Due to their active surface area, these NPs can be incorporated in polymeric and ceramic membranes to improve properties such as roughness, permeability and antifouling resistance. Several effects in membrane modification are expected, due to its excellent stability provided from the nanostructures, which increases crystallinity (into the polymeric matrix) [28,71,72]. these NPs promote the increase of the surface-to-volume ratio, which together with its low cost results in a low-cost device [28].

The ZnO materials used as filler in polymeric membranes, have demonstrated to improve fouling properties and the permeation flux. As an example, Pang et al. [3] studied the effect of multiwalled carbon nanotubes (MWCNT) and ZnO addition on a PES membrane, prepared via non-solvent phase separation, and loaded with different amounts of both kinds of materials. The synergism of both fillers improved membrane porosity and hydrophilicity, leading to the improvement of the membrane permeate flux, and resulting on a PES membrane with enhanced antifouling properties. The filtration performance was tested with a humic acid solution, being the best results obtained with a membrane containing 0.5 wt% of each material.

Several studies have been carried out on the antifouling behavior of nano-ZnO in membranes, as shown by the bibliographic survey described on Table 3.

The incorporation of ZnO NPs as a filler in polymeric membranes has been widely studied, as well as its use in different membrane applications. The performances reached by the modified membranes showed that the presence of ZnO NPs improve some characteristics which are responsible by the reduction of fouling. Literature also points out ZnO as an alternative to other expensive nanomaterials with similar characteristics, like the TiO_2 [16].

In Figure 4 is possible to observe the morphological difference of a PES membrane when incorporated with ZnO NPs.

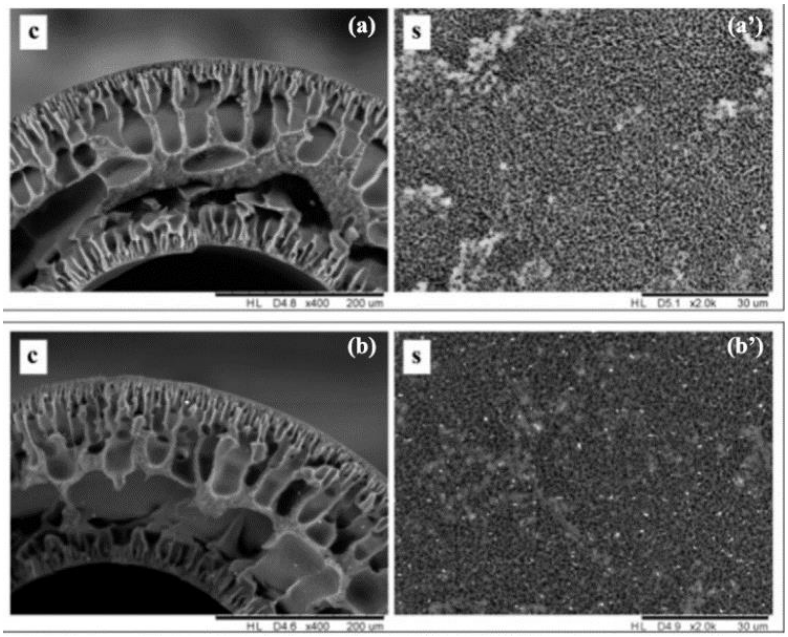

Figure 4. SEM images of PES/PVP membranes at different ZnO NPs loading: (a) and (a') no ZnO, (b) and (b') 0.5 wt%. The left images indicate the cross-sectional SEM and the right images refers to SEM surface.
Source: Adapted from [43]

As an alternative to the low selectivity and fouling problem in the biodiesel purification step, Kusworo et al. [73] studied the modification of PES membranes incorporating ZnO NPs. The PES-nano ZnO membrane was synthesized by preparing a solution composed of PES (17 wt%), nano ZnO (1.5 wt%) and N-methyl Pyrrolidone (NMP) as a solvent. UV irradiation, PVP addition (6 wt%), and thermal treatments were conducted to modify fabricated nanohybrid membranes. The modified membrane increased the flow by up to 200%. The glycerol rejection for the modified membrane was 91.54%, being higher than the unmodified membrane. Also, exhibited significant enhancement of hydrophilicity by lowering the water contact angle value and presented less foulant deposition on the membrane surface. The modified membrane of PES-nano ZnO decreased membrane fouling.

Table 3. Scope of ZnO nanomaterial used as filler in polymeric membranes

Polymer	NPs Loading (wt%)	Fabrication Method	Performance	Ref.
PES	0.0085, 0.013, 0.017, 0.1 and 0.5	Wet phase separation	The antifouling properties were improved with the incorporation of ZnO and properties (surface hydrophilicity, porosity, and surface pore size) increased	[4]
PSF	1, 2, 3 and 4	Phase inversion method	Reduced the hydrophobicity of the membrane using 2 wt%. Water permeability was enhanced, and thermal stability was improved. In a filtration test the membrane exhibit less flux decline.	[21]
PES	0.2, 0.4, 0.6 and 0.8	Phase inversion method	Improvement of the porosity, water flux and antifouling ability when 0.4wt% of ZnO is present.	[22]
PVDF	0.001, 0.005, 0.01, 0.1 and 1	Phase inversion method	Hydrophilicity was improved and roughness of the membrane was decreased, enhancing the anti-fouling performance. The best performance was with 0.005wt%.	[23]
PVDF	0.001, 0.01, 0.1 and 1	Phase inversion method	Membrane fouling resistance decreased with an increase in the ZnO content. The mechanical strength was reinforced.	[24]
PES	0.035, 0.07, 0.085, 0.125, 0.250, 0.375, 1, 2 and 4	Phase inversion induced by immersion precipitation	The blended membrane showed lower flux decline and a better permeability. The rejection of methylene blue increased to 82.3% for blended membranes, with a 0.035wt% of NPs.	[28]
PES	0, 0.5, 2, 3.62 and 5	Dry-jet wet phase inversion	The membrane fouling resistance decreased when used in a filtration test with humic acid. When used with river water the optimized membrane had an improvement in fouling resistance.	[43]
PES	0.01, 0.10, 1.0	Phase inversion precipitation technique	Increased the membrane hydrophilicity and water flux. The best performance (antifouling property) was obtained with 0.1wt% of NPs.	[45]
PVDF	1, 2, 3 and 4	Non-solvent induced phase separation	PVDF membrane demonstrated significant anti-irreversible fouling properties. The mechanical strength was reinforced, and the anti-irreversible fouling properties were enhanced.	[74]

2.4.3.2 Iron oxide NPs incorporated in membranes

Iron is one of the most abundant metals in the earth's crust and the most ubiquitous of the transition metals. Its reactivity in microscopy application is important, however, at the nanoscale, as pure metal, iron NPs are extremely reactive, which made them difficult to study, thus being their applications restricted [16]. On the other hand, iron oxides have specific characteristics and are relatively stable at the nanoscale, making them interesting for some applications.

Iron compounds have low toxicity, hydrophilic nature, high surface modifiability, great biocompatibility and chemically inert. In addition to these characteristics, their crystallographic structures provide high surface area/volume ratio. Many works have investigated the incorporation of iron oxide NPs, such as Fe_2O_3 and Fe_3O_4, in membranes [75].

It was reported that the presence of Fe_2O_3 increase oxygen content on membrane surfaces, which is expected to decrease the contact angle and to enhance hydrophilicity, promoting permeate flux. With lower contact angles, those membranes may improve their performance and anti-fouling characteristics when Fe_2O_3 is incorporated [25].

Several studies have reported the fabrication of membranes modified by iron oxide NPs and it is believed that the impregnation of this NPs is a solution for problems associated with polymeric membrane applications. For example, Ghaemi et al. [44] tested PES- Fe_3O_4 composites nanofiltration membranes in the removal of copper from water. It was found that the highest Cu removal (92%) can be reached in the presence of 0,1 wt% Fe_3O_4 due to the high copper adsorption. It was also reported that this combination led to an increase in the hydrophilicity and pure water flux of membrane.

In the same field, Gholami et al. [76] studied the effect of the blend ratio of polyvinylchoride (PVC), cellulose acetate and ferrosoferric oxide nanoparticle. The membrane was prepared by the phase inversion method being then used to remove lead from water. Different concentrations of Fe_3O_4 (0.01, 0.1 and 1 wt%) were used to study its effect on membrane rejection. Among the nanoparticle concentrations incorporated, the membrane with 0.1% of Fe_3O_4 showed better flux and rejection, when compared to the others.

As described, iron oxides NPs have been used for water treatment, but it can also be applied to minimize the fouling of the membrane and to enhance some properties, such as hydrophilicity, porosity and pore size, as several studies have reported. Some of these works are listed in Table 4.

Table 4. Scope of iron oxide nanomaterials used as filler in polymeric membranes

NP	Polymer	NPs Loading (wt%)	Fabrication Method	Performance	Ref.
Fe_2O_3 and multi-walled carbon nanotubes (MWCNTs)	PVDF	0-2	Immersion precipitation	1 wt% Fe_2O_3 and 0.2wt% MWCNTs significantly improved membrane morphology and presented a significant reduction in membrane fouling.	[25]
Fe_3O_4	PVP and PSF	20.5-84.4	Phase inversion method	An ideal performance in terms of pure water flux, rejection and antifouling ability when a concentration of 58.3wt% Fe_3O_4 is present.	[26]
Fe_3O_4	PVDF	0-80	Phase inversion process	The rejection of PVDF-Fe_3O_4 ultrafiltration membrane increased with the nanoparticle presence. Membrane reached from 65 to 75wt% had a high pure water flux, high rejection, good fouling-resistance and good compaction-resistance ability.	[27]
Fe_2O_3	PVC (Polyvinyl chloride)	0-2	Phase inversion method	Enhanced water flux (782 L/m^2h), higher sodium alginate (SA) rejection rate (91.9%) and better antifouling properties.	[77]
FeO	PES	0, 0.05 and 0.2	Interfacial polymerizatio n method	The membrane increased the removal of hydrophobic contaminants and reduced the fouling. Mechanical and thermal stability were improved.	[78]

Most of the iron oxides nanomaterial applications are in water and wastewater treatment. The incorporation of this nanomaterial in polymeric membranes, to reduce the fouling phenomenon, has not been widely studied but has a good potential to contribute to this objective, as described on the table review (Table 4). This makes its use an interesting possibility to achieve the main goal of the present study. Figure 5 shows the morphological structure of a PES membrane incorporated with iron oxides NPs.

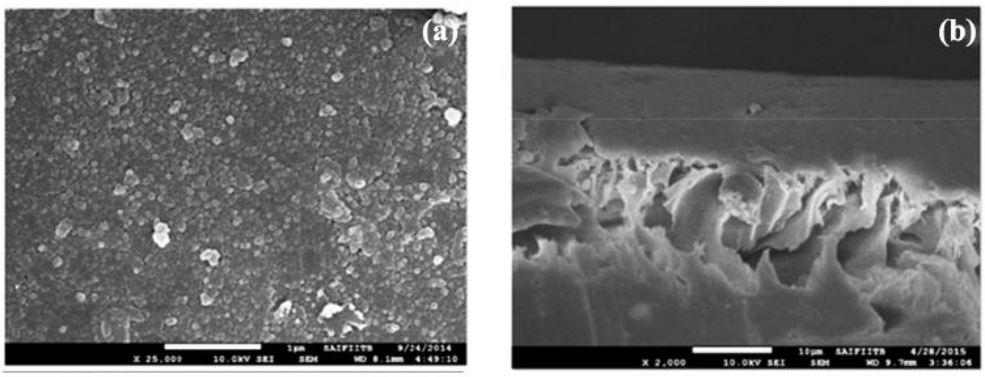

Figure 5. SEM images of PES membrane with 0.2 wt% FeO NPs. (a) refers to SEM surface membrane image, (b) refers to cross-sectional membrane image.
Source: Adapted from [78]

After a careful literature search, a lack was found concerning the application of membranes incorporated with iron oxides NPs in the biodiesel purification step, which is a future potential application for the produced membranes in this present study.

MATERIALS AND METHODS

3 MATERIALS AND METHODS

3.1 Reactants

The reactants used in this work are given in the following sections being separated according to the intended application.

3.1.1 Synthesis of the nanoparticles

For the synthesis of ZnO and iron oxides NPs, the used zinc and iron sources were a solution of Zinc chloride, $ZnCl_2$, (extra pure, Fischer Scientific UK, England) and a solution of Iron (III) chloride hexahydrate, $FeCl_3.6H_2O$, (97 wt%, Merck, Germany). The precipitating agent, ammonium hydroxide, was produced from a NH_3 solution (30%, Mer, Germany) diluted in distilled water, to obtain NH_4OH with a concentration of 1M. Distilled water was used to wash the precipitate, as well as ethanol absolute (99,9%, Fischer, Loughborough, England).

3.1.2 Synthesis of the membranes

For the synthesis of the membranes, Polyethersulfone (PES, Mw = 58,000) in pellets (GoodFellow Cambridge Limited, Hungtindon, England), Polyvinylpyrrolidone (PVP, Mw = 40,000) in powder (Sigma-Aldrich, Saint Louis), N, N-Dimethylformamide (DMF) (99,9%, CARLO EBRA Reagents S.A.S) were used to prepare the casting solutions.

3.2 Synthesis

The experimental procedures adopted in this work are given below, separated by the type of synthesized material.

3.2.1 Nanoparticles

ZnO and iron oxides NPs were synthesized by the coprecipitation method. The metals precursors ($ZnCl_2$ and $FeCl_3.6H_2O$) were dissolved in distilled water to obtain a 0,027 M solution, then each one was stirred continuously with a magnetic stirrer at room temperature. NH_4OH was added dropwise using a peristaltic pump (ISM 845, ISMATEC) until pH 9 was reached, according to the steps shown in Figure 6.

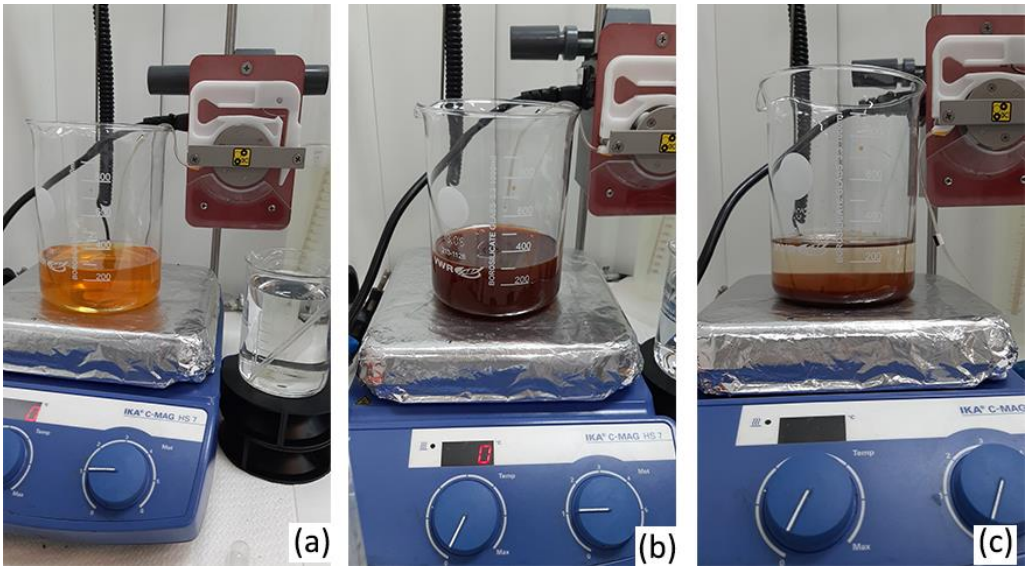

Figure 6. Production of iron oxides NPs. (a) is the beginning of the process, (b) is when pH 9 was reached, (c) is the precipitate at the bottom.

The obtained precipitate was then washed with distilled water until neutral pH, using centrifugation at 600 rpm during 5 minutes in an MPW- 260R centrifuge (MPW Med. Instruments). After, the obtained product was washed with ethanol absolute. The resultant material was dried in a drying oven (Binder FD 115) overnight at 60 °C.

The NPs were stored until the necessary amount to the next step of this study was reached, 5 g of each material. Thereafter, ZnO and iron oxides NPs were transferred to a crucible and placed in a muffle, being heated at 600°C for 3h to remove any of the remaining residues of ammonium and chlorides.

3.2.2 Polymeric membranes

All membranes were prepared by the phase-inversion method. For that, the DMF solution was stirred for 5 minutes at 50ºC, then the NPs were added to the solution, stirred for 5 minutes and ultrasonicated (Ultrasons-H, P- Selecta) for 10 minutes at room temperature. Subsequently the PVP was added to the mixture under stirring. After 5 minutes, the PES was also added, and the stirring maintained for 12 hours at 50ºC to obtain the casting solution. The compositions of each membrane are shown in Table 5.

Table 5. Composition of the casting solution.

Membrane	DMF (g)	PES (g)	PVP (g)	ZnO (g)	Iron Oxides (g)
M1	8.00	1.50	0.50	0	0
M2	7.50	1.50	1.00	0	0
M3	7.00	1.50	1.50	0	0
M4	7.95	1.50	0.50	0.05	0
M5	7.85	1.50	0.50	0.15	0
M6	6.95	1.50	1.50	0.05	0
M7	6.85	1.50	1.50	0.15	0
M8	7.40	1.50	1.00	0.10	0
M9	7.95	1.50	0.50	0	0.05
M10	7.85	1.50	0.50	0	0.15
M11	6.95	1.50	1.50	0	0.05
M12	6.85	1.50	1.50	0	0.15
M13	7.40	1.50	1.00	0	0.10

Each membrane composition presented represents a different level of the factorial experimental design, where the percentage of polymer and embedded nanoparticles were chosen as independent variables and hydraulic permeability, residual masses obtained by the TGA study and porosity were chosen as dependent variables. The experimental design is shown at Table 6.

Table 6. Experimental design

Test	Polymers composition (%)	Nanoparticle composition (%)	XT	XR
1	20	0,5	-1	-1
2	20	0,5	-1	-1
3	20	1,5	-1	1
4	20	1,5	-1	1
5	30	0,5	1	-1
6	30	0,5	1	-1
7	30	1,5	1	1
8	30	1,5	1	1
9	25	1,0	0	0
10	25	1,0	0	0
11	25	1,0	0	0

The statistical significance of the experimental data and the construction of the response surface were determined using the Statistica 10.0 program.

Figure 7 shows the system used to prepare the membrane solution in the stirring step.

Figure 7. Stirring process.

After 12 hours, the casting solution was ultrasonicated for 15 minutes at room temperature. Thereafter, the mixture was spread onto a glass plate with a glass rod at room temperature. The generated membrane was kept on the glass plate for 1 minute that was then immersed in a distilled water bath maintained at room temperature for 4 h. Finally, the membrane was dried at room temperature for 24 h.

3.3 Characterization techniques

3.3.1 Fourier Transform Infrared Spectroscopy (FTIR)

The obtained membranes were analysed by Fourier transform infrared spectroscopy (FTIR), using an ABB Inc., model MB3000 (Quebec, Canada) equipment operating in attenuated reflectance mode (ATR) using a diamond crystal. The analysis was done using a resolution of 4 cm^{-1} and 32 cumulative scans, being the spectra acquired in a wavenumber range from 550 to 4000 cm^{-1}. All the measurements were done using the solid samples at room temperature.

3.3.2 Laser diffraction (LD)

The size distributions of the produced NPs were measured using a laser diffraction (LD) equipment (Malvern, Mastersizer 3000 Hydro MV, UK). For the analysis, the samples were added into deionized water contained in the dispersion unit. The software Malvern Access Controller was used to perform the particle size analysis and calculate size distributions and average sizes.

3.3.3 Thermogravimetric Analysis (TGA)

The thermal degradation of the samples was determined by Thermogravimeric analysis (TGA) using a Netzsch equipment model TG209F3 Tarsus (Selb, Germany). The samples were weighted (5-10 mg) and placed in alumina crucibles, thereafter, heated from 25 to 800°C at a heating rate of 10°C/min under a N_2 flow at 30 mL.min^{-1}. Thermograms were acquired and processed using Netzsch Proteus thermal analysis software, v.5.2.1.

3.3.4 Water uptake and porosity

Water uptake was determined by measuring the dry and wet mass of the membrane samples following a methodology adapted from Eren et al. (2015) [47]. The membranes (1 cm^2) were dried in a convective drying oven for 24 h at 100ºC and weighed. Then, they were placed in a beaker containing 20 mL of distilled water for 24 h at room temperature being then weighed. The test was performed in duplicate. Water uptake, expressed in percentage, was calculated by Equation 4, and porosity of the membranes was determined with Equation 3. Both equations were previously introduced in section 2.3.

$$\%\, Water\ uptake = \frac{W_w - W_d}{W_d}\ X\ 100 \qquad (4)$$

Where W_w stands for the membrane weight in the wet state, and W_d stand for the membrane weight after the drying process. The porosity of the membranes was determined with Equation 3.

$$\varepsilon = \frac{W_w - W_d}{\rho_w . A . L} \qquad (3)$$

Where A stands for the membrane area (cm²), ρ_w is the density of pure water (g.cm^{-3}) and L is the thickness of the membrane (cm).

3.3.5 Optical microscopy (OM)

A sample of the membrane was placed on a microscope slide and placed on an optical microscope (OM) Ni-U (Nikon Eclipse Ni, Nikon Corp., Japan) apparatus, coupled with a digital camera. The displayed images were monitored using NIS-Elements Documentation

software at 40 and 100x magnifications. The pore size was evaluated by measuring 30 pores per image at 100X magnification.

3.3.6 Hydraulic Permeability

The membranes were compacted to ensure the structural accommodation of the polymeric material and to ensure that no interference in the permeate flux values during the experiments. The module was filled with distilled water and the pressure adjusted to 3 bar. This pressure was chosen because it was greater than or equal to the working pressures and after compaction, the flow of distilled water was measured at pressures of 1, 1.5, 2 and 2.5 bar.

The pure solvent flux was determined using Equation 5.

$$J_{perm} = \frac{m_p}{A.t} \quad (5)$$

Where J_{perm} is the permeate flux ($kg.h^{-1}.m^{-2}$), m_p the permeate mass, A the membrane filtration area (m^2) and t time (h).

The hydraulic permeability of the membranes was calculated using equation 6, which corresponds to the angular coefficient of the straight line obtained by the permeate flow versus the pressure gradient.

$$J_{perm} = L_p * \Delta P \quad (6)$$

Where L_p stands for the hydraulic permeability of the membrane ($kg.h^{-1}.m^{-2}.bar$) and ΔP for pressure gradient.

3.3.7 Nanoparticle's characterization

After following the synthesis procedure described in the experimental section (3.1.1), the NPs were obtained and stored in plastic flasks as can be seen in Figure 8. The prepared NPs were characterized by FTIR, LS and TGA.

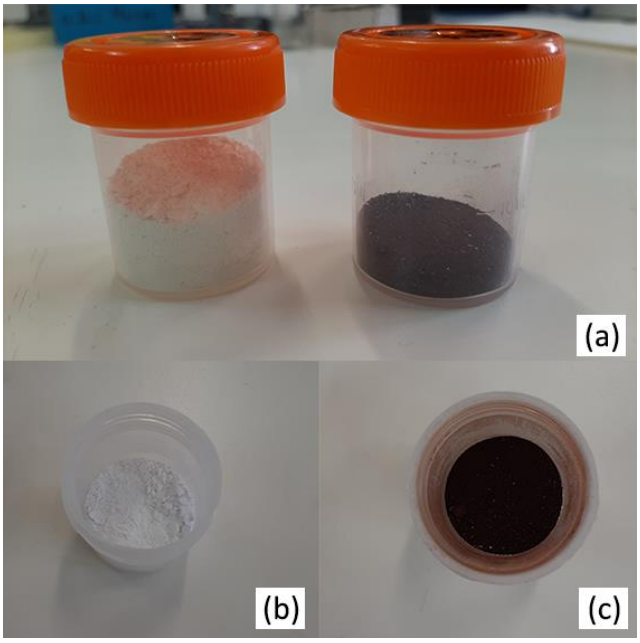

Figure 8. Produced NPs. (a) ZnO NPs (left) and iron oxides NPs (right), (b) ZnO NPs and (c) iron oxides NPs.

3.3.8 Membrane's characterization

The membranes were synthesized following the procedure described in the previous experimental section (3.2.2) in Chapter 3. Figure 17 represents some of the produced samples with different characteristics.

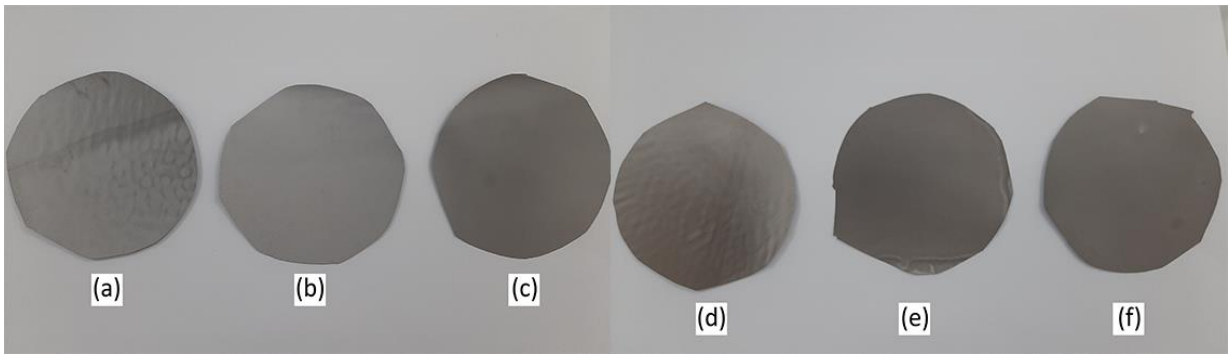

Figure 9. Produced membranes. The membranes refer to (a) M4; (b) M5; (c) M6; (d) M10; (e) M11 and (f) M12.

These membranes, as the other produced in this work, were characterized by TGA, porosity and water uptake, morphology (optical microscopy) and hydraulic permeability.

RESULTS AND DISCUSSION

4 RESULTS AND DISCUSSION

4.1 Characterization of the materials

4.1.1 Fourier Transform Infrared Spectroscopy (FTIR)

FTIR spectra of the synthesized ZnO and iron oxides nanoparticles are shown in Figure 9 and 10, respectively. The absorption bands in the spectra show the stretching and bending vibrations of the metal-oxygen bonds.

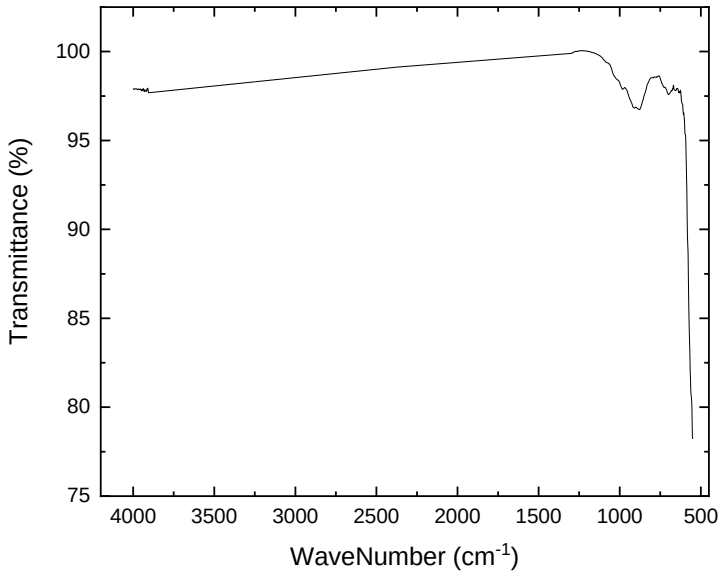

Figure 10. FTIR spectra of the produced ZnO NPs.

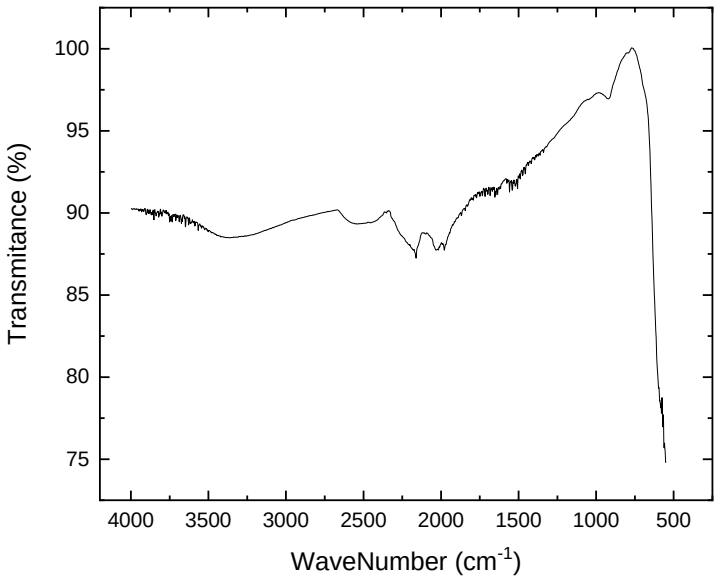

Figure 11. FTIR spectra of produced iron oxides NPs.

The stretching vibrations of Metal-Oxygen (M-O) bonds are found in the range 540-1600 cm^{-1} for tetrahedral structures of the ions and in the range of 400-1480 cm^{-1} for the octahedral ones [79].The obtained spectrum in Figure 9 shows ZnO absorption vibrations in the region 500 and 1000 cm^{-1}. These peaks were attributed to Zn and O bonding vibrations and stretching, confirming the formation of ZnO NPs. The strong characteristic band at 549 cm^{-1} corresponds to the standard peak of ZnO due to the stretching frequency of Zn–O bonds, which confirms the presence of M-O vibrational peaks [65,66,80]. The absence of significant impurities in this sample is confirmed due to the non-existence of peaks related to any other functional group.

In Figure 10 it can be observed the iron oxides with absorption bands in the region 500 and 1000 cm^{-1}. A sharp drop in the range of 700-500 cm^{-1} was noticed where, related with the stretching of Fe-O bond. Data available in the literature indicated that Fe-O shows absorption peaks in the range of 400–600 cm^{-1}, depending on their position in the composite/material [81].

4.1.2 Laser diffraction (LD)

Laser diffraction allows the determination of the particle size distribution of the dispersed particles. The samples of produced NPs were analysed by LD, being obtained the mean particle size based on the respective numerical and volumetric distributions. The obtained results are described in Table 7 and Table 8. Volumetric and numeric distributions for ZnO NPs are represented, respectively, in Figure 11 and 12.

Table 7. Particle size percentile values for the distributions obtained with ZnO NPs.

Sample Name	Diameter	Percentile values		
		Dx (10) (μm)	Dx (50) (μm)	Dx (90) (μm)
ZnO	Number distribution	0.0799 ± 0.0006	0.1070 ± 0.0001	0.1600 ± 0.0008
	Volume distribution	0.5020 ± 0.0084	2.4800 ± 0.0400	31.3000 ± 0.4200

Table 8. Particle size percentile values for the distributions obtained with iron oxides NPs.

Sample Name	Diameter	Percentile values		
		Dx (10) (μm)	Dx (50) (μm)	Dx (90) (μm)
Iron Oxides	Number distribution	0.8300 ± 0.0002	1.1700 ± 0.0009	2.3200 ± 0.0016
	Volume distribution	14.7000 ± 0.8300	108.0000 ± 2.1600	466.0000 ± 6.6000

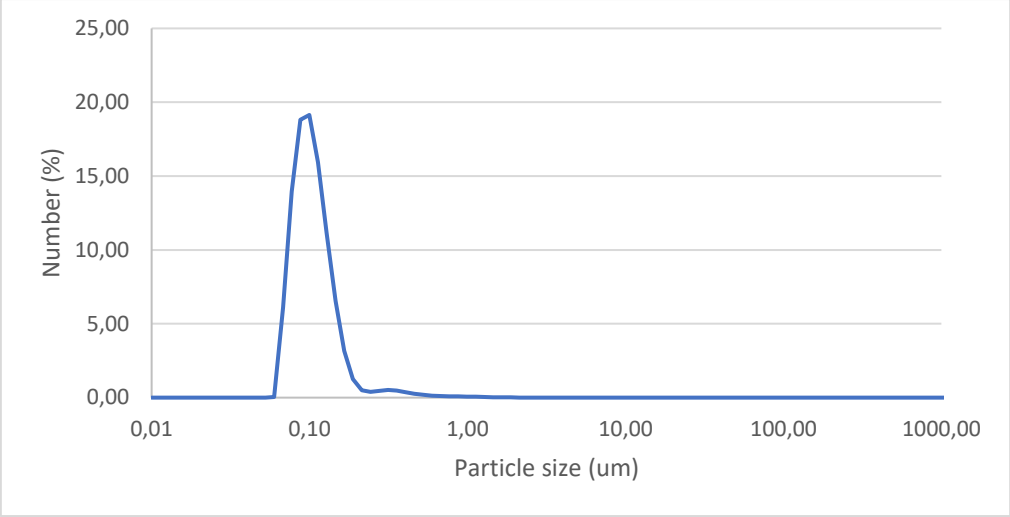

Figure 12. Size distribution in number of ZnO particles obtained by LS.

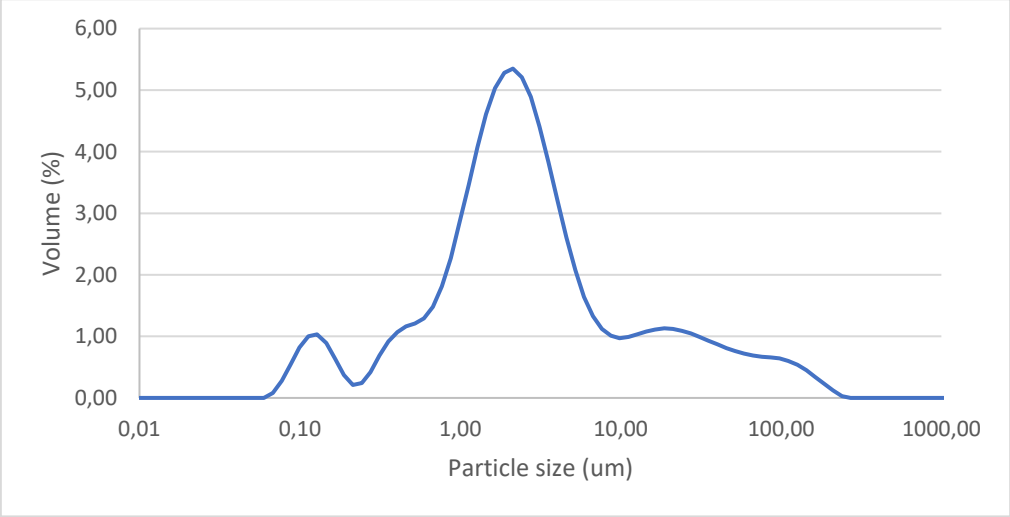

Figure 13. Size distribution in volume of ZnO particles obtained by LS.

Analysing Figure 12, it can be noted that the particles have sizes between 0.06 and 2.75 μm, with a unimodal distribution. For the volume distribution, a multimodal distribution is identified, putting in evidence the presence of NPs with different cluster sizes, having however, a mean size of 2.48 μm to the volume of ZnO NPs as shown in Table 7. It is also possible to observed that the particles have a higher concentration in the range of 0.10 μm, which represents the average particle size for the ZnO particles.

Volumetric and numeric dispersions for iron oxides NPs are represented, respectively, in Figures 14 and 15.

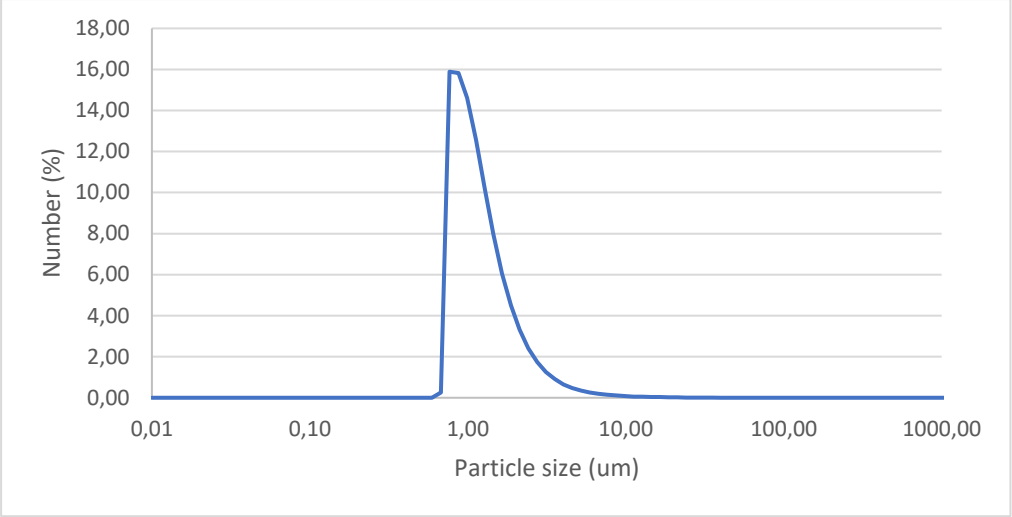

Figure 14. Size distribution by number of iron oxides particles obtained by LS.

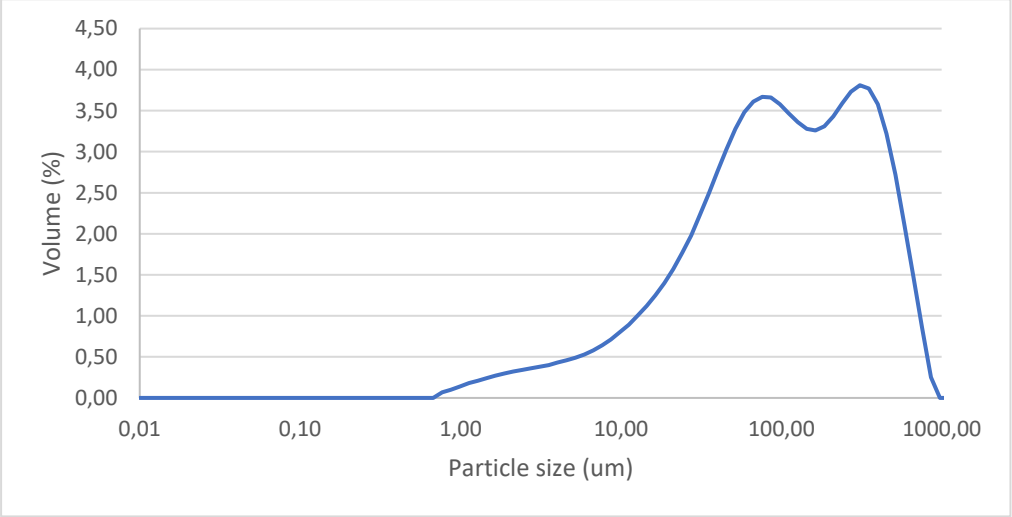

Figure 15. Size distribution by volume of iron oxides particles obtained by LS.

Analysing Figure 14, it is noted that the iron oxides particles have sizes between 0.68 and 35.30 μm. It is also possible to observe a higher number of particles in the range around 1.17 μm, which represents the average particle size of the iron oxides particles, as shown in Table 8. The large peak of the volume distribution noted in Figure 15 can be explained by the agglomeration of particles.

4.1.3 Thermogravimetric Analysis (TGA)

The thermal degradation of the NPs was evaluated. Figure 16 represents the analysis done with the ZnO material. As can be observed from the Figure 16, a weight loss in the range

of room temperature (20ºC) to 100ºC occurs, which is related to the dehydration of surface-adsorbed water.

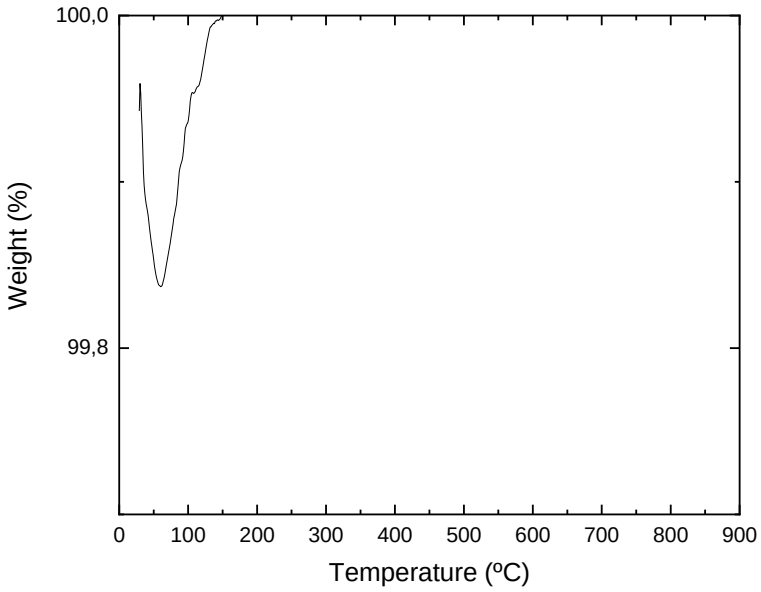

Figure 16. TGA of ZnO NPs.

For higher temperatures, no other significant mass loss was detected, indicating that the higher thermal stability of these materials when under nitrogen atmosphere. The mass gain must be associated to equipment error since the variation is insignificant and the mass gain exceeds the initial sample weight. Figure 17 represents the analysis to iron oxides material. As can be seen in the figure, for this material there is a insignificant weight loss in the same region previously identified for ZnO.

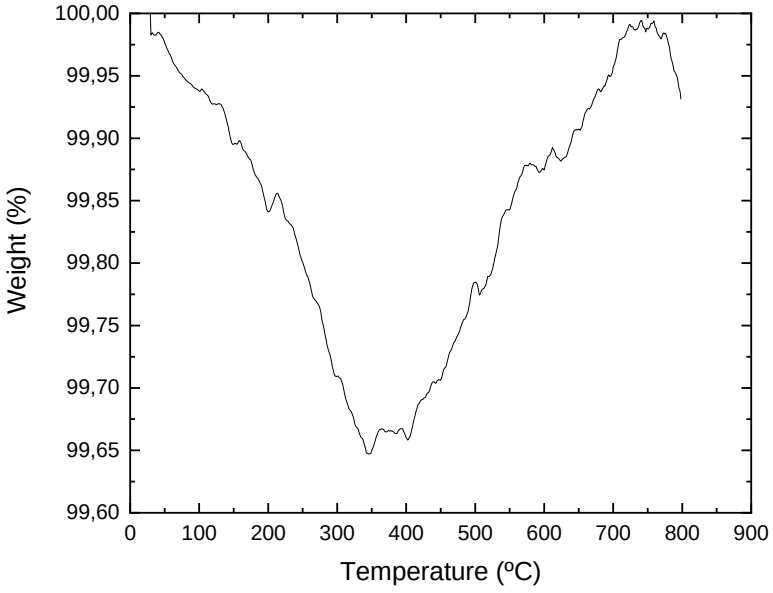

Figure 17. TGA of iron oxides NPs.

The loss of mass up to 100ºC is also related to dehydration of the material. Also, no other significant mass loss is noticed, indicating that the material is thermically stable and does not present any other residual component in its structure. The mass gain, beginning at 400 ºC until 700 ºC, suggests the oxidation of the iron phases existing in the sample. Also, the equipment must has presented an error when measuring the masses, since the mass variations are small.

4.2 Characterizations of the membranes

4.2.1 Porosity and water uptake

This type of analysis requires repeatability to calculate a mean value. It was therefore performed in duplicate, according to the described procedure in section 3.3.4. Table 9 shows the average values found for water absorption and porosity of the membranes produced in this study.

Table 9. Water Uptake and Porosity of the produced membranes.

Membrane		Water Uptake (%)	Porosity (%)
Name	Composition (wt%)		
M1	5% PVP	416.73 ± 40.43	51.33 ± 3.15
M2	10% PVP	401.44 ± 12.18	54.75 ± 1.87
M3	15% PVP	396.54 ± 125.65	64.03 ± 12.76
M4	5% PVP 0.5% ZnO	453.52 ± 51.21	55.43 ± 5.94
M5	5% PVP 1.5% ZnO	392.93 ± 9.15	51.68 ± 2.62
M6	15% PVP 0.5% ZnO	402.08 ± 25.90	63.54 ± 1.26
M7	15% PVP 1.5% ZnO	366.26 ± 0.14	51.55 ± 2.83
M8	10% PVP 1% ZnO	437.88 ± 4.86	55.39 ± 0.16
M9	5% PVP 0.5% iron oxides	413.71 ± 1.66	59.63 ± 0.57
M10	5% PVP 1.5% iron oxides	558.76 ± 25.56	73.79 ± 1.36
M11	15% PVP 0.5% iron oxides	411.45 ± 47.95	48.71 ± 0.55
M12	15% PVP 1.5% iron oxides	408.59 ± 22.72	60.33 ± 1.77
M13	10% PVP 1% iron oxides	432.28 ± 31.02	57.28 ± 1.06

Analysing the results expressed in Table 9, it can be noted that the comparison between the different membranes can be carried out by analysing the different groups. The first is the group of membranes with 5% of PVP in its polymeric matrix (M1, M4, M5, M9 and M10). The porosity increased up to the NPs content of 0.5 wt%. This can be observed for the two different materials studied, ZnO and iron oxides particles. Comparing the membranes incorporated with different materials, it was noted that iron oxides (M9) has a greater influence

in the membrane porosity (59.63%), comparatively with the membrane M4 incorporated with ZnO (55.43%), even the porosity between is close.

For the membranes with 1.5 wt% of embedded nanomaterial (M5 and M10) in their polymer matrix, showed different behaviours. For M5, which has ZnO incorporated, the porosity slightly higher (51.68%) when compared with M1 (51.33%) but decreased when compared with M4. For M10, which has iron oxides in its polymeric matrix, the porosity increased up to 73.79%. Comparing the performance of the materials, the iron oxides has a greater contribution to membrane porosity.

The second group is the one composed by membranes having 15% of PVP in the matrix (M3, M6, M7, M11 and M12). The porosity of the membranes decreased when compared to the membrane with no additive (M3) that has a porosity of 64%. For the membranes with 0.5% of embedded material, the porosity slightly decreased to 63.54% when ZnO was incorporated (M6) and to 48.71% when iron oxides was incorporated (M11). Among the materials, zinc oxide has a greater contribution to membrane porosity, comparatively with iron oxide.

Comparing the membranes with 1.5 wt% of embedded material, the porosity has also decreased, as described previously. The porosity of the membrane with ZnO (M7) decreased to 51.55%, while the membrane with iron oxides particles (M12) decreased to 60.33%. Between both incorporated materials, the performance of iron oxide was better, once it shows a greater contribution to porosity decrease, keeping the porosity near to the value of M3.

The third group is the one with an intermediate level of PVP and nanoparticles, where the membranes M2, M8, M13 contain 10 wt%. and 1% of PVP and particles, respectively. M2 does not contain any embedded material. In this group, both materials increased the porosity from 54.75% to 55.39% and 57.28% for membranes with ZnO and iron oxides, respectively. Considering the sample deviation, is observed that the values are close and do not allow an effective conclusion of the result.

To evaluate the best combination of polymer and nanoparticle the obtained data were analysed using conventional statistical methodologies program (Statistica 10.0) and the regression model represented by Equation 7 was obtained, when ZnO NPs were incorporated at the membranes and the Equation 8 represents the model obtained when iron oxides NPs were incorporated.

$$\varepsilon\ (\%) = 36{,}685 + 0{,}903x + 0{,}006x^2 + 12{,}730y - 0{,}824xy \qquad (7)$$

$$\varepsilon\ (\%) = 151{,}905 - 7{,}637x + 0{,}133x^2 + 19{,}250y - 0{,}2545xy \qquad (8)$$

Where x represents the amount of polymer (%) in the membrane and y the amount of nanomaterial (%) incorporated at the polymeric matrix. The coefficient of determination (R2) obtained for these models were 0.7857 for the ZnO and 0.9898 to the iron oxides, indicating that the model provides a good response estimate in the studied region so that 78,57% of the porosity to membranes with ZnO can be explained by this model and that 98.98% of the porosity to membranes with iron oxides.

From these models it is possible to estimate values for the porosity of membranes in the ranges of levels of the variables studied. According to these models, the response surface were constructed, as shown in Figures 18 and 19, in order to evaluate the conditions in which the highest percentage values of porosity of the membrane are obtained.

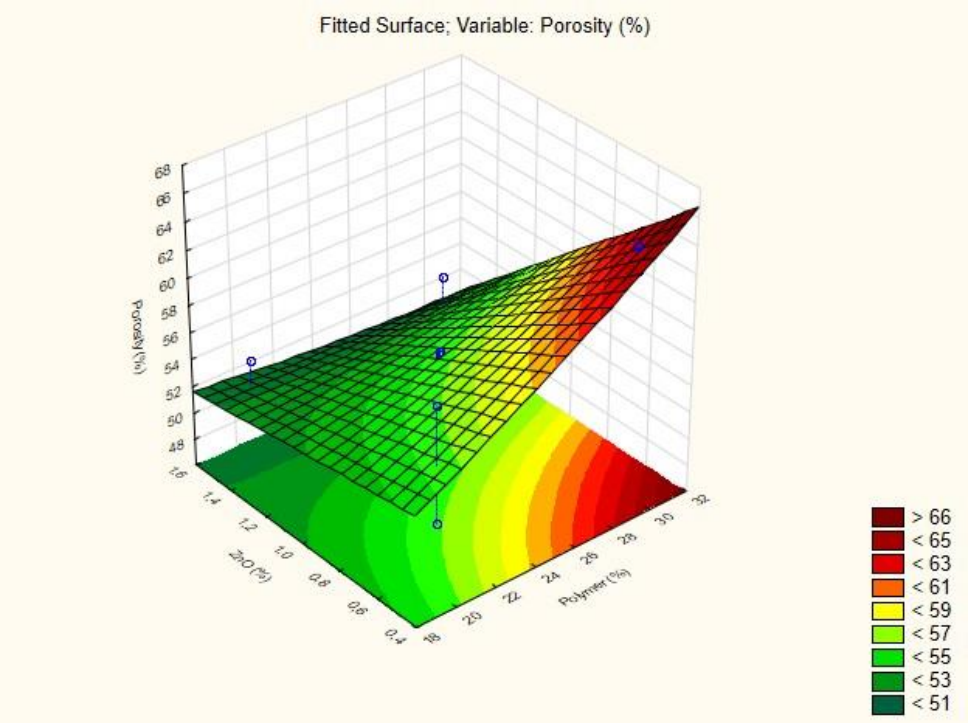

Figure 18. Porosity Response surface to ZnO NPs

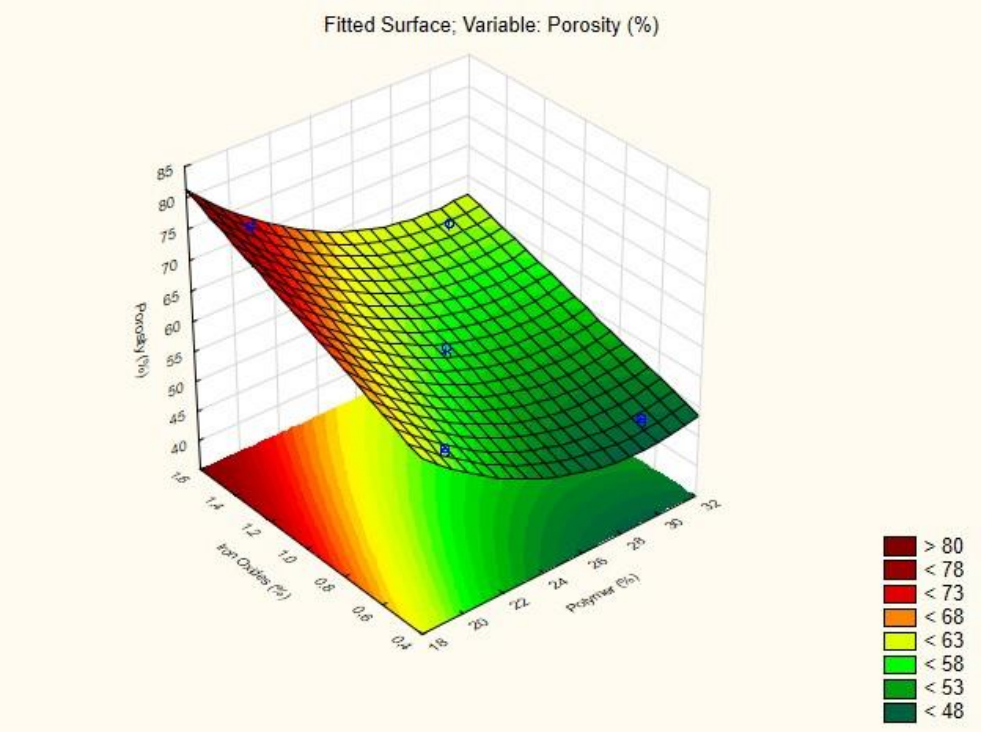

Figure 19. Porosity Response Surface to iron oxides NPs

Analysing the Figures 18 and 19, different behaviour can be seen for the nanoparticles used in this study. When ZnO was used as an additive for the production of the membrane, it was verified that a smaller amount of NPs with a greater amount of polymer used to form the polymer matrix, contributed positively to the porosity of the membrane. While for the iron oxide particles, this behaviour was opposite to that observed previously. That is, the greater the amount of polymer and material incorporated into the membrane, the greater its porosity.

The analysis of variance (ANOVA) for the results obtained is shown in Table X and X. The ANOVA test was performed to determine the significance of the quadratic model fit and the significant effects of the individual terms.

Table 10. ANOVA results to ZnO/PES membranes

Variables	Degrees of freedom	Medium Square	F_{calc}	p-value
X	31,8402	1	31,8402	3,07733
X^2	0,0410	1	0,0410	0,00396
Y	123,8738	1	123,8738	11,97232
XY	33,9488	1	33,9488	3,28113
Error	51,7334	5	10,3467	
Total	241,4372	9		

Table 11. ANOVA results to iron oxides/PES membranes

Variables	Degrees of freedom	Medium Square	F_{calc}	p-value
X	297,0703	1	297,0703	221,3754
X^2	17,8089	1	17,8089	13,2711
Y	332,1753	1	332,1753	247,5355
XY	3,2385	1	3,2385	2,4133
Error	6,7096	5	1,3419	
Total	657,0027	9		

According to the tables, only the term referring to the amount of zinc oxide squared is significant for the model, since the p-value found was lower than 5%. This indicates that the analysed parameters are not statistically significant for the test.

It is generally accepted as a common rule that the enhanced exchange rate between the water and the solvent can render the membranes more porous and vice versa [82]. The reasons for the porosity variation can be explained by two effects caused by the incorporation of metal oxide NPs, the hydrophilicity and viscosity effect. Also, due to the PVP content present in the membrane, which is a porogenous agent, meaning that the greater the quantity, the greater the porosity of the membrane. Hydrophilic NPs, such as ZnO and iron oxides, easily drawn the water into the membrane in the phase inversion process. This effect can increase the exchange rate between water and solvent [22].

The variations found for porosity can also be explained by errors in the preparation of the sample to be weighed since not all the water excess can have been removed during the test. The way the particles were dispersed in the solution during their preparation may also have contributed to such changes, since the dispersion could not be uniform within the whole membrane.

Shen et al [22] produced PES membranes with different amounts of ZnO NPs. In this study a range of 0 to 0.4g of material were incorporated in the polymeric matrix. The porosity of the hybrid membranes was improved by adding the NPs. The found porosity values were close to 80%, which was higher than the porosity obtained for the membranes produced with no additive (74%) in their study. Leo et al [21] also study the incorporation of ZnO NPs in PES membranes. This study showed that the porosities of PES/ZnO membranes were much higher than the PES membrane. The porosity showed a range varying from 75% to 77%, while the PES membrane showed 62% of porous in its structure.

4.2.2 Thermogravimetric Analysis (TGA)

To identify the thermal behaviour of the membranes the first part of this study was devoted to the thermal analysis of the used polymeric compounds. Figure 18 shows the thermograms for PES and PVP.

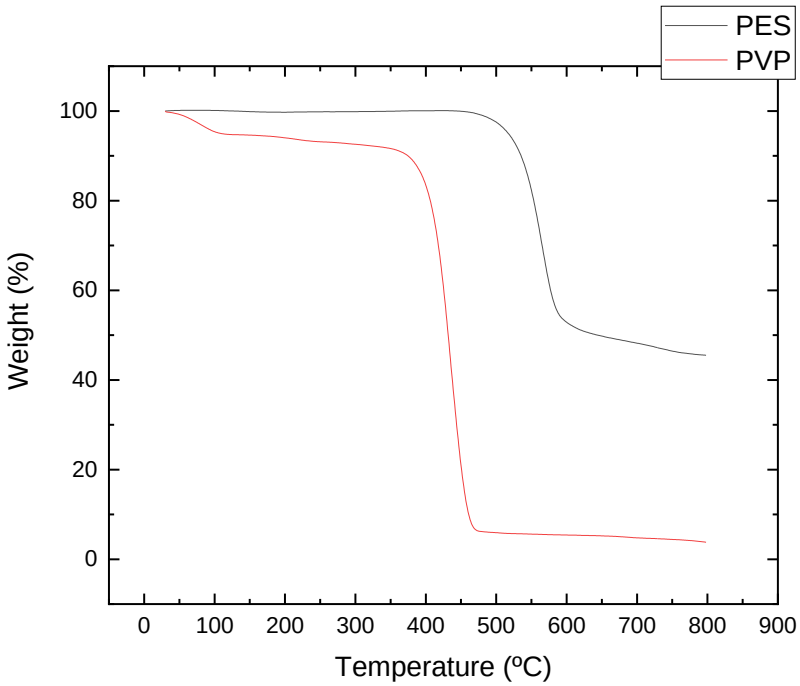

Figure 20.TGA curves of PES and PVP

The thermograms of both polymers consisted of two weight loss peaks between 30–100 °C and 400–730 °C for PES, while for PVP the degradation range was identified between 30–100 °C and 333–533 °C. For both polymers the first weight loss was related with the removal of the residual water present. The second weight loss is associated to the degradation of the polymeric backbone. Analysing the thermal behaviour of polymers, it is seen that PES has a greater thermal stability than PVP. That is confirmed by the temperature at which the thermal degradation begins and by the residual mass of each polymer at the end of the analysis. For PES, the degradation began at 446 ºC and the mass loss in this temperature range was 50.33%, while for PVP, its degradation began at 333 °C and mass loss was 86.33% of its weight.

After knowing the thermal behaviour of the polymers used for the preparation of the membranes, the thermal degradation of the different membranes produced in this study were analysed. Figure 19 represents the thermal behaviour of the first group of membranes, corresponding to the different formulations prepared, namely the ones with 5,10 and 15 wt%.

of PVP, and produced without additives. This study was done aiming at study if the amount of PVP improved the membrane characteristics.

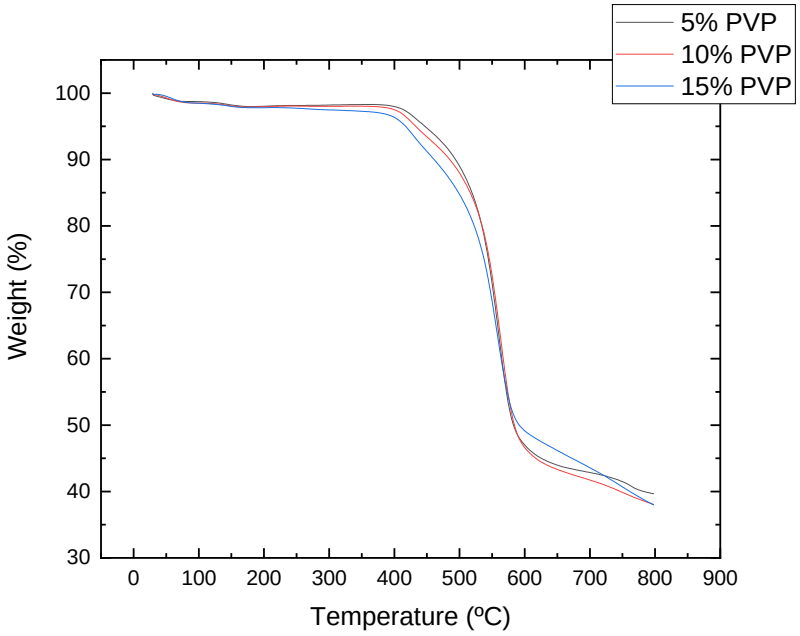

Figure 21. TGA curves of the membranes prepared without additive (M1, M2 and M3).

The thermograms of these membranes have four degradation stages, being these from 30–100 °C, 100–300 ºC, 300–400 °C and 400–730 °C. The first weight loss was due to the loss of residual water. The second is related with the removal of residual DMF, while the third range refers to the degradation of PVP. The degradation of PES occur between 508 and 620 °C.

The thermal study shows that the membranes with 5 (M1) and 10% (M2) of PVP in their composition had a similar behaviour, since until 400°C this membrane lost 2.02% of its initial weight while M2 lost 2.50%. The membrane with 15% of PVP in its composition has the lower thermal resistance among this set of samples. M3 lost 3.71% of its initial mass until 400°C. At the temperature of 800°C, the residual masses were 39.66%, 38.03% and 37.94% for M1, M2 and M3, respectively, being this related with the content of PES present in each formulation.

To study the effect of the NPs addition on the thermal properties of the membranes, these were also analysed by TGA. Figure 20 shows the thermal behaviour when the produced ZnO NPs were incorporated in the membranes with 5% of PVP.

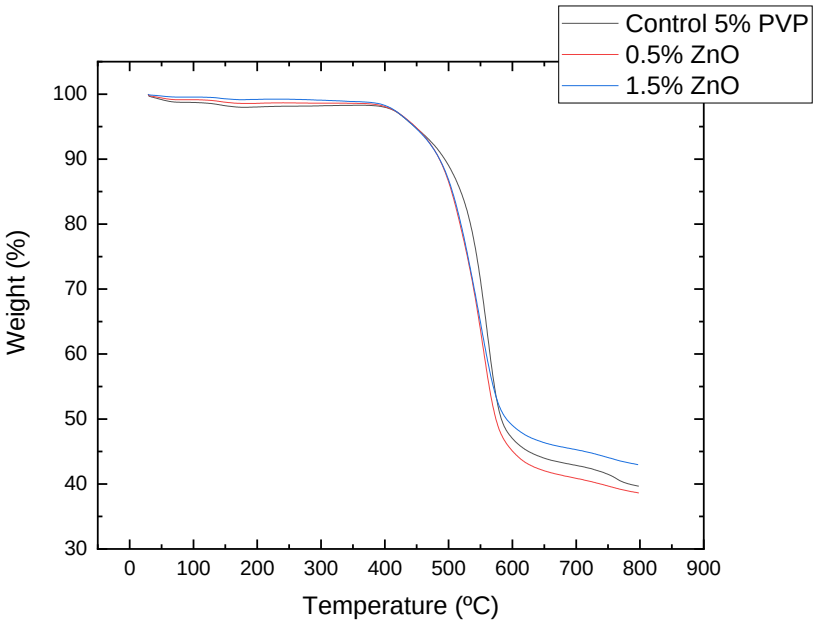

Figure 22. TGA curves of the membranes with 5% PVP with different amounts of ZnO NPs (M1, M4 and M5).

As seen observed for the membranes without additives in its composition, the TGA curves of these membranes present also four degradation stages located in the range 30–100 °C, 100–300 ºC, 300–400 °C, and 400–730 °C. However, the incorporation of ZnO nanoparticles changed the thermal resistance of the membrane. The membranes showed a mass loss of 1.92% and 1.73% until 400°C and a residual mass of 38.62% and 42.97%, for M4 and M5, respectively. The membrane with the larger amount of ZnO in its structure, have higher resistance than the others, since its mass had a smaller loss till 400°C being this also reflected on the residue obtained at the end of the analysis. On the other hand, M4 (0.5% of ZnO) has a similar behaviour to M1, but it was noticed a reduction of mass loss until 400 °C, since the membrane without additive lost 2.02% of its mass.

The thermal behaviour for the membranes with 5% of PVP and iron oxides NPs embedded in its polymeric matrix are shown in Figure 21.

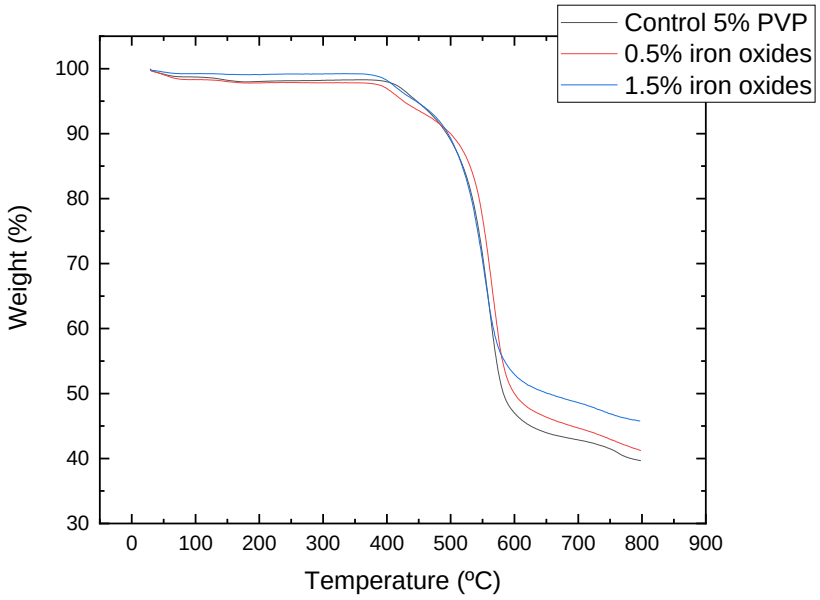

Figure 23. TGA curves of the membranes with 5% PVP with different amounts of iron oxides NPs (M1, M9 and M10).

Analysing the obtained TGA curves, the same behaviour previously observed for the decomposition of the membranes components was noticed. As observed in the Figure 21, the incorporation of iron oxides nanoparticles also changed the thermal degradation of the membranes. As seen for the membranes with 5% of PVP and ZnO, the membrane with the larger amount of iron oxides in its structure showed a lower weight loss than the others (M10 – mass loss until 400 °C of 1.80% and residual mass of 45.74%). On the other hand, M9 composition did not improved the membrane thermal resistance when compared with M1, which has no additive embedded. The mass loss of M9 until 400 °C was 3.14% of its initial mass, while the residual mass at the end of the analysis was 41.19%, due to the presence of the NPs.

Analysing the results obtained for the membrane with 5% of PVP, it can be concluded that the higher amount of embedded material, both ZnO and iron oxides, increases the thermal resistance of the membrane.

The NPs were also incorporated into the membranes with 15% of PVP. The TGA curves to this group of samples is represented in Figure 22.

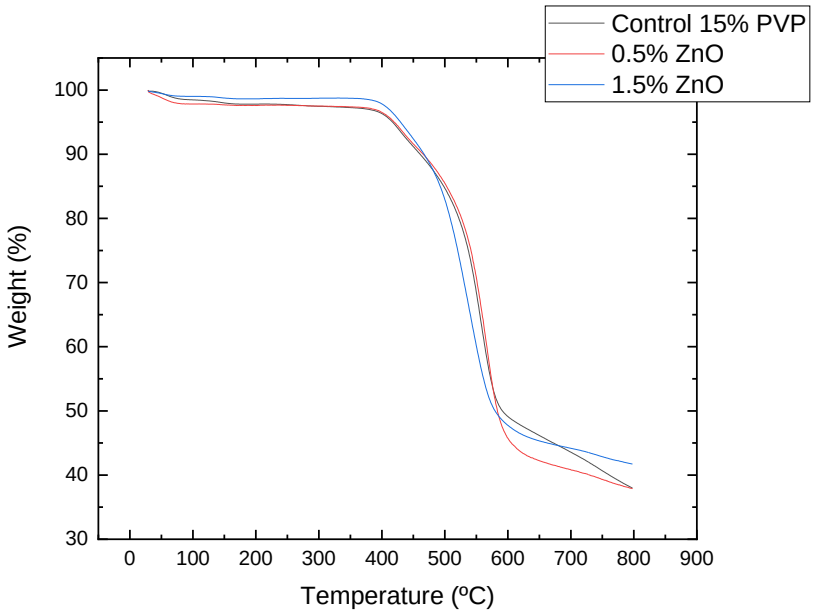

Figure 24. TGA curves of the membranes with 15% PVP with different amounts of ZnO NPs (M3, M6 and M7).

Analysing the obtained thermograms, a similar behaviour can be identified. The mass loss obtained until 400 °C for these samples was 3.53 and 2.14% for M6 and M7, respectively. The membranes also have a residual mass of 37.85% and 41.70%, respectively. The membranes with incorporated iron oxides were also studied for these conditions and the obtained thermograms are represented in the Figure 23.

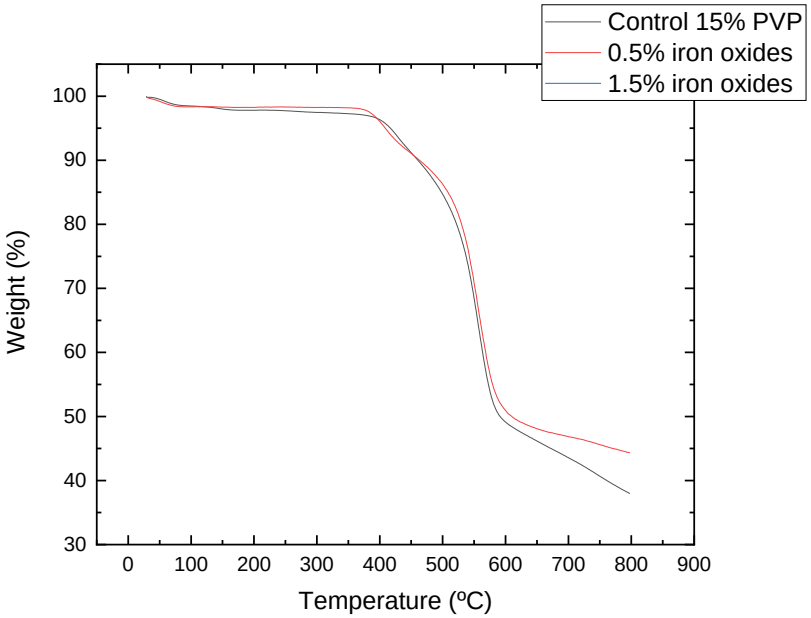

Figure 25. TGA curves of the membranes with 15% PVP with different amounts of iron oxides NPs (M3, M11 and M12).

The iron oxides NPs embedded in a membrane with a higher amount of PVP, showed a very similar behaviour to the membrane without any additive (M3). In Figure 23, is possible to notice that the NPs have a contribution to the thermal behaviour of the membranes. The higher amount added to the membrane lead to an increase of the thermal resistance, since the mass loss obtained until 400 °C was 3.91% and 2.14% for M11 and M12, respectively. The membranes also showed a residual mass of 44.31% and 42.40%, respectively.

Analysing the results obtained for the membrane with 15% of PVP in its structure, it can be concluded that the higher the amount of NPs is the higher is the thermal resistance of the membrane.

In the following, the thermal analysis of the membranes with intermediate amounts of NPs (0.10%) and PVP (10%) in its polymeric solution is discussed, being the thermograms of the samples shown in Figure 24.

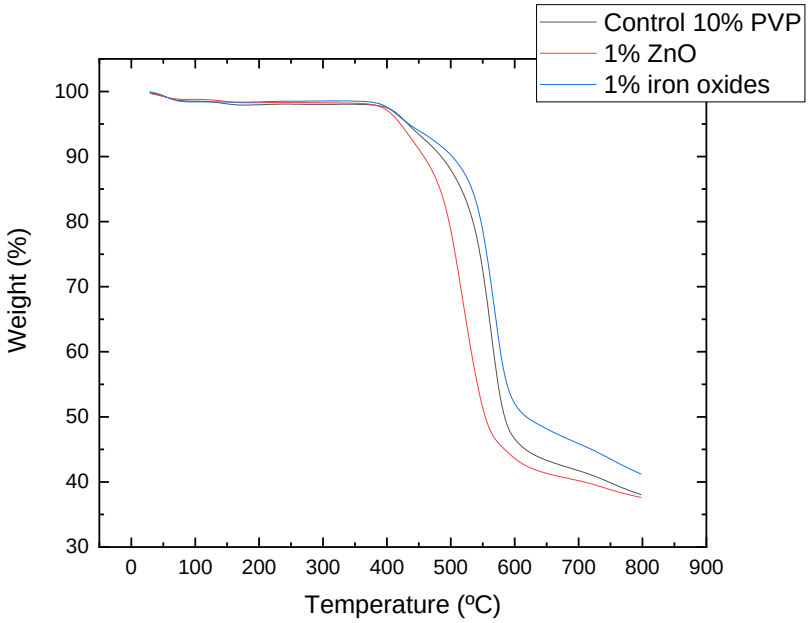

Figure 26. TGA curves of the membranes with 10% PVP and 1% of ZnO or iron oxides NPs (M2, M8 and M13).

Figure 24 allows the comparison between the different produced NPs where is possible to observe that iron oxides has a contribution higher than the ZnO to the membrane thermal stability. The ZnO membrane reveals has a higher thermal degradation comparatively with the membrane composed only by the base polymers, indicating that this combination is not suitable in terms of thermal resistance. The masses losses obtained until 400°C for these samples were 2.89 and 2.41% for M8 and M13, respecitvely. The membranes also showed a residual mass of 37.60% and 42.40%, respectively.

To better understand the effect of the different membrane compositions, the thermograms of the samples added with different ZnO contents are shown in Figure 25, while those with iron oxides are shown in Figure 26.

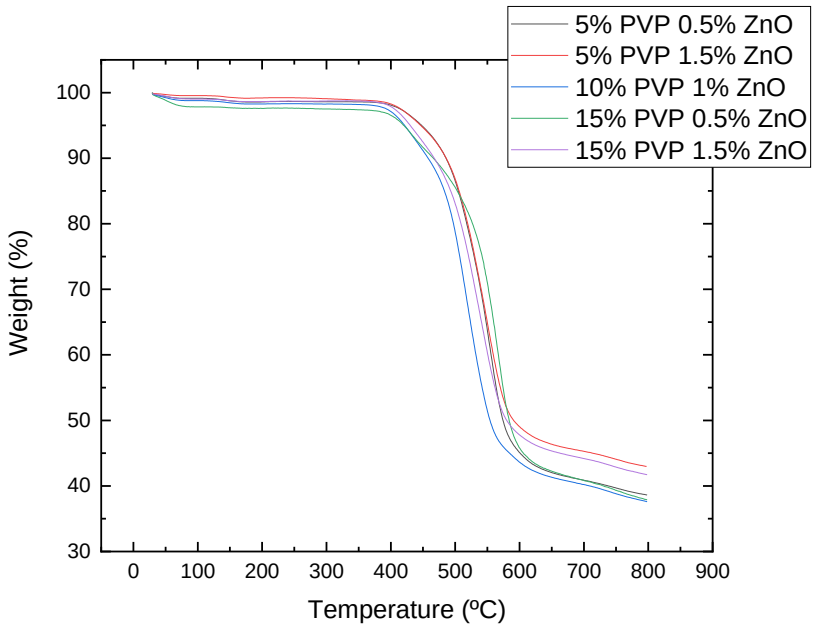

Figure 27. TGA curves of the membranes with ZnO.

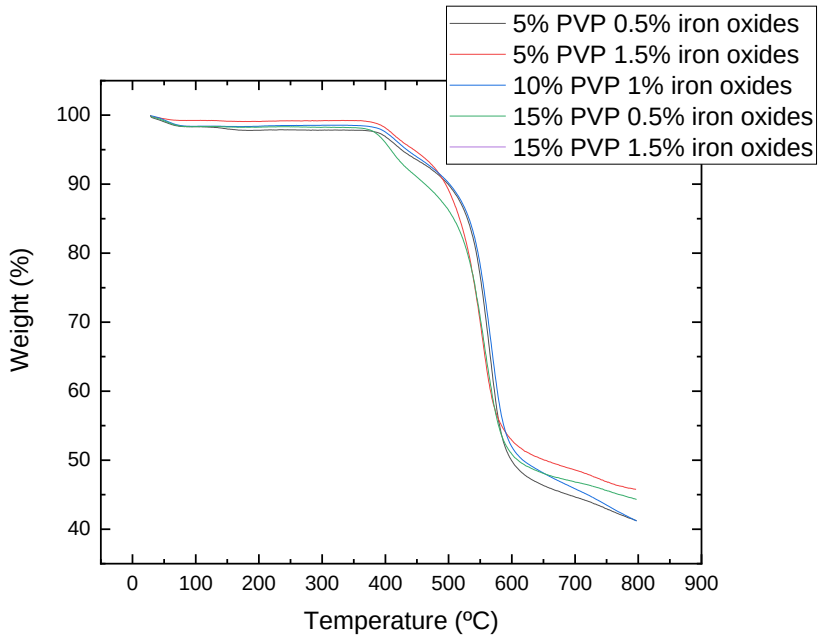

Figure 28. TGA curves of the membranes with iron oxides.

As was done to the porosity parameter in the previous section (4.2.1) to evaluate the best combination of polymer and nanoparticle the obtained data were analysed using conventional statistical methodologies program (Statistica 10.0). The regression model

represented by Equation 9 was obtained, when ZnO NPs were incorporated at the membranes and the Equation 10 represents the model obtained when iron oxides NPs were incorporated.

$$Residual\ Mass\ (\%) = 101{,}925 - 5{,}422x + {,}1074x^2 + 5{,}350y - 0{,}050xy \qquad (9)$$

$$Residual\ Mass\ (\%) = \ 50{,}455 - 1{,}385x + 0{,}0404x^2 + 17{,}470y - 0{,}646xy \qquad (10)$$

Where x represents the amount of polymer (%) in the membrane and y the amount of nanomaterial (%) incorporated at the polymeric matrix. From these model, the response surface were constructed, as shown in Figures 29 and 30, in order to evaluate the conditions in which the highest percentage values of residual mass of the membrane are obtained after the TGA study was done.

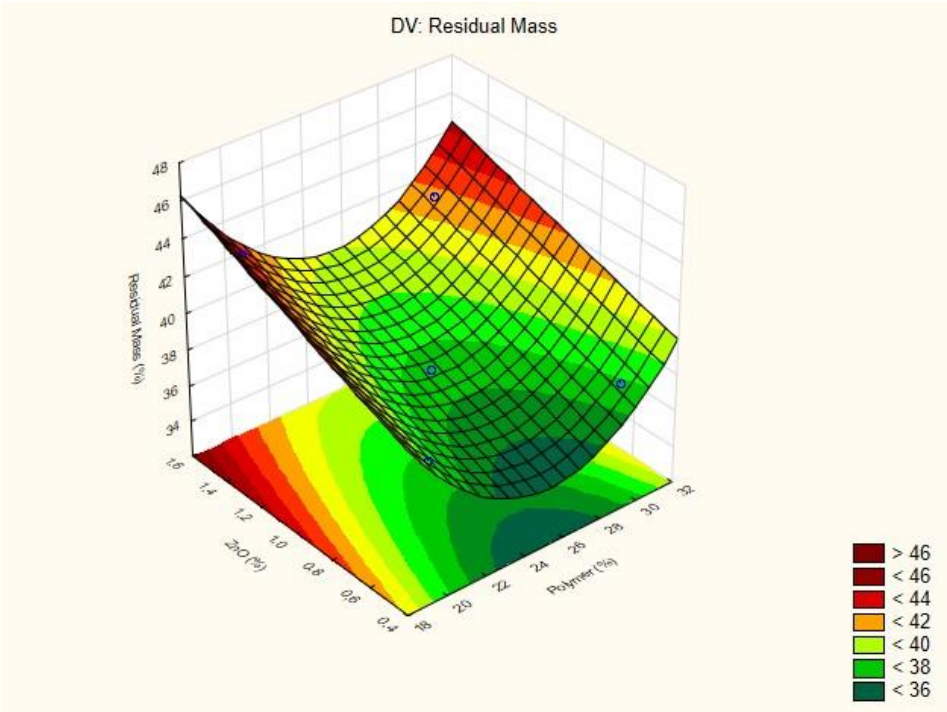

Figure 29. Residual Mass Response to ZnO

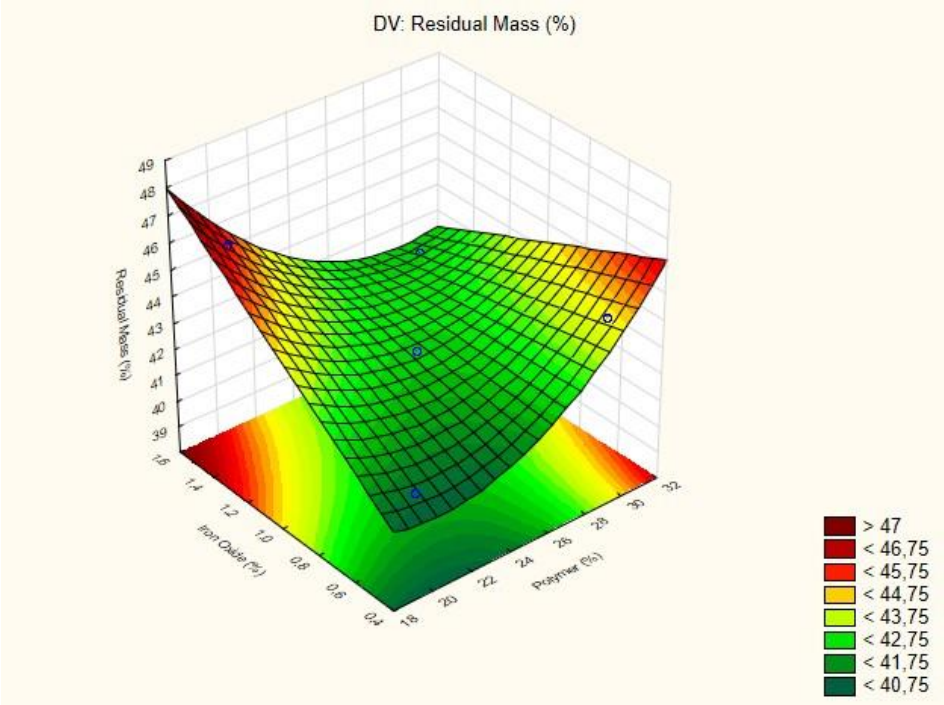

Figure 30. Residual Mass Response to Iron Oxides

Analysing the Figures 29 and 30, it is noticed a different behaviour in the membranes embedded with the different nanomaterial synthesized in this study. When ZnO was used as an additive in the production of membranes, a greater residual mass at the end of the TGA study was noticed, when a greater amount of nanoparticles was used to compose the casting solution of the membrane, that is, 1.5 wt% regardless of the amount of polymer used in the composition of the casting solution. This fact allows to conclude that 1.5 wt% of ZnO NPs combined in PES membranes, provides a better thermal stability to the membrane.

Membranes embedded with the produced iron oxides NPs, according to Figure 30, presented a higher residual mass after the TGA study was done, when 1.5 wt% of NPs is combined with 5% of PVP to compose the casting solution (M10). It was also verified that M13 showed a significant thermal stability once the residual mass was higher than the others membranes embedded with iron oxides, regardless M10.

Summarizing, the thermal degradation profiles presented shows that the better combination of PVP and NPs is when 5% of PVP and 1.5% of NPs are combined with PES to form the membrane matrix. Even if the performances are close to each other, as discussed before, it is possible to confirm that the incorporation of metal oxide nanoparticles into polymeric membranes improves their thermal behaviour.

The results are similar to other studies in the literature that also verified changes in the thermal stability of polymeric membranes after the incorporation of metallic oxide nanoparticles. Lakhotia et al. [78] verified that the introduction of the FeO nanoparticles improved the thermal stability of the membranes once the degradation temperature of the membrane increased. Shen et al. [22] have observed that the decomposition temperature (Td) increased continuously with increased weights of added nano-ZnO. At their study, when the weight of added nano-ZnO reaches to 0.4 g, the Td of the ZnO/PES hybrid membrane was improved by 94.4 °C relative to that of the PES membrane.

To this parameter was not possible to apply an ANOVA test in order to find out if the results are significant because the hydraulic permeability performance was performed once. So, the model can be used to preview the membrane behaviour with characteristic similar to those studied in this work.

4.2.3 Optical Microscopy (OP)

Figures 27 to 29 represent the displayed images obtained by the digital camera coupled to the apparatus system for the membranes without NPs, where it is possible to observe the membrane porous that were formed in the non-solvent bath phase of the synthesis.

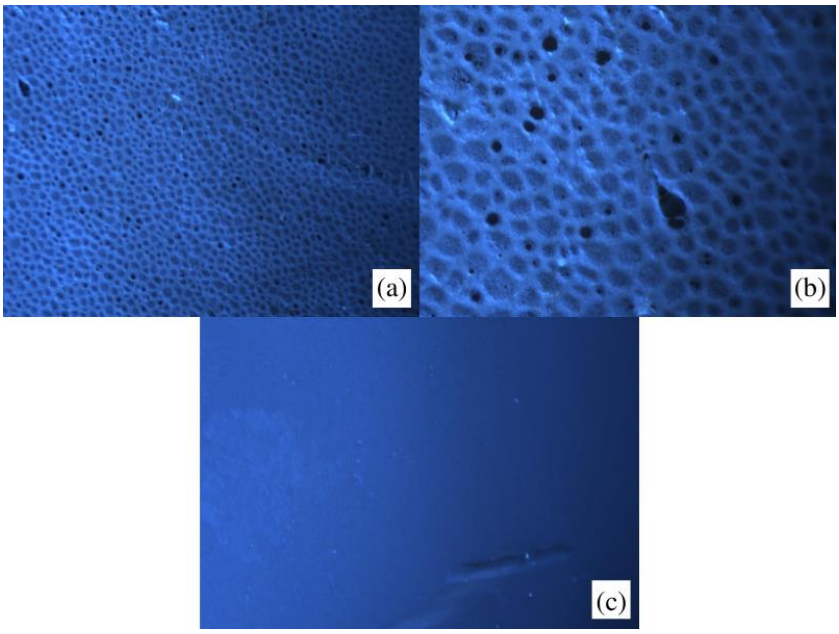

Figure 31. Image of M1 (5% PVP). The images refer to magnification of: (a) 40x membrane's front; (b) 100x membrane's front and (c) 40x membrane's back.

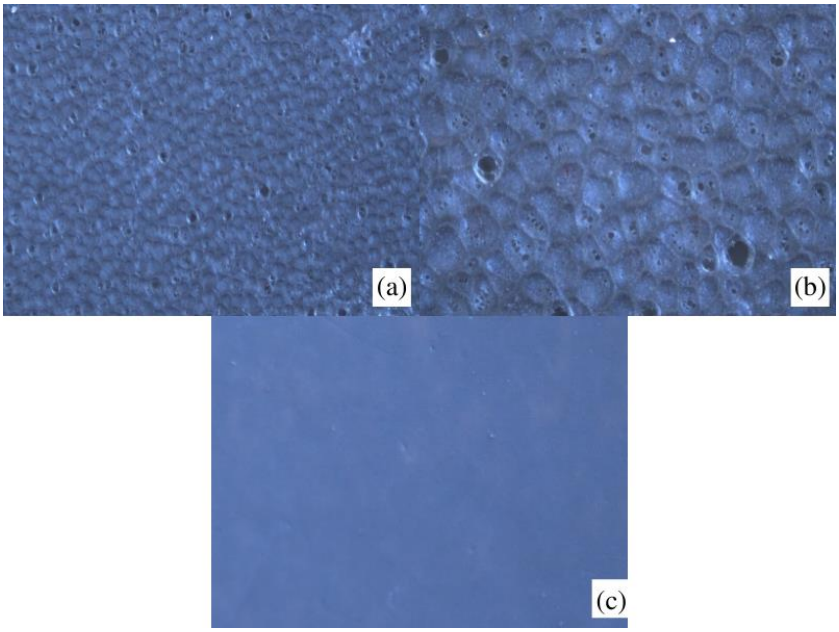

Figure 32. Image of M2 (10% PVP). The images refer to magnification of: (a) 40x membrane's front; (b) 100x membrane's front and (c) 40x membrane's back.

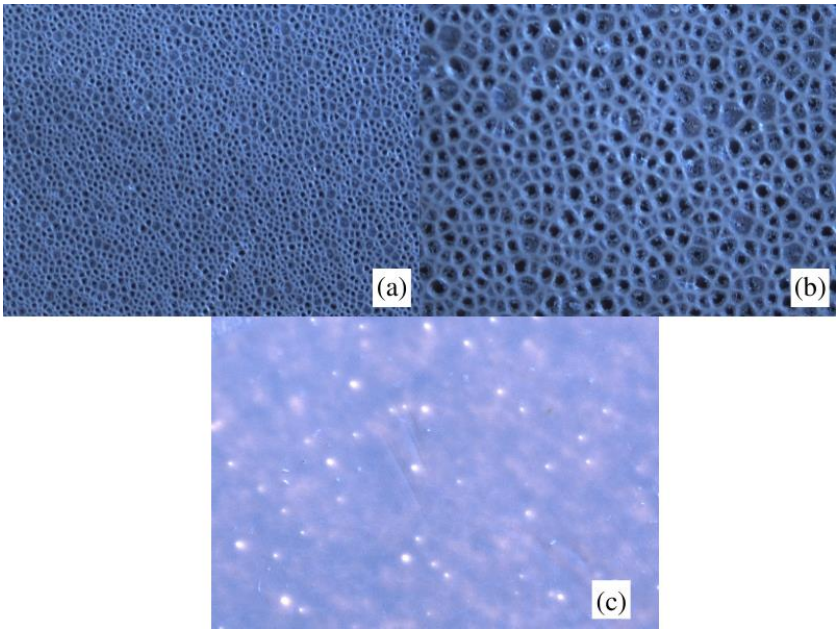

Figure 33. Image of M3 (15% PVP). The images refer to magnification of: (a) 40x membrane's front; (b) 100x membrane's front and (c) 40x membrane's back.

By analysing the images provided in Figures 27 to 29, it is possible to conclude that the membranes have a defined pore structure. M3 visually presents a greater number of pores, in addition to having a more uniform pore distribution. It is also possible to note that a higher amount of PVP in the polymer matrix generates a greater number of pores in the non-solvent bath phase. This fact is corroborated by the previous porosity analysis described in Water uptake and porosity section (4.2.1).

Figures 30 to 34 represent the images obtained by the digital camera coupled in the apparatus system for the membranes composed by different amounts of PVP and ZnO NPs in its polymeric matrix.

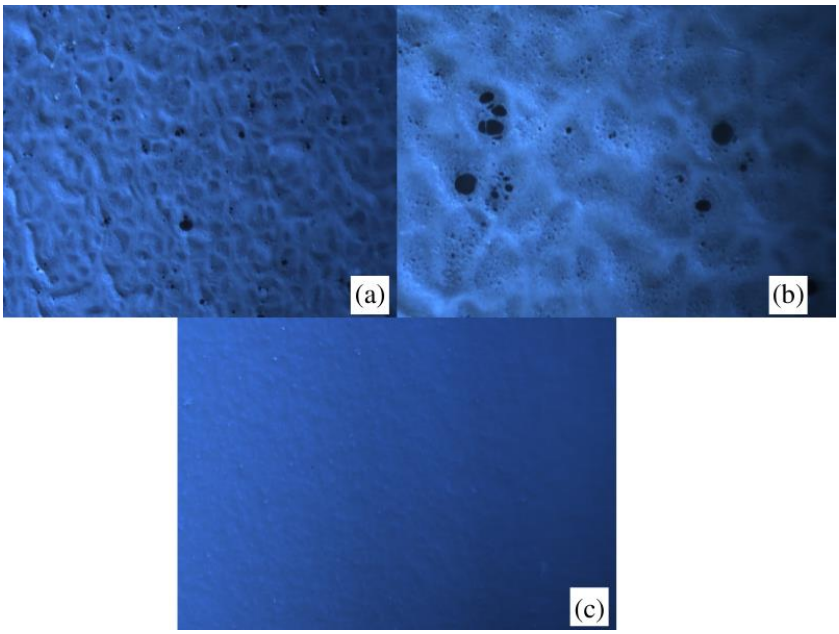

Figure 34. Image of M4 (5% PVP and 0.5% ZnO). The images refer to magnification of: (a) 40x membrane's front; (b) 100x membrane's front and (c) 40x membrane's back.

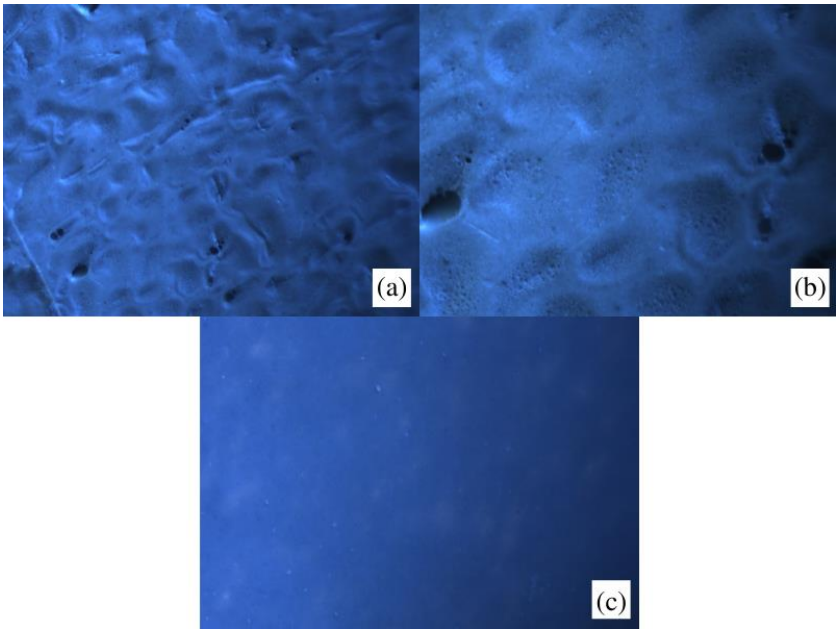

Figure 35. Image of M5 (5% PVP and 1.5% ZnO). The images refer to magnification of: (a) 40x membrane's front; (b) 100x membrane's front and (c) 40x membrane's back.

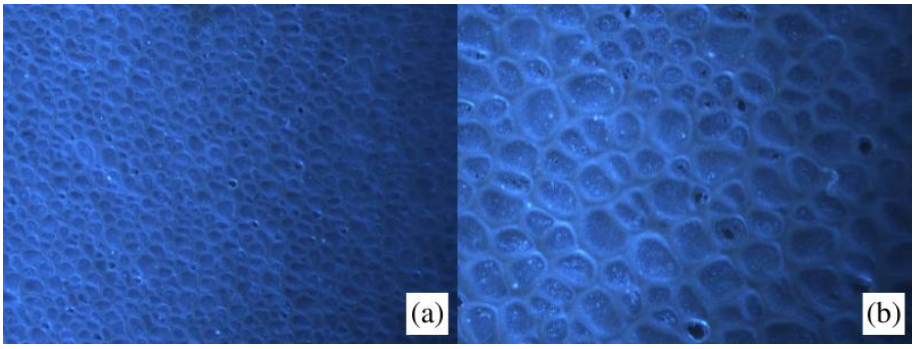

Figure 36. Image of M6 (15% PVP and 0.5% ZnO). The images refer to magnification of: (a) 40x membrane's front and (b) 100x membrane's front.

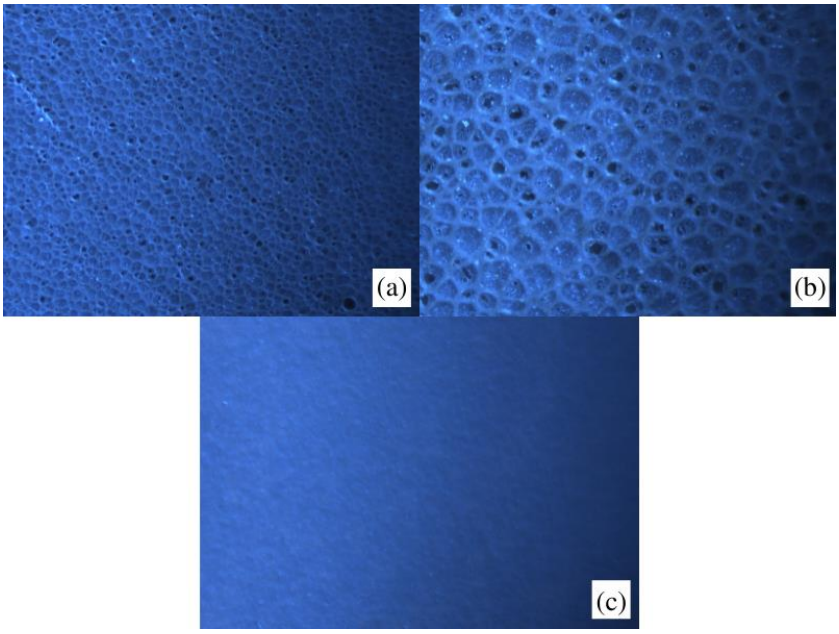

Figure 37. Image of M7 (15% PVP and 1.5% ZnO). The images refer to magnification of: (a) 40x membrane's front; (b) 100x membrane's front and (c) 40x membrane's back.

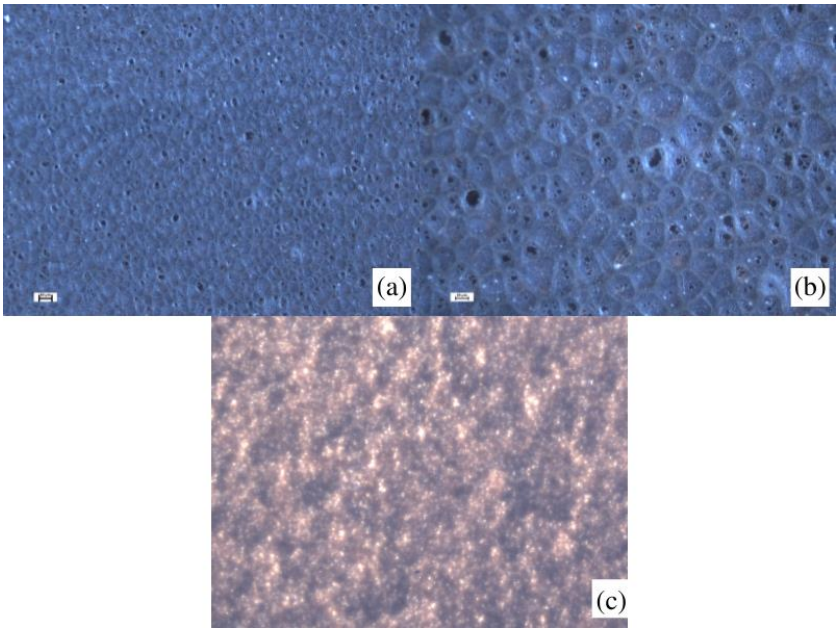

Figure 38. Image of M8 (10% PVP and 1% ZnO). The images refer to magnification of: (a) 40x membrane's front; (b) 100x membrane's front and (c) 40x membrane's back.

Comparing the membranes with and without ZnO NPs in the membrane structure, a difference in the dispersion and in the apparent size of the pores is noted. Even with this difference the water uptake and porosity analysis (4.2.1) indicated that the porosity was kept similar to the one of membranes with no addition of ZnO NPs. By the images inspection it is possible to observe that the pores sizes in the membranes with ZnO are larger than the one observed for the membranes without ZnO. The mean size for each membrane is shown in Table 12. The figures also indicate a difference in the pores structure of M5 when compared with the others, but still presenting pores as shown by the porosity analysis.

For the last sequence of pictures, the membranes with different amounts of PVP and iron oxides NPs in its polymeric matrix are represented (Figures 35 to 39).

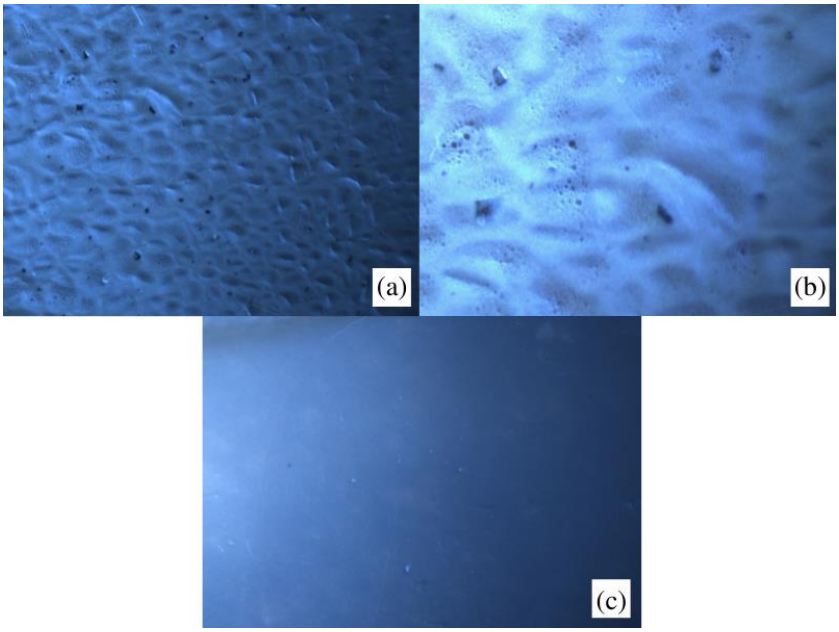

Figure 39. Image of M9 (5% PVP and 0.5% Iron oxides). The images refer to magnification of: (a) 40x membrane's front; (b) 100x membrane's front and (c) 40x membrane's back.

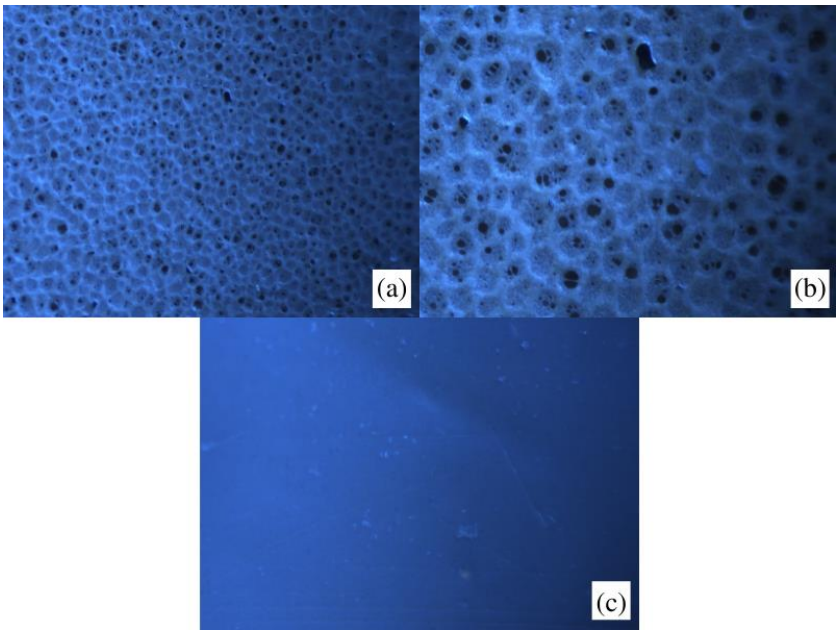

Figure 40. Image of M10 (5% PVP and 1.5% Iron oxides). The images refer to magnification of: (a) 40x membrane's front; (b) 100x membrane's front and (c) 40x membrane's back.

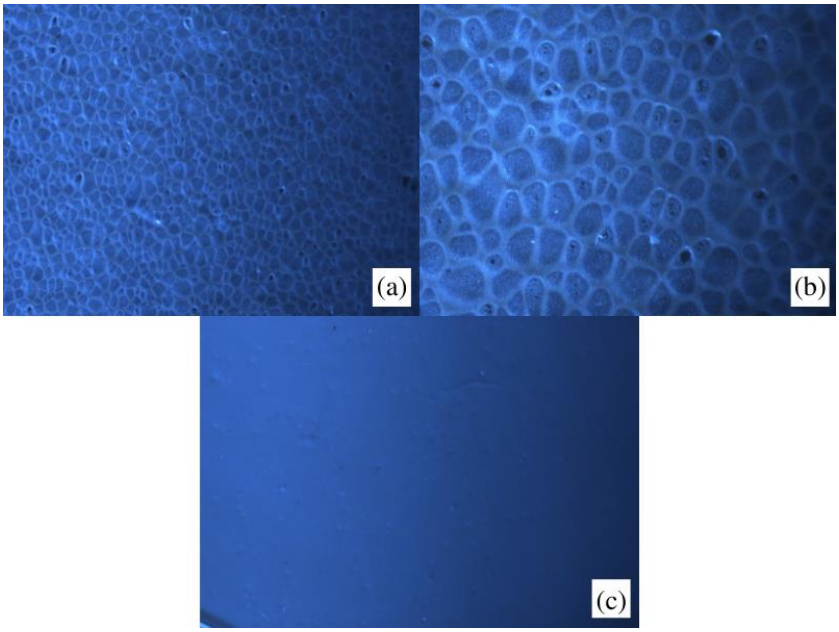

Figure 41. Image of M11 (15% PVP and 0.5% Iron oxides). The images refer to magnification of: (a) 40x membrane's front; (b) 100x membrane's front and (c) 40x membrane's back.

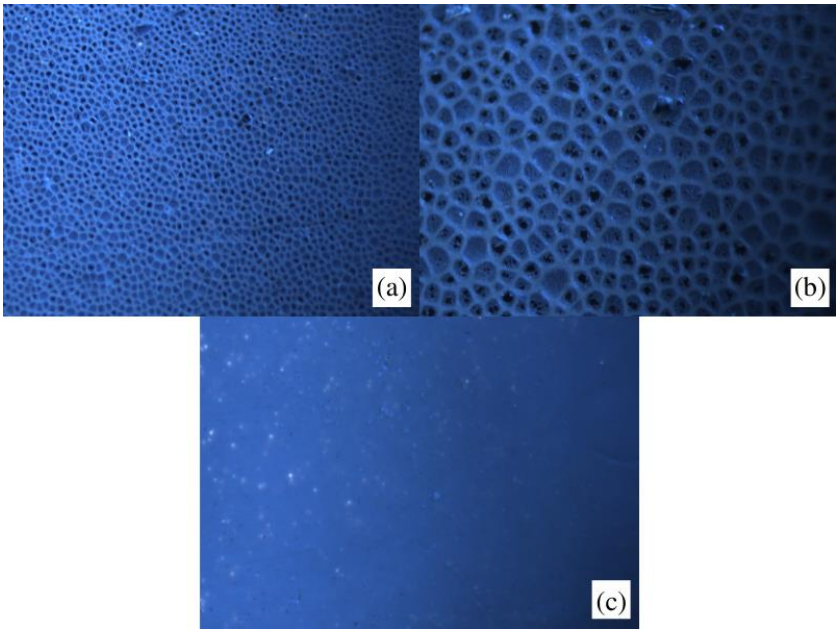

Figure 42. Image of M12 (15% PVP and 1.5% Iron oxides). The images refer to magnification of: (a) 40x membrane's front; (b) 100x membrane's front and (c) 40x membrane's back.

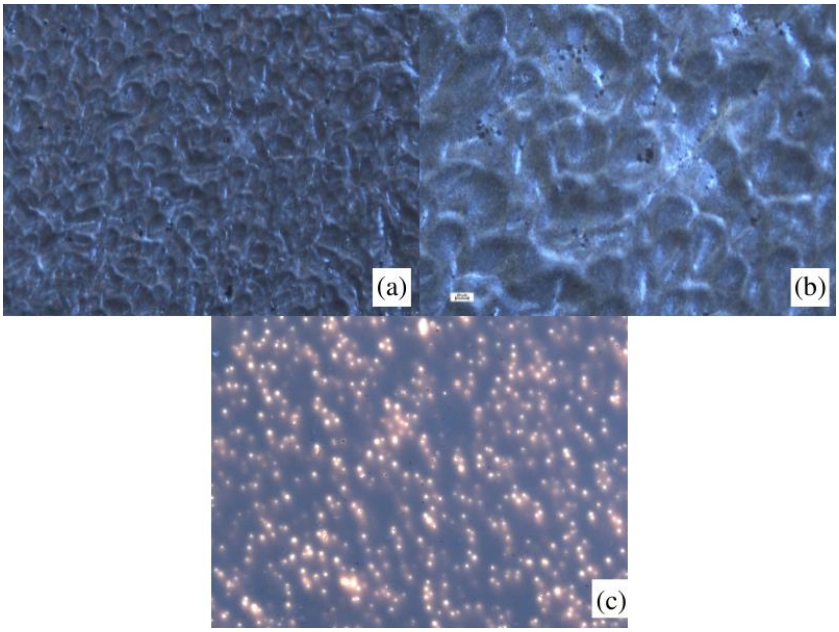

Figure 43. Image of M13 (10% PVP and 1% Iron oxides). The images refer to magnification of: (a) 40x membrane's front; (b) 100x membrane's front and (c) 40x membrane's back.

Comparing the Figures 35 to 39 from this group of membranes, it is noticed a difference in its structure. M10 and M12 visually presents a better distribution of pores as well a higher pore amount, indicating a larger porosity. M10 shows a larger amount of pores, which can be confirmed by the porosity analysis, since the porosity of this membrane increase to 73.79%.

This group of membranes presented a better distribution of pores than the group with ZnO NPs. There is a small difference in the porous structure of M9 when compared to other membranes in this group, which have also occurred for M5 in the previous group. Both showed differences when the membrane was synthesized with 5% PVP in its structure, but the amount of NPs was different.

Using optical microscopy, it was possible to analyse the structure of the prepared membranes on a larger scale. The displayed images of the membranes were monitored at magnifications of 40 and 100x. Based on these images it was possible to determine the average pore size. The results for this analysis are presented in Table 12.

Table 12. Mean pore size of produced membranes

Membrane	Composition (wt%..)	Length (µm)		
		Mean	Minimum	Maximum
M1	5% PVP	6.66 ± 6.64	1.58	37.5
M2	10% PVP	5.83 ± 4.67	0.93	20.6
M3	15% PVP	9.38 ± 6.61	1.6	22.44
M4	5% PVP 0.5% ZnO	12.07 ± 9.89	3.57	40.46
M5	5% PVP 1.5% ZnO	10.58 ± 12.84	2.94	70.17
M6	15% PVP 0.5% ZnO	8.77 ± 5.20	2.89	26.57
M7	15% PVP 1.5% ZnO	13.03 ± 6.10	3.33	23.2
M8	10% PVP 1% ZnO	6.95 ± 5.44	1.46	29.56
M9	5% PVP 0.5% iron oxides	2.81 ± 1.05	1.2	5.83
M10	5% PVP 1.5% iron oxides	13.25 ± 8.38	4.21	37.96
M11	15% PVP 0.5% iron oxide	8.65 ± 4.93	3.1	22.09
M12	15% PVP 1.5% iron oxides	13.67 ± 7.14	1.86	26.74
M13	10% PVP 1% iron oxides	7.46 ± 5.01	3.6	20.35

Analysing the results in Table 10 it is possible to compare the data of the three different groups, as previously done with porosity and water uptake analysis. The increase of membrane porosity is important to prevent the fouling, so the membrane performance is not changed by this phenomenon. The first group composed by membranes with 5% of PVP in the polymeric matrix (M1, M4, M5, M9 and M10) shows an increase in the mean pore size for M4, M5 and M10 when compared to M1. M9 presented a significant decrease. However, the result did not interfere with the porosity of the membrane, which increased when compared with M1, as already described.

In the second group, composed by membranes with 15% of PVP in the polymeric matrix (M3, M6, M7, M11 and M12), it is possible to notice that the membranes with a smaller amount of NPs, for both materials, didn’t show significant change in the mean pores size when compared with the membranes without NPs, while the membranes with higher amount of NPs embedded increased the mean pore sizes, indicating that an amount of 1.5 wt% is the best option to increase this parameter.

The third group (M2, M8 and M13), composed by membranes with 10% of PVP in its polymeric matrix, shows that for both materials the mean pore sizes were increased by the addition of NPs. Between the two studied NPs, iron oxides was the material presenting a greater contribution to increase this parameter.

Leo et al [21] verified that the addition of ZnO nanoparticles to the PSf membranes made the average pore size of membranes with incorporated material to be larger than the average pore size of the membrane without ZnO NPs incorporated. The average pore size of

the membranes synthesized in this study increased from 0.067 microm (when no NPs were used) to 0.080 and 0.105 microm when 3 and 4 w.t.% of ZnO NPs were incorporated, respectively.

4.2.4 Hydraulic Permeability

This type of analysis allows to study the behaviour of the membrane's filtration properties at room temperature (25°C) and at different pressure values. To analyse all membranes, groups were chosen to describe its behaviour, as done previously in the other analysis of this study. In all the following groups present figures which describe how the permeate flow (J_{perm}) of all membranes gradually decrease over time and how the mean permeate flow ($\overline{J_{perm}}$) varies with a pressure gradient.

The first group is the one corresponding to the membranes without in its polymeric matrix, which include M1, M2 and M3. Figure 40 shows the permeate flow (J_{perm}) behaviour of this group.

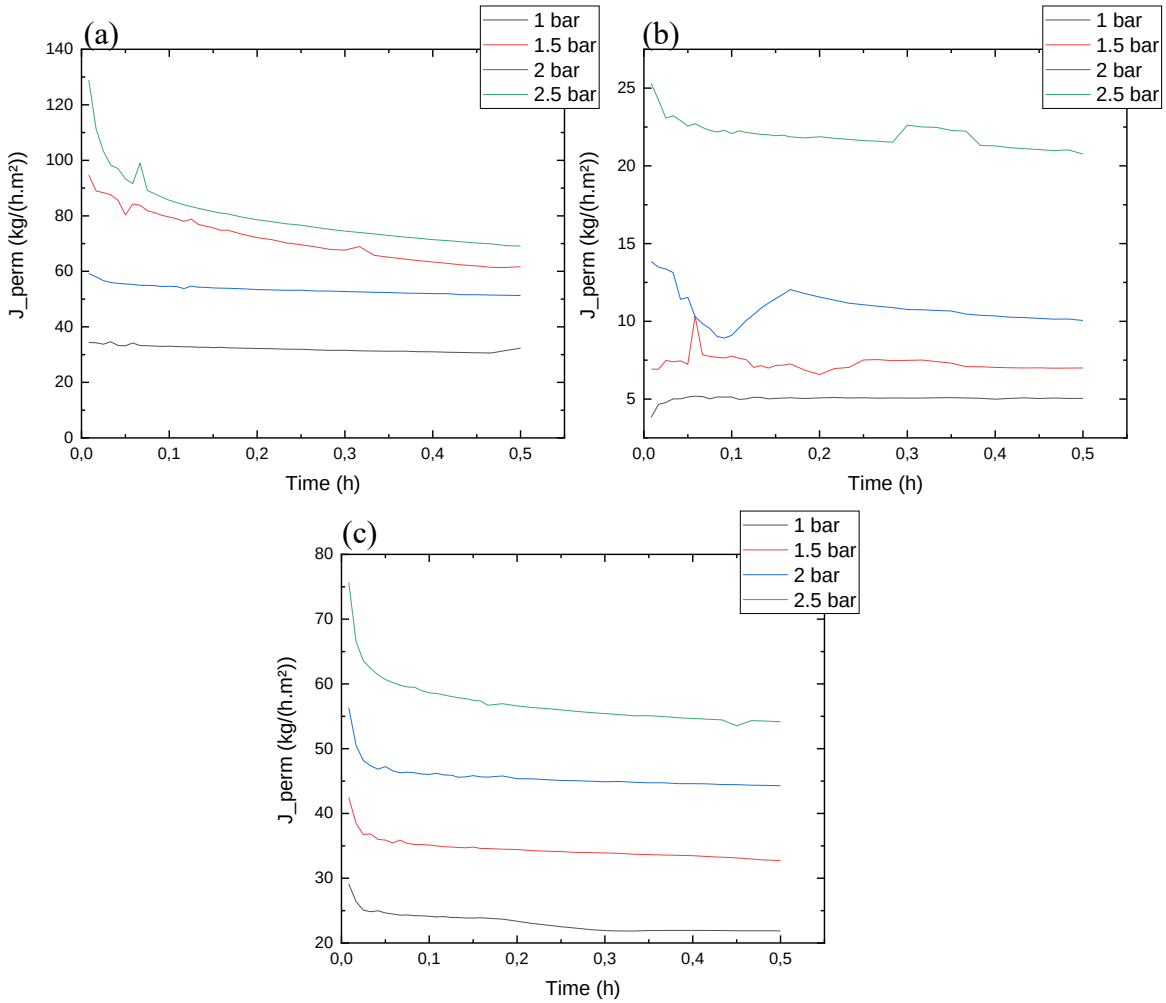

Figure 44. Permeate flux of membranes without NPs. Images refer to: (a) M1 (5% PVP); (b) M2 (10% PVP) and (c) M3 (15% PVP)

The results presented show that M1 became mechanically stable and compacted after 0.20 h when the gradient pressure applied was 1 and 2 bar. On the other hand, for the same membrane, when 1.5 and 2.5 bar was applied in the filtration process the membrane became mechanically stable and compacted after 0.35 h. M1 presented the greatest decline in permeate flow when the gradient pressure was 2.5 bar.

In membrane filtration processes that use a pressure as driving force, the permeate flow is directly proportional to the pressure gradient [20]. The stabilized permeate flux of each membrane was used to see how this parameter changes with the applied pressure during the membrane filtration process.

For this group of membranes without nanoparticles, a linear increase in the mean permeate flux was observed as the pressure increases, as seen in Figure 41. However, analysing the variation of this parameter, it is possible to see that each membrane presented a different behaviour since different values for the mean permeate flux were obtained. In Table 11, the values obtained for the hydraulic permeability of the membranes are represented.

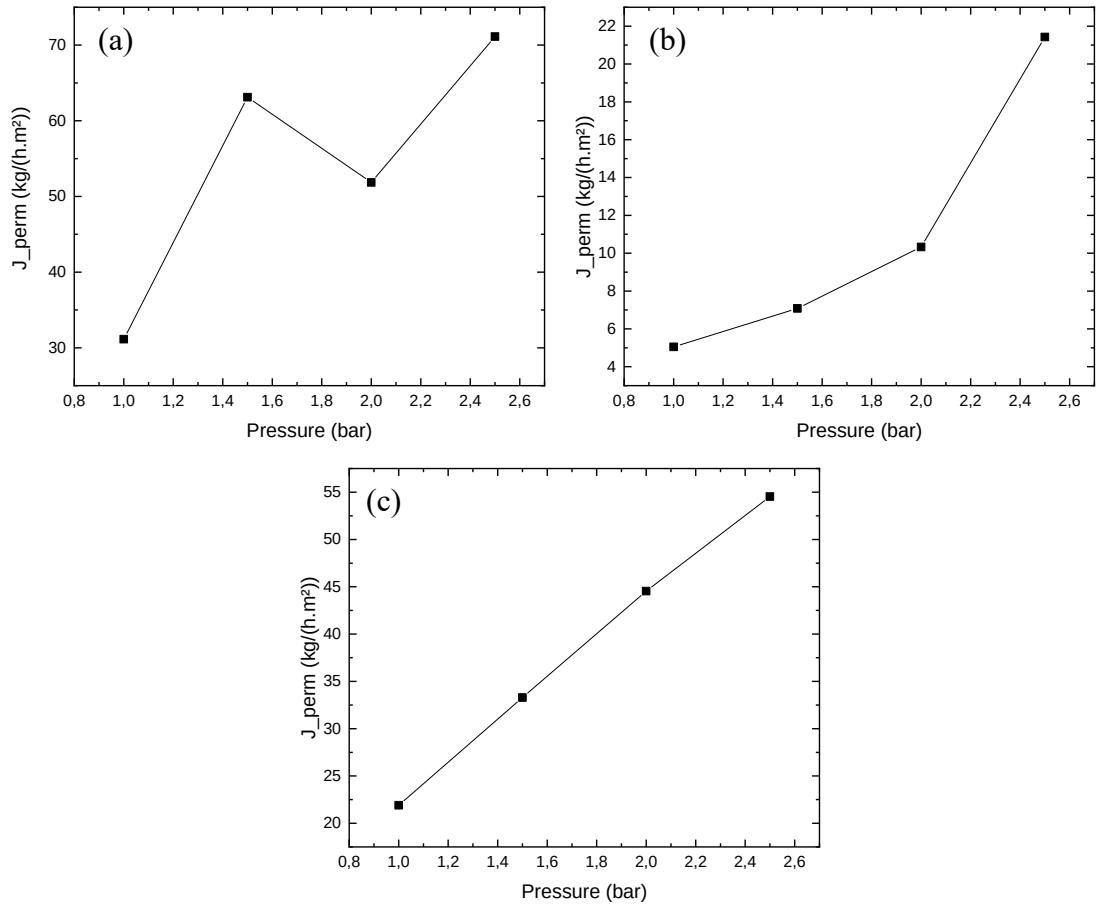

Figure 45. Mean permeate flux over the pressure variation in membranes without NPs. Images refer to (a) M1; (b) M2 and (c) M3

To study whether the addition of the particles produced changes in the filtration properties, the analysis of the added samples was also performed. Figure 42 shows the behaviour when ZnO NPs were incorporated into the membranes with 5 and 15% of, which corresponds to the second group of analysis.

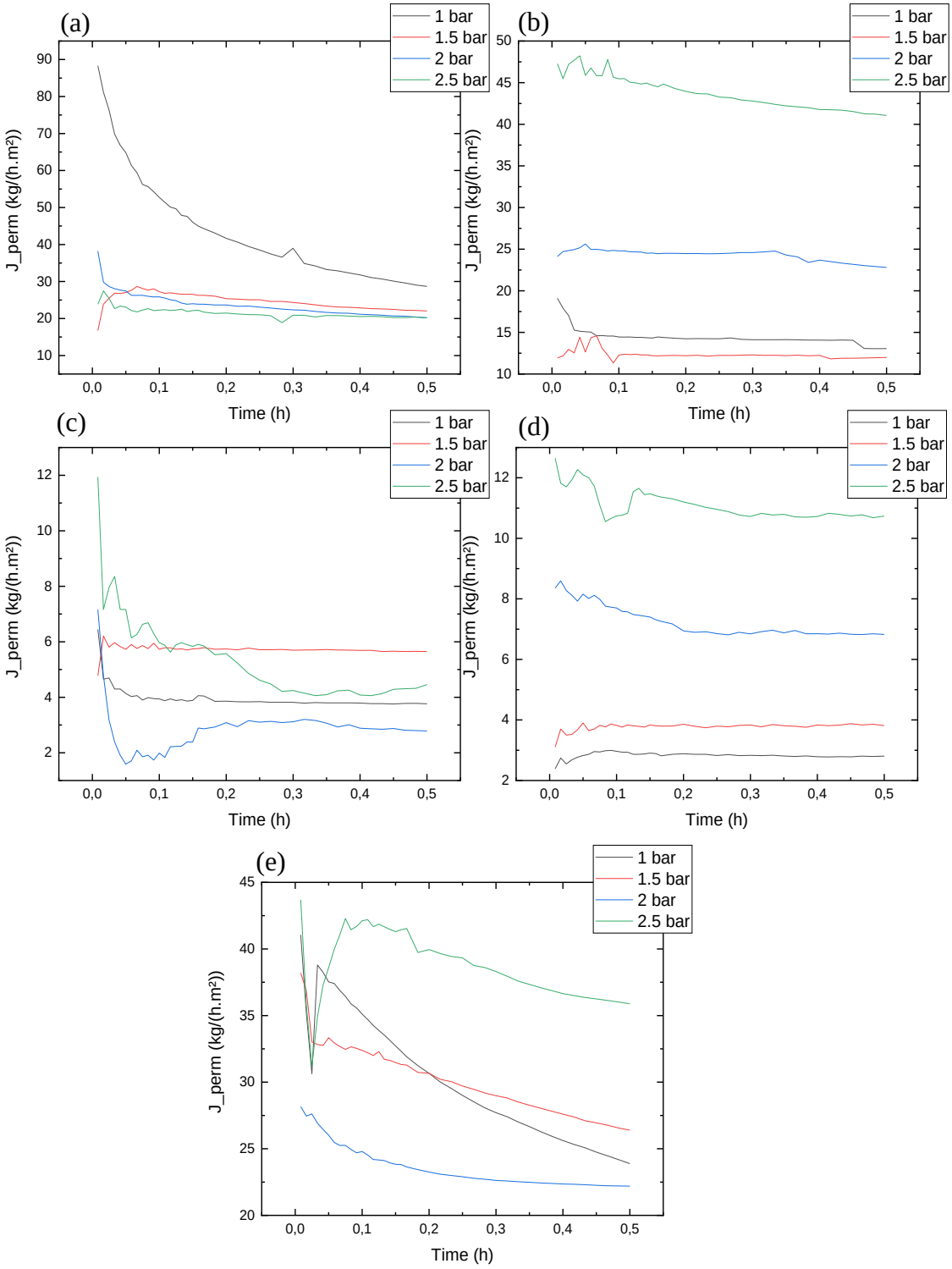

Figure 46. Permeate flux of membranes with ZnO NPs. Images refer to: (a) M4; (b) M5; (c) M6; (d) M7 and (e) M8

The obtained results show that M4 became mechanically stable and compacted after 0.35 h when the gradient pressure range for 1 to 2 bar, and after 0.45 h when a pressure of 2.5 bar was used, which also showed the greatest decline in the permeate flow. For M5, results show that the membrane became stable after 0.10 h in the range from 1 to 2 bar and after 0.40 h for 2.5 bar. The last studied pressure was also the one that lead to the greatest decline in J_{perm}. M6 presented a different behavior among the previous studied membranes. J_{perm} was practically constant for the pressure of 1.5 bar, while for the other pressures the membrane stabilized after 0.30 h. For M7 it was observed that, for the studied pressures of 1, 1.5 and 2 bar, a stability of the permeate flux was reached after 0.20 h and after to 0.30 h for the pressure of 2.5 bar were achieved.

For the last membrane of this group, M8, the stability was reached after 0.40 h when a pressure of 1,1.5 and 2.5 bar was applied in the permeate flux analysis. For the pressure of 2 bar, the J_{perm} became stable after 0.20 h.

For membranes with ZnO incorporated in their polymeric matrix, a linear increase in the mean permeate flux was observed as the pressure increased for all membranes from this group, as can be observed in Figure 43. Except for M4, which presented a decreasing trend, possibly due to the higher influence of the structural characteristics of the membranes, such as the porosity and the pore radius, which is related to the formation of macrovoids due to the applied pressure, which can change the size of the pores during the penetration of the distilled water [46].

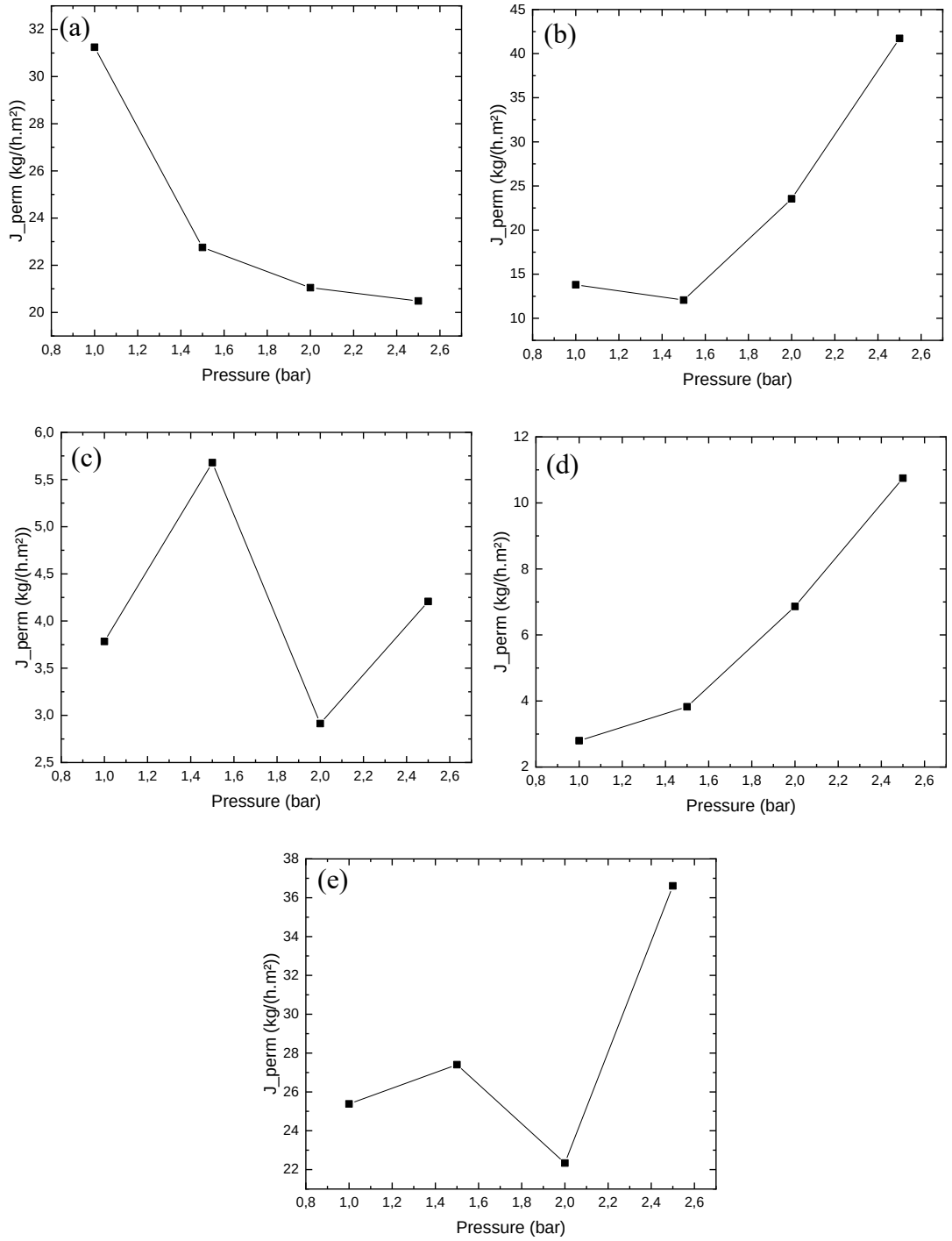

Figure 47. Mean permeate flux over the pressure variation of membranes with ZnO NPs. Images refer to: (a) M4; (b)M5; (c)M6; (d) M7 and (e) M8

When the range of obtained mean permeate flux of this group of membranes is compared with the membranes without NPs, a lower variation of this parameter was reached, except for M8 which presented the higher interval for the mean permeate flux.

Once the effect of ZnO nanoparticles on membrane filtration characteristics has been described, the effect of the second material of interest, iron oxides nanoparticles, was analysed.

Figure 44 shows the behaviour for this last group of membranes, which was produced with incorporation of iron oxides with different amounts of PVP.

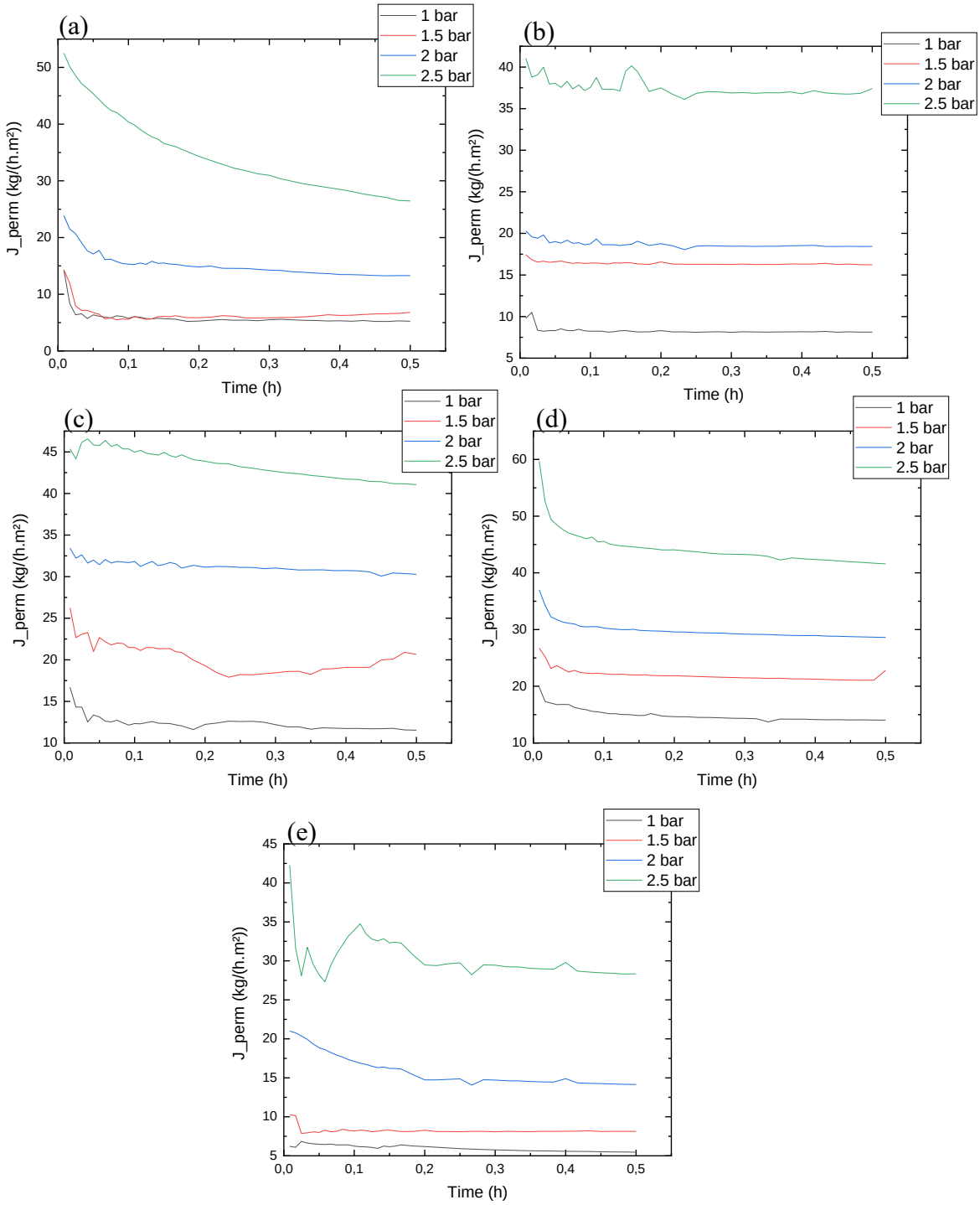

Figure 48. Permeate flux of membranes with iron oxides NPs. Images refer to: (a) M9; (b) M10; (c) M11; (d) M12 and (e) M13

The results show the stability and compactness of M9 after 0.30 h when the applied pressure was 1, 1.5 and 2 bar. For a pressure of 2 bar, no complete stabilization was observed, only a decrease in the drop of the permeate flow after 0.35 h was perceived. On the other hand,

M10, which has the same percentage of PVP, but a higher amount of iron oxides NPs (1.5 wt%), was compacted becaming mechanically stable for all tested pressures after a period of 0.30 h.

Membranes M11 and M12, which present 15 wt% of PVP in its composition have its permeate flux stabilized, meaning that the membrane compacted after a period of 0.30 h for both amounts of tested iron oxides NPs.

For the membrane with an intermedium value of the components, M13, the permeate flux remained practically constant for the studied pressures of 1 and 1.5 bar, since had only a small variation from the beginning of the experiment. The compaction occurred after 0.20 h for both pressures. For a pressure of 2 bar, the permeate flux was stable after 0.20 h and did not show a very sharp drop, as noted in Figure 44**.** When the membrane was subjected to 2.5 bar, it presented oscillations in the permeate flux, until stabilization after 0.3 h.

For membranes with iron oxides incorporated in their polymeric matrix, a linear increase in the mean permeate flux was observed as the pressure increases for all membranes from this group, as can be seen in Figure 45**.** The performance of membranes with 10 and 15% of PVP in their structure is highlighted. Analyzing the range of mean permeate flux, it is observed that M11, M12 and M13 performed better than M2 and M3 samples.

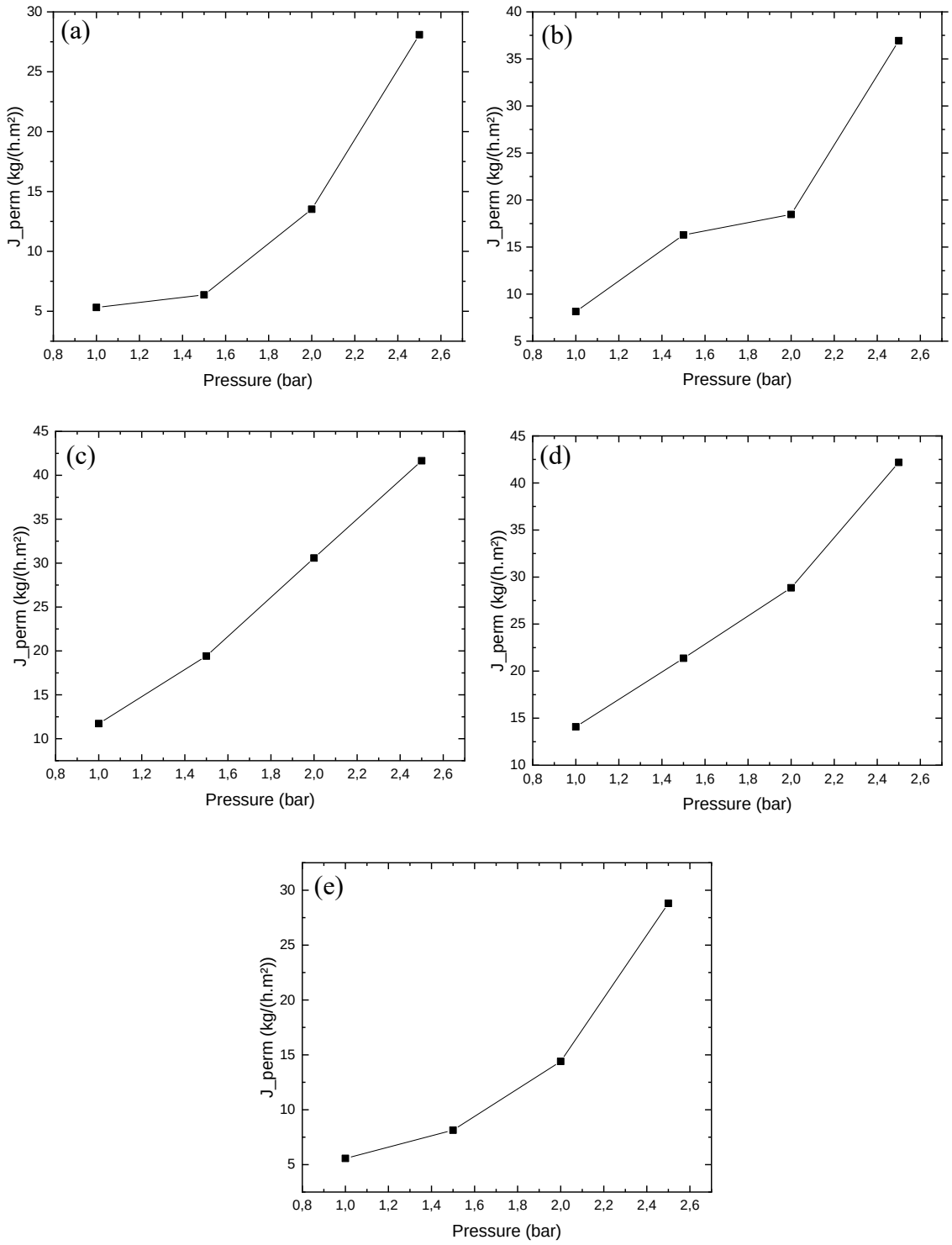

Figure 49. Mean permeate flux over the pressure variation to membranes with iron oxides NPs. Figures refer to (a) M9; (b)M10; (c)M11; (d) M12 and (e) M13

The hydraulic permeability represents how much the permeate flux will vary with the increase or decrease of the pressure applied to the membrane flux, due to its compaction during the process, which is needed to apply to the membrane. In Table 11 it is possible to observe the hydraulic permeation of each studied membrane.

Table 13. Hydraulic Permeability of all membranes

Membrane	L_p (kg.h^{-1}.m^{-2}.bar)
M1	30.17
M2	6.66
M3	22.02
M4	11.75
M5	13.58
M6	2.12
M7	3.64
M8	15.01
M9	8.31
M10	11.99
M11	15.27
M12	15.51
M13	8.78

For this study, it was noted that the higher is the permeate flux value is, the higher is the hydraulic permeability of the membrane is, and that the incorporation of the synthesized nanoparticles have contributed to reduce the hydraulic permeability of membranes when compared to the membranes without nanoparticles in its polymeric matrix.

To evaluate the behaviour of hydraulic permeability as the polymer and nanoparticle change the obtained data were analysed using conventional statistical methodologies program (Statistica 10.0) and the regression model represented by Equation 11 was obtained, when ZnO NPs were incorporated at the membranes and the Equation 12 represents the model obtained when iron oxides NPs were incorporated.

$$L_p = -143{,}915 + 13{,}527x - 0{,}289x^2 + 2{,}450y - 0{,}031xy \quad (11)$$

$$L_p = 84{,}870 - 7{,}112x + 0{,}159x^2 + 10{,}560y - 0{,}344xy \quad (12)$$

Where x represents the amount of polymer (%) in the membrane and y the amount of nanomaterial (%) incorporated at the polymeric matrix. From these model, the response surface were constructed, as shown in Figures 50 and 51.

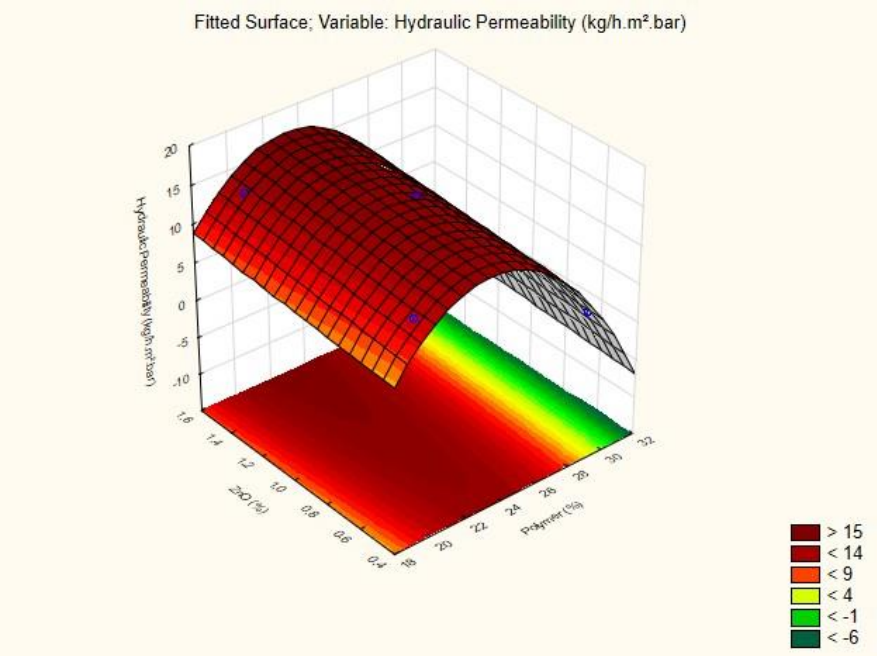

Figure 50. Hydraulic Permeability Response Surface to ZnO

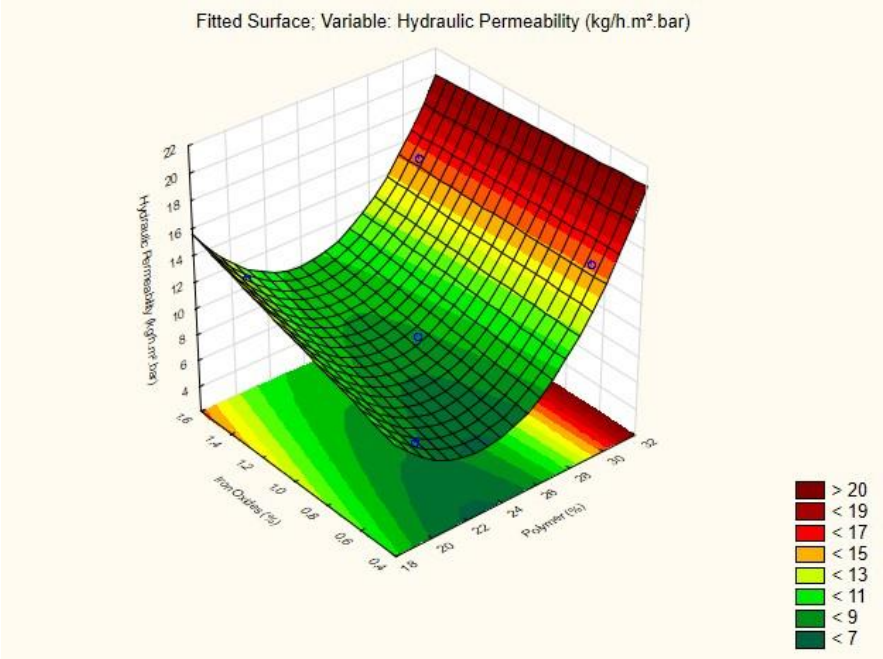

Figure 51. Hydraulic Permeability Response Surface to iron oxides

For membranes that had ZnO incorporated into their polymer matrix, a negative effect of hydraulic permeability was noted with the increase in the amount of polymer, as well as nanoparticles. The model indicates that the range that has the best performance to the analysed parameter is when a smaller amount of polymer was used to compose the membrane casting solution.

For membranes incorporated with iron oxide, the effect of increasing the amount of polymer and the amount of incorporated material was positive for hydraulic permeability. The model indicates that the greater the amount of polymer combined with a greater amount of iron oxides, the greater the permeability of the membrane, which represents the highest level of the experimental planning proposed in this study. To this parameter was not possible to apply an ANOVA test in order to find out if the results are significant because the hydraulic permeability performance was performed once. So, the model can be used to preview the membrane behaviour with characteristic similar to those studied in this work.

Knowing how much the permeate flux of each membrane was reduced is also important, as well knowing the hydraulic permeability. This analysis allows examine the performance of the membrane permeability without looking at the range of the permeate flux. The reduction of this important parameter is represented in Table 12. The percentage reduction in permeate flux was calculated based on the difference between the value obtained at the beginning and end of the experiment.

Table 14. Permeate flux reduction (%)

Membrane	Pressure (bar)			
	1,00	1,50	2,00	2,50
M1	5,94%	34,92%	13,38%	46,41%
M2	1,78%	6,44%	27,36%	17,96%
M3	24,93%	22,98%	21,41%	28,43%
M4	67,52%	7,67%	47,08%	15,33%
M5	31,63%	1,54%	5,43%	13,15%
M6	41,60%	8,97%	61,11%	62,67%
M7	0,70%	2,14%	18,33%	15,16%
M8	41,84%	30,90%	21,23%	17,86%
M9	63,33%	52,50%	44,33%	49,62%
M10	16,95%	6,92%	9,14%	8,89%
M11	30,95%	21,36%	9,40%	9,47%
M12	29,22%	14,69%	22,67%	30,30%
M13	11,99%	20,78%	32,67%	32,94%

The decrease of the permeate flux over time can be justified by the pores becoming denser and closer as the distilled water passes through the membranes due to mechanical instability of the membrane as a function of the applied pressure, even if the distilled water has a low concentration of impurities. In addition, a small physical-chemical interaction of the distilled water with the membrane may cause the swelling of the polymer matrix [46].

In Table 12, is noticed that the membranes which showed the lowest reduction in the permeate flux were M7 and M10. They represent a sample for each incorporated material,

showing that the effect of the incorporated NPs was positive in modifying the permeate flux of the membranes. It is also possible to observe that among the membranes embedded with ZnO NPs, the best conditions leading to the smallest drop in the permeate flux were when a pressure of 1.5 bar was applied. In this case, the greater amount (1.5 wt%) of NPs contributed to this result, as shows M5 and M7 analysis.

For the membranes in which iron oxides NPs were incorporated, the best conditions were when a pressure of 2 bar was applied. It presented the lowest values of the permeate flux reduction. Differently from the other tested material, the iron oxides NPs had a better performance in membranes M10 and M11. These membranes have different amounts of NPs and PVP in their polymeric matrix. The results indicate that the material contribute to change the membrane's properties when compared to the membranes without addition of NPs.

Other authors have studied flux variation in membranes. Lakhotia et al. [78] verified that the flux for each membrane showed a linear increase with an increase in pressure. The results indicate that the presence of FeO nanoparticles in the membrane (i.e., NHPDM1 and NHPDM2) enhanced the pure water permeate flux compared to membranes without FeO nanoparticles (i.e., HDPM). Esfahani et al [2] verified an increase of the water fluxes in all ZnO/PES membranes studied in his work, as the weight of added ZnO NPs is increased. The highest water flux (125.40 kg/m^2h) was achieved when the weight of added ZnO NPs was 0.2 g. This flux represents an improvement of 254% over that of the PES membrane without ZnO in its structure.

CONCLUSIONS AND FUTURE WORK

5 CONCLUSIONS

Metal oxide nanoparticles (ZnO and iron oxides) were synthesized by the co-precipitation method and incorporated into polymeric membranes during the synthesis of the membranes by phase inversion methodology. This study has shown that was possible to incorporate the NPs in the membrane polymeric matrix of PES/PVP.

The incorporation of ZnO and iron oxides NPs has changed the PES/PVP membrane characteristics. The impact of their incorporation in the membrane was studied by TGA analysis, which showed that the residual mass was higher for membranes with NPs, comparatively with the ones without incorporated NPs. The NPs also increased the thermal resistance of the membranes. The combination leading to the best thermal behavior was the composition 5 wt% of PVP and 1.5 wt% of NPs combined with PES to form the membrane matrix, which was verified by the TGA study and the experimental planning used in this work.

Since permeability depends on porosity and hydrophilicity, it was possible to verify that M10, which presented the higher value of porosity, was the membrane presenting the most stable permeate flux over time and the one with less reduction of the permeate flux. In addition, it corresponds to the combination presenting the better thermal behaviour as previously described. It was also verified that a smaller amount of ZnO NPs (0.5wt%) combined with 15wt% of PVP to compose the matrix of PES/ZnO membranes had the best performance to the porosity parameter. While the iron oxides NPs had the best performance to this parameter when 1.5wt% of material was combined with 5wt% of PVP to constitute the casting solution of the membrane.

Even the membranes were not tested in a filtration process, the study with distilled water presented a preliminary overview how it is the membrane behaviour for the permeate flux and its reduction over time. Considering that the used solvent, has low concentration of impurities, it is believed that the flow reduction occurred predominantly due to mechanical instability of the membrane as a function of the applied pressure. Also, it can be considered that a small physical-chemical interaction of distilled water with the membrane can cause the swelling of the polymer matrix. Therefore, comparing the results obtained in this work with the studies presented in chapter 2, they are promising for the incorporation in PES membranes since fouling characteristics of the membranes were changed.

Hydraulic permeability was analyzed statistically and determined that the best combination of factors for this parameter is when 0.5% nanomaterial with 5% PVP are combined to form the membrane structure. To the iron oxides nanoparticles the best

performance of hydraulic permeability is when 15wt% of PVP and 1.5wt% of nanomaterial were combined to compose the membrane structure.

Analyzing the results described for all the factors studied in this work, there is a better operating condition of the membranes when the structure is formed by 15wt% of PVP. However, the amount of incorporated material presented differences. The best structure was obtained when this amount of PVP was combined with 0.5% of ZnO and for iron oxide when 1.5% of material was used.

Since the search for the composition that best provides antifouling characteristics for the incorporated membranes is achieved, it is expected that the synthesized membranes tend to achieve results similar to those presented in chapter 2 when applied in the separation process, reducing the fouling phenomenon in the application of membranes in separation process.

6 FUTURE RESEARCH

ZnO and iron oxides NPs were synthesized by a coprecipitation method, the simplest technique to obtain large quantities of NPs. Nevertheless, for this method the control of size and chemical uniformity, are the main challenge due to the uncontrolled aggregation of the particles. Also, this method requires a large amount of water in the washing step due to a strong base solution that is used. In this context, it would be interesting in future works to evaluate other preparation methods in order to control the aggregation of particles and perform the characterization of synthesized materials by X-ray diffraction, to identify the metallic phases present in the synthesized NPs, mainly for the iron oxide. It would be also interesting to incorporate those NPs in the membranes, since particles better dispersed could improve the characteristics of the studied membranes, contributing to prevent the fouling phenomenon. In addition, another research focused would be to test the application of the membranes in a filtration process to better evaluate the membrane performance and to analyze the fouling.

7 REFERENCES

[1] X. Li, X. Fang, R. Pang, J. Li, X. Sun, J. Shen, W. Han, L. Wang, Self-assembly of TiO_2 nanoparticles around the pores of PES ultrafiltration membrane for mitigating organic fouling, J. Memb. Sci. 467 (2014) 226–235. https://doi.org/10.1016/j.memsci.2014.05.036.

[2] M.R. Esfahani, S.A. Aktij, Z. Dabaghian, M.D. Firouzjaei, A. Rahimpour, J. Eke, I.C. Escobar, M. Abolhassani, L.F. Greenlee, A.R. Esfahani, A. Sadmani, N. Koutahzadeh, Nanocomposite membranes for water separation and purification: Fabrication, modification, and applications, Sep. Purif. Technol. 213 (2019) 465–499. https://doi.org/10.1016/j.seppur.2018.12.050.

[3] W.Y. Pang, A.L. Ahmad, N.D. Zaulkiflee, Antifouling and antibacterial evaluation of ZnO/MWCNT dual nanofiller polyethersulfone mixed matrix membrane, J. Environ. Manage. 249 (2019). https://doi.org/10.1016/j.jenvman.2019.109358.

[4] S. Zhao, W. Yan, M. Shi, Z. Wang, J. Wang, S. Wang, Improving permeability and antifouling performance of polyethersulfone ultrafiltration membrane by incorporation of ZnO-DMF dispersion containing nano-ZnO and polyvinylpyrrolidone, J. Memb. Sci. 478 (2015) 105–116. https://doi.org/10.1016/j.memsci.2014.12.050.

[5] B.H. Jume, M.A. Gabris, H. Rashidi Nodeh, S. Rezania, J. Cho, Biodiesel production from waste cooking oil using a novel heterogeneous catalyst based on graphene oxide doped metal oxide nanoparticles, Renew. Energy. 162 (2020) 2182–2189. https://doi.org/10.1016/j.renene.2020.10.046.

[6] E. Bet-Moushoul, K. Farhadi, Y. Mansourpanah, A.M. Nikbakht, R. Molaei, M. Forough, Application of CaO-based/Au nanoparticles as heterogeneous nanocatalysts in biodiesel production, Fuel. 164 (2016) 119–127. https://doi.org/10.1016/j.fuel.2015.09.067.

[7] D. Singh, D. Sharma, S.L. Soni, S. Sharma, P. Kumar Sharma, A. Jhalani, A review on feedstocks, production processes, and yield for different generations of biodiesel, Fuel. 262 (2020). https://doi.org/10.1016/j.fuel.2019.116553.

[8] M. Vijay Kumar, A. Veeresh Babu, P. Ravi Kumar, The impacts on combustion, performance and emissions of biodiesel by using additives in direct injection diesel engine, Alexandria Eng. J. 57 (2018) 509–516. https://doi.org/10.1016/j.aej.2016.12.016.

[9] M.J. Alves, S.M. Nascimento, I.G. Pereira, M.I. Martins, V.L. Cardoso, M. Reis,

Biodiesel purification using microand ultrafiltration membranes, Renew. Energy. 58 (2013) 15–20. https://doi.org/10.1016/j.renene.2013.02.035.

[10] S. Chozhavendhan, M. Vijay Pradhap Singh, B. Fransila, R. Praveen Kumar, G. Karthiga Devi, A review on influencing parameters of biodiesel production and purification processes, Curr. Res. Green Sustain. Chem. 1–2 (2020) 1–6. https://doi.org/10.1016/j.crgsc.2020.04.002.

[11] T. Sokač, M. Gojun, A.J. Tušek, A. Šalić, B. Zelić, Purification of biodiesel produced by lipase catalysed transesterification by ultrafiltration: Selection of membranes and analysis of membrane blocking mechanisms, Renew. Energy. 159 (2020) 642–651. https://doi.org/10.1016/j.renene.2020.05.132.

[12] N.R. Uliana, A. Polloni, M. Paliga, J.G. Veneral, M.B. Quadri, J.V. Oliveira, Acidity reduction of enzymatic biodiesel using alkaline washing, Renew. Energy. 113 (2017) 393–396. https://doi.org/10.1016/j.renene.2017.06.001.

[13] J.J. Torres, N.E. Rodriguez, J.T. Arana, N.A. Ochoa, J. Marchese, C. Pagliero, Ultrafiltration polymeric membranes for the purification of biodiesel from ethanol, J. Clean. Prod. 141 (2017) 641–647. https://doi.org/10.1016/j.jclepro.2016.09.130.

[14] Saiful, R. Muliadi, M. Ilham, Fadli, M. Yusuf, Preparation of mixed matrix polymeric membrane for removing of contaminants in crude biodiesel, Res. J. Chem. Environ. 22 (2018) 15–21.

[15] M.C.S. Gomes, P.A. Arroyo, N.C. Pereira, Influence of oil quality on biodiesel purification by ultrafiltration, J. Memb. Sci. 496 (2015) 242–249. https://doi.org/10.1016/j.memsci.2015.09.004.

[16] L.Y. Ng, A.W. Mohammad, C.P. Leo, N. Hilal, Polymeric membranes incorporated with metal/metal oxide nanoparticles: A comprehensive review, Desalination. 308 (2013) 15–33. https://doi.org/10.1016/j.desal.2010.11.033.

[17] M. Zou, W. Zhang, R. Wu, H. Jiang, F. Cao, E. Su, Removal of ginkgotoxin from the Ginkgo biloba seeds powder by adopting membrane separation technology, J. Clean. Prod. 280 (2021) 124452. https://doi.org/10.1016/j.jclepro.2020.124452.

[18] I.M. Atadashi, M.K. Aroua, A.A. Aziz, Biodiesel separation and purification: A review, Renew. Energy. 36 (2011) 437–443. https://doi.org/10.1016/j.renene.2010.07.019.

[19] G.Q. Lu, J.C. Diniz da Costa, M. Duke, S. Giessler, R. Socolow, R.H. Williams, T. Kreutz, Inorganic membranes for hydrogen production and purification: A critical review and perspective, J. Colloid Interface Sci. 314 (2007) 589–603. https://doi.org/10.1016/j.jcis.2007.05.067.

[20] M. Mulder, Basic principles of membrane technology, (1991). https://doi.org/10.1524/zpch.1998.203.part_1_2.263.

[21] C.P. Leo, W.P. Cathie Lee, A.L. Ahmad, A.W. Mohammad, Polysulfone membranes blended with ZnO nanoparticles for reducing fouling by oleic acid, Sep. Purif. Technol. 89 (2012) 51–56. https://doi.org/10.1016/j.seppur.2012.01.002.

[22] L. Shen, X. Bian, X. Lu, L. Shi, Z. Liu, L. Chen, Z. Hou, K. Fan, Preparation and characterization of ZnO/polyethersulfone (PES) hybrid membranes, Desalination. 293 (2012) 21–29. https://doi.org/10.1016/j.desal.2012.02.019.

[23] J. Hong, Y. He, Effects of nano sized zinc oxide on the performance of PVDF microfiltration membranes, Desalination. 302 (2012) 71–79. https://doi.org/10.1016/j.desal.2012.07.001.

[24] J. Hong, Y. He, Polyvinylidene fluoride ultrafiltration membrane blended with nano-ZnO particle for photo-catalysis self-cleaning, Desalination. 332 (2014) 67–75. https://doi.org/10.1016/j.desal.2013.10.026.

[25] A. Alpatova, M. Meshref, K.N. McPhedran, M. Gamal El-Din, Composite polyvinylidene fluoride (PVDF) membrane impregnated with Fe_2O_3 nanoparticles and multiwalled carbon nanotubes for catalytic degradation of organic contaminants, J. Memb. Sci. 490 (2015) 227–235. https://doi.org/10.1016/j.memsci.2015.05.001.

[26] Z.Q. Huang, K. Chen, S.N. Li, X.T. Yin, Z. Zhang, H.T. Xu, Effect of ferrosoferric oxide content on the performances of polysulfone-ferrosoferric oxide ultrafiltration membranes, J. Memb. Sci. 315 (2008) 164–171. https://doi.org/10.1016/j.memsci.2008.02.028.

[27] Z.Q. Huang, F. Zheng, Z. Zhang, H.T. Xu, K.M. Zhou, The performance of the PVDF-Fe_3O_4 ultrafiltration membrane and the effect of a parallel magnetic field used during the membrane formation, Desalination. 292 (2012) 64–72. https://doi.org/10.1016/j.desal.2012.02.010.

[28] S. Balta, A. Sotto, P. Luis, L. Benea, B. Van der Bruggen, J. Kim, A new outlook on membrane enhancement with nanoparticles: The alternative of ZnO, J. Memb. Sci. 389 (2012) 155–161. https://doi.org/10.1016/j.memsci.2011.10.025.

[29] A.L. Ahmad, A.A. Abdulkarim, B.S. Ooi, S. Ismail, Recent development in additives modifications of polyethersulfone membrane for flux enhancement, Chem. Eng. J. 223 (2013) 246–267. https://doi.org/10.1016/j.cej.2013.02.130.

[30] L. Marbelia, M.R. Bilad, I.F.J. Vankelecom, Gradual PVP leaching from PVDF/PVP blend membranes and its effects on membrane fouling in membrane bioreactors, Sep.

Purif. Technol. 213 (2019) 276–282. https://doi.org/10.1016/j.seppur.2018.12.045.

[31] G. Wu, S. Gan, L. Cui, Y. Xu, Preparation and characterization of PES/TiO_2 composite membranes, Appl. Surf. Sci. 254 (2008) 7080–7086. https://doi.org/10.1016/j.apsusc.2008.05.221.

[32] E. Saljoughi, S.M. Mousavi, Preparation and characterization of novel polysulfone nanofiltration membranes for removal of cadmium from contaminated water, Sep. Purif. Technol. 90 (2012) 22–30. https://doi.org/10.1016/j.seppur.2012.02.008.

[33] E. Yuliwati, A.F. Ismail, Effect of additives concentration on the surface properties and performance of PVDF ultrafiltration membranes for refinery produced wastewater treatment, Desalination. 273 (2011) 226–234. https://doi.org/10.1016/j.desal.2010.11.023.

[34] H. Song, J. Shao, Y. He, B. Liu, X. Zhong, Natural organic matter removal and flux decline with PEG-TiO_2-doped PVDF membranes by integration of ultrafiltration with photocatalysis, J. Memb. Sci. 405–406 (2012) 48–56. https://doi.org/10.1016/j.memsci.2012.02.063.

[35] A. V. B., S. Mohanty, S.K. Nayak, Preparation and characterization of porous polyethersulfone (PES) membranes with improved biocompatibility by blending sulfonated polyethersulfone (SPES) and cellulose acetate (CA) – A comparative study, Mater. Today Commun. 25 (2020) 101544. https://doi.org/10.1016/j.mtcomm.2020.101544.

[36] J. Guo, J. Kim, Modifications of polyethersulfone membrane by doping sulfated-TiO_2 nanoparticles for improving anti-fouling property in wastewater treatment, RSC Adv. 7 (2017) 33822–33828. https://doi.org/10.1039/c7ra06406c.

[37] A. Aguilar-Sanchez, B. Jalvo, A. Mautner, S. Nameer, T. Pöhler, T. Tammelin, A.P. Mathew, Waterborne nanocellulose coatings for improving the antifouling and antibacterial properties of polyethersulfone membranes, J. Memb. Sci. (2020). https://doi.org/10.1016/j.memsci.2020.118842.

[38] S. Zhao, Z. Wang, X. Wei, X. Tian, J. Wang, S. Yang, S. Wang, Comparison study of the effect of PVP and PANI nanofibers additives on membrane formation mechanism, structure and performance, J. Memb. Sci. 385–386 (2011) 110–122. https://doi.org/10.1016/j.memsci.2011.09.029.

[39] Y. Kourde-Hanafi, P. Loulergue, A. Szymczyk, B. Van der Bruggen, M. Nachtnebel, M. Rabiller-Baudry, J.L. Audic, P. Pölt, K. Baddari, Influence of PVP content on degradation of PES/PVP membranes: Insights from characterization of membranes with

controlled composition, J. Memb. Sci. 533 (2017) 261–269. https://doi.org/10.1016/j.memsci.2017.03.050.

[40] S. Mohsenpour, A. Safekordi, M. Tavakolmoghadam, F. Rekabdar, M. Hemmati, Comparison of the membrane morphology based on the phase diagram using PVP as an organic additive and TiO_2 as an inorganic additive, Polymer (Guildf). 97 (2016) 559–568. https://doi.org/10.1016/j.polymer.2016.05.069.

[41] X. Meng, D. Luosang, S. Meng, R. Wang, W. Fan, D. Liang, X. Li, Q. Zhao, L. Yang, The structural and functional properties of polysaccharide foulants in membrane fouling, Chemosphere. 268 (2021) 129364. https://doi.org/10.1016/j.chemosphere.2020.129364.

[42] N. Sankar, S. Joseph, Membrane Filtration Techniques Through Polymer Nanocomposites, in: Transp. Prop. Polym. Membr., Elsevier, 2018: pp. 265–300. https://doi.org/10.1016/B978-0-12-809884-4.00014-8.

[43] A.L. Ahmad, A.A. Abdulkarim, Z.M.H. Mohd Shafie, B.S. Ooi, Fouling evaluation of PES/ZnO mixed matrix hollow fiber membrane, Desalination. 403 (2017) 53–63. https://doi.org/10.1016/j.desal.2016.10.008.

[44] N. Ghaemi, S.S. Madaeni, P. Daraei, H. Rajabi, S. Zinadini, A. Alizadeh, R. Heydari, M. Beygzadeh, S. Ghouzivand, Polyethersulfone membrane enhanced with iron oxide nanoparticles for copper removal from water: Application of new functionalized Fe_3O_4 nanoparticles, Chem. Eng. J. 263 (2015) 101–112. https://doi.org/10.1016/j.cej.2014.10.103.

[45] H. Rajabi, N. Ghaemi, S.S. Madaeni, P. Daraei, B. Astinchap, S. Zinadini, S.H. Razavizadeh, Nano-ZnO embedded mixed matrix polyethersulfone (PES) membrane: Influence of nanofiller shape on characterization and fouling resistance, Appl. Surf. Sci. 349 (2015) 66–77. https://doi.org/10.1016/j.apsusc.2015.04.214.

[46] L.D. Fiorentin-Ferrari, K.M. Celant, B.C. Gonçalves, S.M. Teixeira, V. Slusarski-Santana, A.N. Módenes, Fabrication and characterization of polysulfone and polyethersulfone membranes applied in the treatment of fish skin tanning effluent, J. Clean. Prod. 294 (2021) 126127. https://doi.org/10.1016/j.jclepro.2021.126127.

[47] E. Eren, A. Sarihan, B. Eren, H. Gumus, F.O. Kocak, Preparation, characterization and performance enhancement of polysulfone ultrafiltration membrane using PBI as hydrophilic modifier, J. Memb. Sci. 475 (2015) 1–8. https://doi.org/10.1016/j.memsci.2014.10.010.

[48] J.M. Rami, C.D. Patel, C.M. Patel, M. V Patel, Materials Today : Proceedings Thermogravimetric analysis (TGA) of some synthesized metal oxide nanoparticles,

Mater. Today Proc. (2020) 1–5. https://doi.org/10.1016/j.matpr.2020.12.554.

[49] E. Mahmoudi, L.Y. Ng, W.L. Ang, Y.T. Chung, R. Rohani, A.W. Mohammad, Enhancing Morphology and Separation Performance of Polyamide 6,6 Membranes By Minimal Incorporation of Silver Decorated Graphene Oxide Nanoparticles, Sci. Rep. 9 (2019) 1–16. https://doi.org/10.1038/s41598-018-38060-x.

[50] R.T. Sataloff, M.M. Johns, K.M. Kost, Nanostructured Materials and Nanotechnology, n.d.

[51] Maiti, Bidinger, Crystals Growth, Morphology and Perfection, 1st ed., Cambridge University Press, New York, 1981.

[52] F. Ahangaran, A.H. Navarchian, Recent advances in chemical surface modification of metal oxide nanoparticles with silane coupling agents: A review, Adv. Colloid Interface Sci. 286 (2020) 102298. https://doi.org/10.1016/j.cis.2020.102298.

[53] A. Kumar, Sol gel synthesis of zinc oxide nanoparticles and their application as nano-composite electrode material for supercapacitor, J. Mol. Struct. 1220 (2020) 128654. https://doi.org/10.1016/j.molstruc.2020.128654.

[54] M. Sheikh, M. Pazirofteh, M. Dehghani, M. Asghari, M. Rezakazemi, C. Valderrama, J.L. Cortina, Application of ZnO nanostructures in ceramic and polymeric membranes for water and wastewater technologies: A review, Chem. Eng. J. 391 (2020) 123475. https://doi.org/10.1016/j.cej.2019.123475.

[55] C.B.D. Marien, C. Marchal, A. Koch, D. Robert, P. Drogui, Sol-gel synthesis of TiO_2 nanoparticles: effect of Pluronic P123 on particle's morphology and photocatalytic degradation of paraquat, Environ. Sci. Pollut. Res. 24 (2017) 12582–12588. https://doi.org/10.1007/s11356-016-7681-2.

[56] P.S. Wu, Y.C. Lee, Y.C. Kuo, C.C. Lin, Development of octyl methoxy cinnamates (OMC)/silicon dioxide (SiO_2) nanoparticles by sol-gel emulsion method, Nanomaterials. 7 (2017). https://doi.org/10.3390/nano7120434.

[57] F.H. Saboor, A.A. Khodadadi, Y. Mortazavi, M. Asgari, Microemulsion synthesized silica/ZnO stable core/shell sensors highly selective to ethanol with minimum sensitivity to humidity, Sensors Actuators, B Chem. 238 (2017) 1070–1083. https://doi.org/10.1016/j.snb.2016.07.127.

[58] Y.L. Pang, S. Lim, H.C. Ong, W.T. Chong, Research progress on iron oxide-based magnetic materials: Synthesis techniques and photocatalytic applications, Ceram. Int. 42 (2016) 9–34. https://doi.org/10.1016/j.ceramint.2015.08.144.

[59] T.Q. Bui, S.N.C. Ton, A.T. Duong, H.T. Tran, Size-dependent magnetic responsiveness

of magnetite nanoparticles synthesised by co-precipitation and solvothermal methods, J. Sci. Adv. Mater. Devices. 3 (2018) 107–112. https://doi.org/10.1016/j.jsamd.2017.11.002.

[60] S. Akbari, S.M. Masoudpanah, S.M. Mirkazemi, N. Aliyan, PVA assisted coprecipitation synthesis and characterization of $MgFe_2O_4$ nanoparticles, Ceram. Int. 43 (2017) 6263–6267. https://doi.org/10.1016/j.ceramint.2017.02.030.

[61] C. Altavilla, E. Ciliberto, Inorganic Nanoparticles: Synthesis Application and perspectives, n.d.

[62] W.M. Rangel, R.A.A. Boca Santa, H.G. Riella, A facile method for synthesis of nanostructured copper (II) oxide by coprecipitation, J. Mater. Res. Technol. 9 (2020) 994–1004. https://doi.org/10.1016/j.jmrt.2019.11.039.

[63] I. Nkurikiyimfura, Y. Wang, B. Safari, E. Nshingabigwi, Temperature-dependent magnetic properties of magnetite nanoparticles synthesized via coprecipitation method, J. Alloys Compd. 846 (2020). https://doi.org/10.1016/j.jallcom.2020.156344.

[64] O. Singh, N. Kohli, R.C. Singh, Precursor controlled morphology of zinc oxide and its sensing behaviour, Sensors Actuators, B Chem. 178 (2013) 149–154. https://doi.org/10.1016/j.snb.2012.12.053.

[65] W. Ahmad, D. Kalra, Green synthesis, characterization and anti microbial activities of ZnO nanoparticles using Euphorbia hirta leaf extract, J. King Saud Univ. - Sci. 32 (2020) 2358–2364. https://doi.org/10.1016/j.jksus.2020.03.014.

[66] A. Fathima Beevi, G. Sreekala, B. Beena, Synthesis, characterization and photocatalytic activity of SnO_2, ZnO nanoparticles against congo red: A comparative study, Mater. Today Proc. (2021). https://doi.org/10.1016/j.matpr.2020.10.755.

[67] S.K. Sharma, J.M. Vargas, K.R. Pirota, S. Kumar, C.G. Lee, M. Knobel, Synthesis and ageing effect in s nanoparticles: Transformation to core-shell FeO/Fe_3O_4 and their magnetic characterization, J. Alloys Compd. 509 (2011) 6414–6417. https://doi.org/10.1016/j.jallcom.2011.03.072.

[68] I. de la Calle, M. Menta, M. Klein, F. Séby, Screening of TiO_2 and Au nanoparticles in cosmetics and determination of elemental impurities by multiple techniques (DLS, SP-ICP-MS, ICP-MS and ICP-OES), Talanta. 171 (2017) 291–306. https://doi.org/10.1016/j.talanta.2017.05.002.

[69] E. Abdulkarem, Y. Ibrahim, M. Kumar, H.A. Arafat, V. Naddeo, F. Banat, S.W. Hasan, Polyvinylidene fluoride (PVDF)-α-zirconium phosphate (α-ZrP) nanoparticles based mixed matrix membranes for removal of heavy metal ions, Chemosphere. 267 (2020)

128896. https://doi.org/10.1016/j.chemosphere.2020.128896.

[70] P.S. Goh, B.C. Ng, W.J. Lau, A.F. Ismail, Inorganic nanomaterials in polymeric ultrafiltration membranes for water treatment, Sep. Purif. Rev. 44 (2015) 216–249. https://doi.org/10.1080/15422119.2014.926274.

[71] W. Hu, S. Chen, B. Zhou, H. Wang, Facile synthesis of ZnO nanoparticles based on bacterial cellulose, Mater. Sci. Eng. B Solid-State Mater. Adv. Technol. 170 (2010) 88–92. https://doi.org/10.1016/j.mseb.2010.02.034.

[72] M. Sheikh, M. Pazirofteh, M. Dehghani, M. Asghari, M. Rezakazemi, C. Valderrama, J.L. Cortina, Application of ZnO nanostructures in ceramic and polymeric membranes for water and wastewater technologies: A review, Chem. Eng. J. 391 (2020) 123475. https://doi.org/10.1016/j.cej.2019.123475.

[73] T.D. Kusworo, W. Widayat, D.P. Utomo, Y.H.S. Pratama, R.A.V. Arianti, Performance evaluation of modified nanohybrid membrane polyethersulfone-nano ZnO (PES-nano ZnO) using three combination effect of PVP, irradiation of ultraviolet and thermal for biodiesel purification, Renew. Energy. 148 (2020) 935–945. https://doi.org/10.1016/j.renene.2019.10.177.

[74] S. Liang, K. Xiao, Y. Mo, X. Huang, A novel ZnO nanoparticle blended polyvinylidene fluoride membrane for anti-irreversible fouling, J. Memb. Sci. 394–395 (2012) 184–192. https://doi.org/10.1016/j.memsci.2011.12.040.

[75] S. Al Aani, C.J. Wright, M.A. Atieh, N. Hilal, Engineering nanocomposite membranes: Addressing current challenges and future opportunities, Desalination. 401 (2017) 1–15. https://doi.org/10.1016/j.desal.2016.08.001.

[76] A. Gholami, A.R. Moghadassi, S.M. Hosseini, S. Shabani, F. Gholami, Preparation and characterization of polyvinyl chloride based nanocomposite nanofiltration-membrane modified by iron oxide nanoparticles for lead removal from water, J. Ind. Eng. Chem. 20 (2014) 1517–1522. https://doi.org/10.1016/j.jiec.2013.07.041.

[77] E. Demirel, B. Zhang, M. Papakyriakou, S. Xia, Y. Chen, Fe_2O_3 nanocomposite PVC membrane with enhanced properties and separation performance, J. Memb. Sci. 529 (2017) 170–184. https://doi.org/10.1016/j.memsci.2017.01.051.

[78] S.R. Lakhotia, M. Mukhopadhyay, P. Kumari, Iron oxide (FeO) nanoparticles embedded thin-film nanocomposite nanofiltration (NF) membrane for water treatment, Sep. Purif. Technol. 211 (2019) 98–107. https://doi.org/10.1016/j.seppur.2018.09.034.

[79] A.D. Mani, I. Soibam, Effect of the size of the dopants on the dielectric and magnetic properties of $Bi(La,Gd)FeO_3$ multiferroic materials, J. Nano Res. 51 (2018) 61–68.

https://doi.org/10.4028/www.scientific.net/JNanoR.51.61.

[80] S.C. Sharma, ZnO nano-flowers from Carica papaya milk: Degradation of Alizarin Red-S dye and antibacterial activity against Pseudomonas aeruginosa and Staphylococcus aureus, Optik (Stuttg). 127 (2016) 6498–6512. https://doi.org/10.1016/j.ijleo.2016.04.036.

[81] F. Iazdani, A. Nezamzadeh-Ejhieh, FeO-Clinoptilolite nanoparticles: Brief characterization and its photocatalytic kinetics towards 2,4-dichloroaniline, Chem. Phys. 550 (2021) 111305. https://doi.org/10.1016/j.chemphys.2021.111305.

[82] J.H. Kim, K.H. Lee, Effect of PEG additive on membrane formation by phase inversion, J. Memb. Sci. 138 (1998) 153–163. https://doi.org/10.1016/S0376-7388(97)00224-X.